ORDERING AND THE K-STATE IN NICKEL-MOLYBDENUM ALLOYS

By

BRUCE GORDON LEFEVRE

A DISSERTATION PRESENTED TO THE GRADUATE COUNCIL OF
THE UNIVERSITY OF FLORIDA
IN PARTIAL FULFILLMENT OF THE REQUIREMENTS FOR THE
DEGREE OF DOCTOR OF PHILOSOPHY

UNIVERSITY OF FLORIDA

December, 1966

ACKNOWLEDGMENTS

The author would like to acknowledge the assistance of the following people who contributed their time and effort toward a successful conclusion of this work: Professor A. G. Guy (Committee Chairman), Professor J. J. Hren, Graduate Assistant R. W. Newman, Professor R. W. Gould, Professor E. A. Starke, Professor J. E. Spruiell, and Mr. E. J. Jenkins. Professor Guy suggested the topic for this research and provided many helpful suggestions during the course of the experiments and the preparation of the manuscript.

Professor Hren and R. W. Newman are responsible for the success of the field-ion microscopy portion of this work. It was they who built the microscope and developed the techniques used in this study. They also contributed heavily in the interpretation of the micrographs.

Professor R. W. Gould and Professor E. A. Starke (Georgia Institute of Technology) provided many helpful suggestions concerning the x-ray diffraction experiments and the interpretation of the data. Professor J. E. Spruiell and his associates at the University of Tennessee provided the alloys that were used in this research as

well as many helpful suggestions concerning experimental techniques. It was the work of Professor Spruiell and his associates in the Ni-Mo system that stimulated interest in the present research.

Mr. E. J. Jenkins who is the electron microscopist in the metallurgy department of the University of Florida contributed unselfishly of his own time in connection with that portion of the work.

The author is also grateful to the Graduate School of the University of Florida and the National Science Foundation for providing financial support for this research.

Last, but by no means least, the author would like to acknowledge his wife Elaine for her moral support and constant encouragement during the many periods when things "just weren't going right."

TABLE OF CONTENTS

LIST OF FIGURES

LIST OF FIGURES--*Continued*

LIST OF FIGURES--*Continued*

LIST OF FIGURES--*Continued*

LIST OF FIGURES--*Continued*

LIST OF FIGURES--*Continued*

LIST OF FIGURES--*Continued*

Abstract of Dissertation Presented to the Graduate Council in Partial Fulfillment of the Requirements for the Degree of Doctor of Philosophy

ORDERING AND THE K-STATE IN NICKEL-MOLYBDENUM ALLOYS

By

Bruce Gordon LeFevre

December, 1966

Chairman: Dr. A. G. Guy

Major Department: Metallurgical and Materials Engineering

The K-state is a phenomenon that is marked by anomalous property changes in certain alloys without observable macroscopic structural changes. One of these anomalies is a decrease in resistivity with cold work and an increase in resistivity with annealing, an effect which is opposite to that found in normal alloys. Short-range order has frequently been suggested as a possible cause of the K-state. In this work studies were made on Ni-Mo to determine the role of short-range order on the formation of the K-state. Polycrystalline specimens containing 10.5, 14.0, and 20.0 a/o Mo were studied by means of electrical resistivity, x-ray diffuse scattering, electron transmission microscopy, field-ion microscopy, and x-ray small-angle scattering. These specimens were examined after a variety of mechanical and thermal treatments.

Previous studies have shown that the K-state can be formed in Ni-Mo alloys and that short-range order exists in the α-phase region; however, no direct correlation has been made between short-range order and the K-state in this system. The results of the x-ray diffuse-scattering measurements made in this study show that there is a one-to-one correlation between the degree of short-range order and the resistivity changes. It was found that when specimens are treated in such a way that the resistivity increases, there is also a significant increase in the degree of short-range order, and conversely.

A possible explanation of how short-range order increases the resistivity in Ni-Mo alloys was provided by field-ion micrographs of specimens in the ordered and disordered conditions. Ni-14.0 a/o Mo specimens were quenched from the α-phase region and compared with Ni-20.0 a/o Mo alloys which had been annealed to develop the fully-ordered Ni_4Mo structure (β phase). From a comparison of the two it was concluded that short-range order in dilute Ni-Mo alloys consists of small, imperfect domains of Ni_4Mo-type long-range order, approximately 50 Å in diameter. It is suggested that the resistivity increase is caused by a decrease in the number of effective electrons as the degree of short-range increases. A rough calculation

shows that as a result of the Ni_4Mo-type of ordering, the Fermi surface lies closer to a Brillouin-zone boundary than for the case of a random solid solution. This can be attributed to the fact that ordering changes the symmetry of the solid solution and provides new reflecting planes which give rise to superlattice lines.

The early stages of precipitation of the β phase was studied in the Ni-14.0 a/o Mo alloys by means of resistivity, electron microscopy, and small-angle scattering. It was concluded that the small domains which make up the short-range order in the α phase provide nuclei for the precipitation of the β phase at lower temperatures. By direct observation of the precipitation process in an electron-microscope hot stage it was found that the β phase grows directly into platelets without the occurrence of any intermediate metastable phases. The habit plane of the platelets was found to be the {111}.

INTRODUCTION

The effects of solute elements on such mechanical properties of metals as yield strength and hardness have long been known in an empirical way. The science of metallurgy, however, is fast approaching the stage where these effects are considered in a more fundamental way and are explained in terms of structural features such as detailed local atomic arrangements, density and types of lattice defects, early stages of precipitation, vibrational modes of the lattice, and even the density of electronic states and their effect upon the type of atomic bonding. These structures can be inferred from new and sophisticated tools such as x-ray and neutron diffraction, electron microscopy, field-ion microscopy, anelasticity, magnetic susceptibility, calorimetry, thermoelectric power, the Hall constant, the Mössbauer effect, nuclear magnetic resonance, and others. A property of certain alloys that has generated considerable interest in the past few years is the so-called K-state (more properly called the K-effect). Interest in this phenomenon stems from the fact that it is marked by an anomalous change in certain physical properties (notably resistivity) without any observable macroscopic structural changes. At one time or another all of the above mentioned

tools, with the exception of nuclear magnetic resonance and Mössbaur effect have been used in investigating various aspects of the K-state.

The first definitive work done on the K-state was by Thomas in 1951 [1]. In this study he noted certain anomalies in the physical properties of several alloy systems in which at least one component was a transition element. The alloys that he studied were Ni-Cr, Ni-Cu-Zn, Fe-Al, Cu-Mn, Ag-Mn, and Ni-Cu. Upon thermally annealing specimens which has been previously quenched from an elevated temperature or cold-worked he found an unusual increase in resitivity in a certain range of temperature as shown in Figure 1. Such an effect has since been found in a number of other alloys that will be mentioned later. In almost every case one of the components is a transition element, a fact which is important when considering the cause of the resistivity anomaly.

Although this resistivity anomaly has been rather arbitrarily selected as the "definition" of the K-state, primarily because of the ease with which it can be detected, there are other significant property changes which accompany the change in resistivity and these might well be used to monitor the K-state. For example, a 20% increase in hardness was found by Nordheim and Grant [2] and Lifshitz [3]

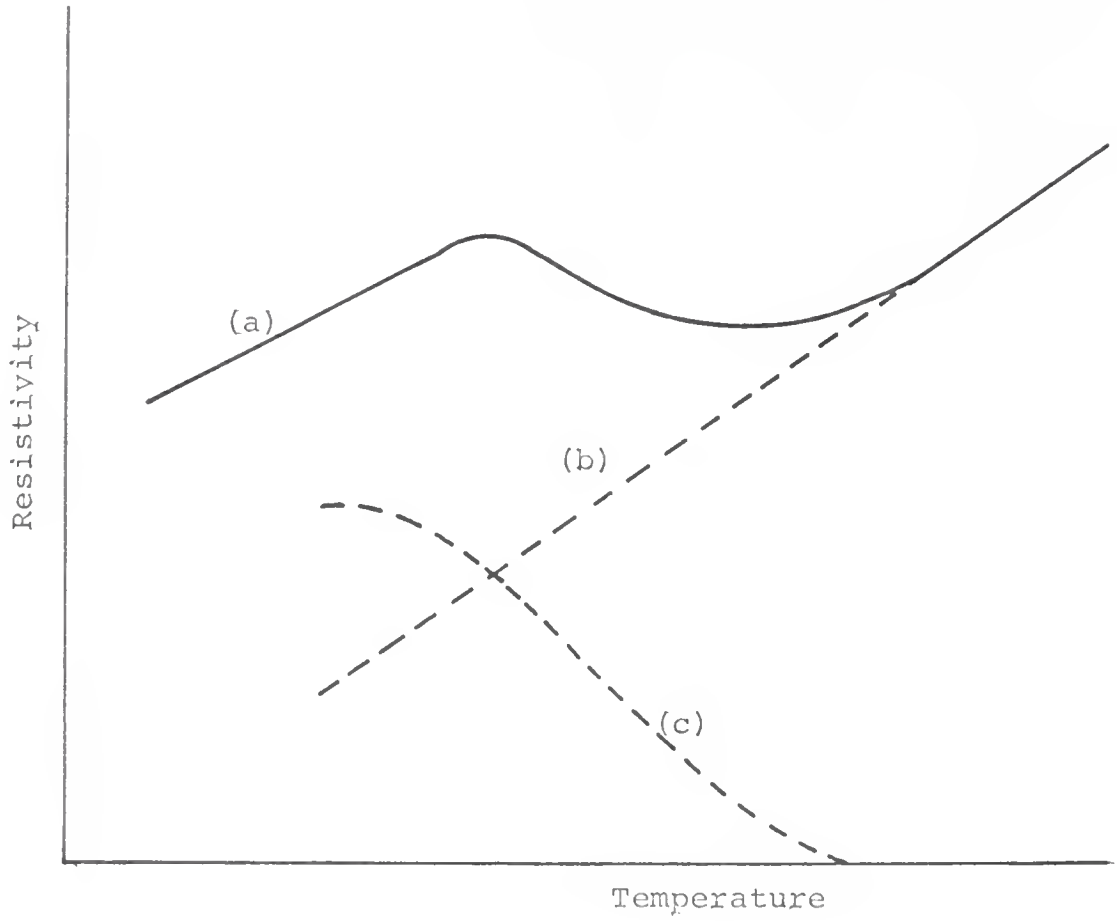

Fig. 1--Schematic resistivity-temperature curve characteristic of K-state alloys. Curve (a), obtained on heating samples quenched from 800°C. Curve (b), characteristic of normal alloys. Curve (c), contribution of K-state (after Thomas).

in a Ni-20a/o Cr alloy upon formation of the K-state. Lifshitz also reported that for a Nichrome alloy in which the K-state has been formed, no increase in hardness was observed for specimens cold-worked in the range 20-80% reduction of area. After 80% reduction of area the K-state was completely destroyed and the normal work-hardening effects were observed. In Ni-8.3a/o Al Kurdyumov *et al.* [4] found a change in elastic modulus upon quenching and annealing. Davies [5] used dilatometry and x-ray diffuse scattering to study the K-state in Fe-Al alloys in the composition range 16-25a/o Al. He observed as much as a 0.03% contraction and a 25% increase in flow stress upon formation of the K-state. In a recent study of K-state phenomena in Ag-Pd alloys, Chen and Nicholson [6] used resistivity, Hall constant, thermoelectric power, and magnetic susceptibility measurements. They found that cold working up to about 20% reduction of area reduced the resistivity of these alloys. Thereafter the resistivity increased as it would under normal conditions. Negative deviations were found in the thermoelectric power upon cold working up to 90% reduction of area. In other recent work in the Ni-Al system by Starke, Gerold and Guy [7] and by Hornbogen and Kreye [8], electron microscopy was used as well as resistivity and x-ray diffuse scattering. In this system the formation of ordered Guinier-Preston (G.P.) zones

of Ni_3Al was found to play an important part. Starke *et al.* also used small-angle x-ray scattering to verify the existence of these zones. Stansbury *et al.* [9] found an anomalous increase in the specific heat of Ni-Cr and Ni-Mo alloys which are known to form the K-state.

The previous examples show the many ways in which the K-state can manifest itself. Müller and Muth [10] have summarized many of these effects. There is a heat evolution, a lattice contraction, a shift in the Hall constant to more positive values, an increase in the effective mass of the charge carriers with a decrease in their mobility, a lowering of the magnetic susceptibility, and an increase in hardness and elastic modulus. And of course, one can add to the list: an increase in specific heat, an increase in thermoelectric power (cold working decreases it and destroys the K-state), and an increase in strength.

As for the nature of the structure which characterizes the K-state, some form of ordering, clustering, or G.P. zones has been suggested by many investigators depending upon the particular system under consideration. Actually there has been little direct observation of such structures by x-ray techniques since the time when ordering was first suggested by Yano [11] in 1940 for the Ni-Cr system. The whole problem has been complicated to some extent by two

factors: (1) Most of the work has been done on Ni-Cr alloys, in which a large effect occurs, but in which x-ray measurements of ordering are extremely difficult because of the small difference in the atomic scattering factors of Ni and Cr [1,2,3,10-23]. (2) Much of the work has been done on alloys in which a proper distinction was not, or could not be, made between effects associated with the early stages of precipitation of a second phase and those effects truly associated with changes in a single-phase solid solution. A large part of the previously mentioned work on Ni-Cr alloys falls into this category as well as some of the earlier work on the Ni-Al system. It should not be surprising to find measurable property changes associated with the precipitation of a second phase, in fact, this is a basis for the determination of equilibrium phase diagrams. Hence a strict definition of the K-effect should not include such systems. However, there is good reason to believe that in many systems the structure of an as-quenched, supersaturated solid solution bears some relationship to the final precipitate. From this standpoint, therefore, the study of two-phase systems in connection with the K-state is of considerable interest.

Davies [5] summarized the theories proposed up to that time for the structural effects responsible for the

K-state. They are: (1) short-range order [1,11,20]; (2) some form of long-range order [12,2]; (3) clustering or G.P. zones [3]; and (4) clustering of some atoms followed by ordering of the matrix [24]. In his own work on Fe-Al alloys, Davies attributed the K-state to an ordered structure with a very small domain size. Since his x-ray patterns indicated the coexistence of short-range and long-range order, it is difficult to determine just how much of a role each of these plays or just what the relationship is between the two forms of order.

In references [7] and [8], mentioned previously, a detailed study was made on Ni-Al alloys both in the single-phase region (the face-centered cubic [FCC] α phase) and in a two-phase region (the α phase + the ordered FCC α' phase with the composition Ni_3Al). It was found that short-range order was responsible for a small but measurable K-effect in the single-phase alloys whereas the formation of coherent G.P. zones of the ordered α' phase was responsible for a much larger K-effect in the two-phase alloys. A maximum in resistivity for the two-phase alloys was found to occur when the G.P. zones had a radius of about 15-20 Å. It appears that the situation here is completely analogous to the maximum of resistivity in Al-Zn alloys [25] where the critical size is about 9 Å. It was assumed by Starke *et al.* that the resistivity maximum is caused by scattering of

the conduction electrons near the Fermi surface by the G.P. zones as suggested by Mott [26]. The maximum presumably corresponds to a size of the zones that is about the wavelength of the conduction electrons and is caused by an increased probability for scattering of these electrons. It could not be definitely concluded whether it was this effect or the accompanying coherency strains in the matrix that plays the larger role. This research on the Ni-Al system was important because a clear distinction has been made between the effects of ordering of the matrix and the effects of heterogenieties in the early stages of precipitation.

Recent work by Baer [27] on Ni-W and Ni-Mo alloys shows a quite larger K-effect present in the single-phase α field. The kinetics of the formation of the K-state in Ni-Mo has also been studied by several Russian workers [28, 29,30] who proceeded on the assumption that the K-effect in this system was in fact due to a form of short-range ordering and therefore involved diffusion-controlled redistribution of atoms. Baer was able to show that short-range order does in fact exist in Ni-W and can be destroyed by subsequent cold work. Although no data were given for Ni-Mo alloys, Baer stated that this system showed a similar behavior. The presence of short-range order in the α phase

in the Ni-Mo system has been shown conclusively by Spruiell [31] from x-ray studies of single crystals and also by McManus [32] from similar studies on polycrystalline specimens. No adequate study has been made in the Ni-Mo system of the correlation between short-range order and resistivity.

The Ni-Mo and Ni-W alloys apparently represent systems in which some condition in the single-phase, solid-solution matrix causes the K-state. This is apparently true also in the Ag-Pd alloys investigated by Chen and Nicholson [6], and by Westerlund and Nicholson [33]. It must be emphasized, however, that even though short-range order has been suggested many times there are other distinct possibilities which will be discussed in more detail later. Guy [34], for example, suggested the possibility of solute concentration at dislocations, the migration of which is enhanced by the presence of excess vacancies in the freshly-quenched specimen.

In summary, the K-state has been attributed to one or more of three factors: (1) the early stages of precipitation of a second phase; (2) departures from randomness in the solid-solution matrix due either to solute concentration at defects or to some form of order, either local or long-range; (3) changes in electronic configuration due to local

lattice distortions. In cases where no second phase is involved, most investigators agree that there is a certain fundamental change in electronic structure of the K-state alloys with appropriate cold working and annealing. Whether this change involves ordering or simply static displacements due to cold work could only be speculated, since there has been little correlation of x-ray analysis with the electronic property changes such as resistivity, Hall constant, and magnetic susceptibility. Much of the speculation could have been eliminated by qualitative diffuse-scattering x-ray measurements on polycrystalline samples. The importance of diffuse x-ray scattering measurements was also emphasized by Baer [27] who attributed the K-state to short-range order and recommended determining the detailed atomic arrangements involved in each alloy system. The determination of the exact nature of the local atomic arrangements appears all the more important in view of recent evidence of a K-effect in the systems Au-Cu [35, 36, 37], Cu-Al [38], and Cu-Zn [38], systems in which no transition element is present.

The present research was undertaken to learn as much as possible about the structural effects which accompany the K-effect in the Ni-Mo system. In particular, the role of short-range order was investigated directly

by diffuse x-ray scattering and was correlated with resistivity measurements made after appropriate mechanical and thermal treatments. These measurements were supplemented by electron-microscopic and field-ion microscopic studies. The Ni-Mo system is particularly convenient for such an investigation because it shows a reasonably large K-effect and is amenable to x-ray studies of ordering because of the large difference in atomic scattering factors. The primary objective of the research was to obtain detailed experimental evidence which would either support or refute the proposal that local order is responsible for the K-effect in the Ni-Mo system. An additional objective was to determine the nature of the local order that is known to exist in dilute alloys of molybdenum in nickel.

CHAPTER I

REVIEW OF THEORY

1.1 *Resistivity of Alloys*

Excellent summaries of the theories of electrical conductivity in metals are given in Chapter 11 in Dekker [39] and in an early review article by Bardeen [40]. These reviews do not go into very much detail concerning the effect of ordering upon resistivity; however, a very detailed treatment of the effect of ordering is given by Krivoglaz and Smirnov [41]. In their treatment, it is assumed that the number of conduction electrons and the density of states into which transitions may be made are unaffected by ordering; thus only the effect of the redistribution of scattering centers is considered. On the other hand, as has been discussed in the Introduction, changes in electronic structure may be extremely important in the case of K-state alloys.

The early theories of Drude and Lorentz [42] were developed before the introduction of the band theory of solids, hence they were severely restricted in much the same way as the early theories of specific heats. These theories contained the essential ideas that the current is carried by electrons which move about more or less

freely and are subject to collisions with the crystalline lattice. Associated with each collision is a mean time τ (relaxation time), and the electron is assumed to lose all the energy gained by the imposed electric field with each collision. This results in an expression for the conductivity given by:

$$\sigma = ne^2\tau/m \qquad (1)$$

where σ = conductivity

n = number of electrons per unit volume

τ = relaxation time or mean time between collisions

m = mass of electron

e = charge on electron.

In this derivation use is made of classical statistics. The theory was later revised by Sommerfeld [43] using Fermi-Dirac statistics with a free-electron approach. This led to the expression:

$$\sigma = ne^2\tau_F/m \qquad (2)$$

where τ_F = relaxation time of electrons at the Fermi level. Finally, a treatment by Mott and Jones [44] using the band approximation gave:

$$\sigma = n_{eff}e^2\tau_F/m \qquad (3)$$

where n_{eff} is the number of "effective" electrons.

The importance of this equation is that one can now distinguish between metals and insulators as well as between good metallic conductors and poor metallic conductors. For example, the number of effective electrons in a filled band is zero, as in the case of insulators. Furthermore, n_{eff}, even for the case of an unfilled band, depends, among other things, on the width of the band, or in other words, on the tightness of binding. n_{eff} also depends upon the level to which the band is filled. Once the band structure for the various metals is known, one can understand the difference between good and poor conductors. The application of equation (3) is based entirely on the terms n_{eff} and τ_F. In other words, the conductivity of a material is determined by the number of effective electrons and by the relaxation time between collisions with the ionic cores for those electrons near the Fermi level.

Several important facts concerning the resistivity of metals are worth reviewing at this point.

1. Although all the electrons of a metal take part in the conduction process, it is the relaxation time (or collision probability) of only those near the Fermi surface that affects the conductivity.

2. A perfectly periodic crystal, i.e., one with no imperfections, at absolute zero would have zero resistance. Deviations from perfect periodicity are caused by:

   a. Lattice vibrations

b. Lattice defects (vacancies, dislocation, grain boundaries, etc.)

c. Foreign impurity atoms.

3. According to Matthiessen's Rule, the resistivity of an alloy can be written as: $\rho = \rho_0 + \rho(T)$ where ρ_0 is a temperature-independent term that includes effects of 2b and 2c above, and $\rho(T)$ is a temperature-dependent term determined by the interaction between electron waves (photons) and lattice vibrations (phonons). ρ_0 is often called the "residual" resistivity. Since it is temperature-independent, resistivity measurements in the study of lattice defects are frequently made at low temperatures to remove the $\rho(T)$ term and increase the precision.

Most of the theory of resistivity is concerned with the evaluation of the terms $\rho(T)$ and ρ_0. The $\rho(T)$ term can only be completely understood in terms of photon-phonon interactions as originally developed by Bloch [45]. In this treatment each lattice vibration is considered as a wave (phonon) having a certain propagation vector $\vec{q}$ which designates its momentum. It also has one of a number of quantized energies in complete analogy with the propogation of electron waves. A complete treatment involves the use of time-dependent perturbation theory. Out of such a treatment comes certain selection rules for photon-phonon interactions, and each interaction of a photon with the lattice results in the absorption or emission of a vibrational quantum. At low temperatures the higher-frequency modes of oscillation are not excited and therefore

the collision of a photon with a low-energy phonon results in only a small deviation of the wave vector $\vec{k}$ and a small loss of energy for the electron. Hence the resistivity decreases with temperature.

The fact that $\rho(T)$ and ρ_0 are ordinarily independent of one another is demonstrated by the work of Linde [46] shown in Figure 2. The temperature-coefficient of resistivity is affected very little by alloying copper with nickel since the primary effect of alloying is to increase ρ_0, i.e., to simply add a constant to the function ρ vs. T. There is, of course, a slight effect of alloying on the $\rho(T)$ term because of the change in the Debye temperature of the crystal with alloying.

Matthiessen's rule, however, does assume that there are no significant changes in the electronic structure as a result of alloying. It must be borne in mind that, although the principle influence on resistivity is ordinarily the distribution of the scattering centers themselves, the electronic effects accompanying alloying, ordering, introduction of defects, etc. may be extremely important. In fact, as previously mentioned, it has been suggested that this is the basis of the K-state phenomenon. The importance of the electronic properties of a metal can be demonstrated as follows. Equation (3) can be rewritten in terms of the

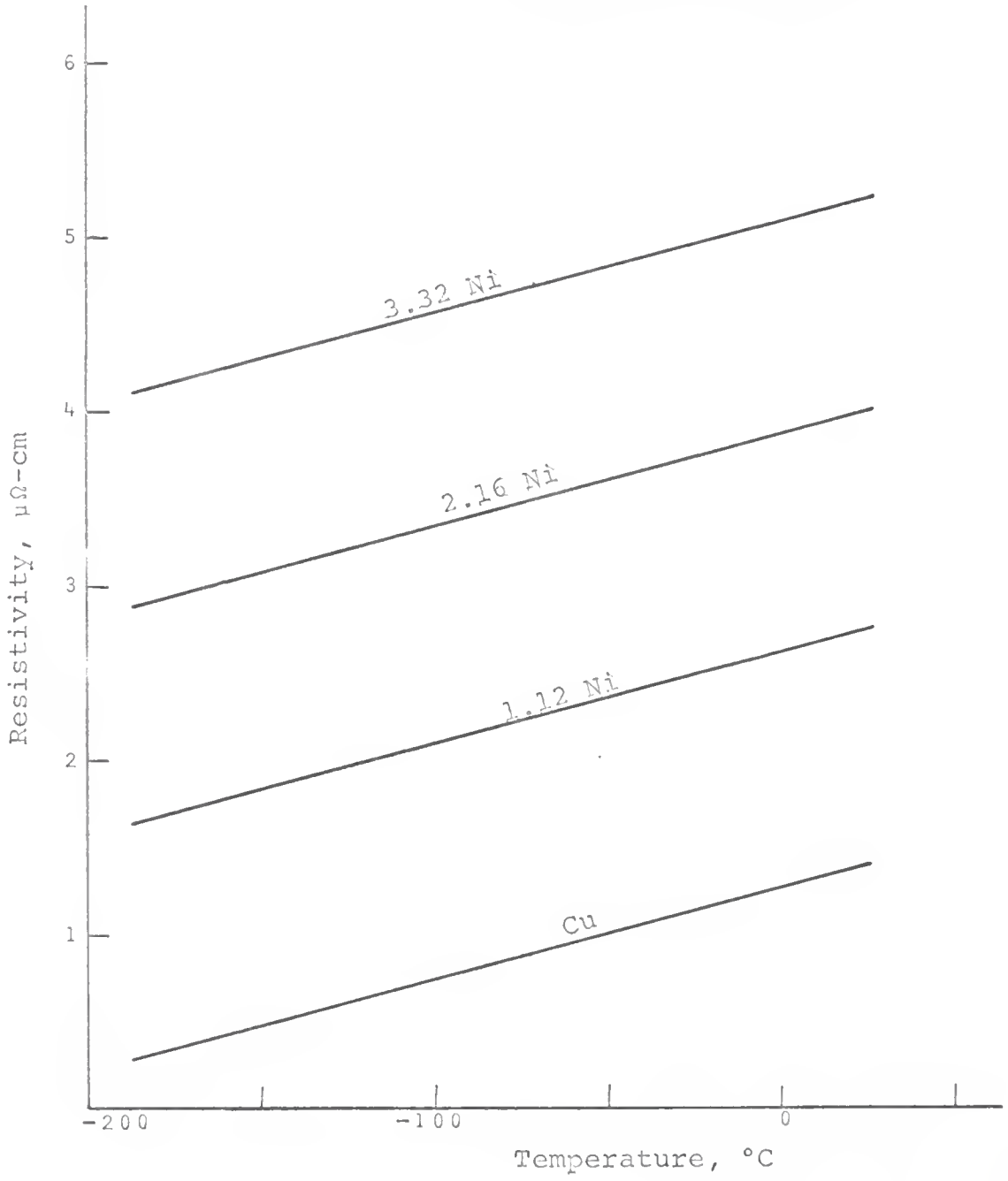

Fig. 2--Curves of resistivity vs. temperature for Cu-Ni alloys (after Dekker).

mean free path of electrons at the Fermi surface Λ_F:

$$\sigma = n_{eff} e^2 \Lambda_F / m V_F \qquad (4)$$

where V_F = velocity of electrons having the Fermi energy. At high temperatures, Λ_F is directly proportional to θ^2, the Debye temperature of the solid, hence:

$$\sigma = KM(\theta^2/T) \qquad (5)$$

where K is a constant containing the terms n_{eff} and V_F, and M is the mass of the atom. A plot of $\sigma/M\theta^2$ versus atomic number at room temperature is given in Figure 3 for various metals. This plot reflects the electronic properties of these metals since the ordinate is a measure of the conductivity per unit of vibrational displacement. Especially noteworthy are the differences between values for monovalent metals and the neighboring divalent metals such as K and Ca, Cu and Zn, Rb and Sr, Ag and Cd, Cs and Ba. The poorer conductivities of the divalent metals is due to the fact that they have fewer effective electrons; i.e., n_{eff} is smaller. Another interesting feature is the low conductivity of the transition elements. This can be seen by comparing the neighboring pairs Ni and Cu, Pd and Ag, Pt and Au. An explanation can be given in terms of the band structure of the transition elements as shown in

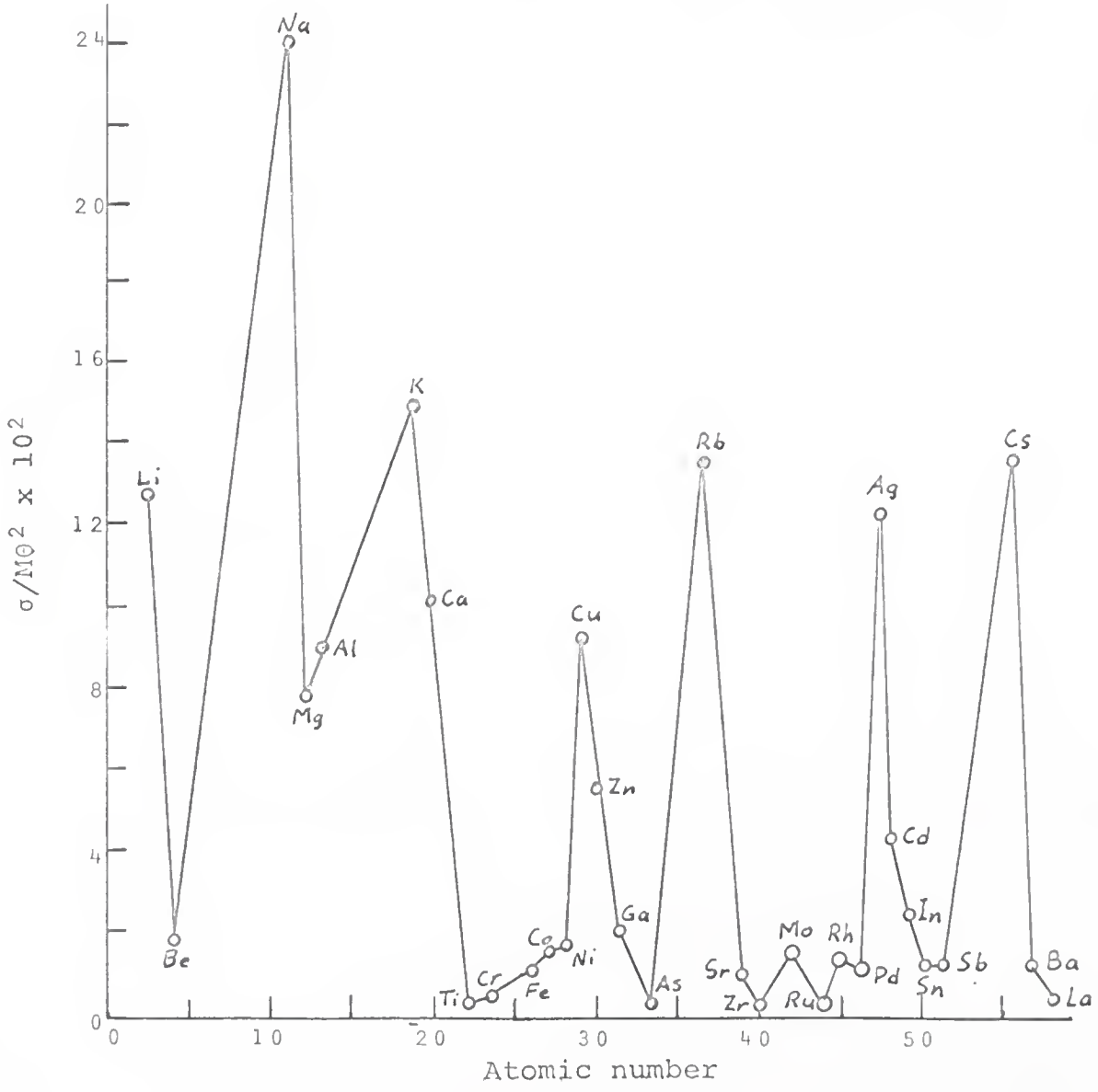

Fig. 3--Values of $\sigma/M\theta^2$ vs. atomic number obtained from conductivity measurements at 0°C (after Mott and Jones).

Figure 4. The transition elements have unfilled overlapping s and d energy bands as shown. The d band is extremely narrow compared to the s band and hence n_{eff} for the d band is very small. Therefore, most of the conduction electrons are contributed by the wide s band. However, transitions after scattering with phonons can now be made from the s band to states in the d band since the Fermi level passes through both bands. The high density of states near the Fermi level in the d band means that there is a relatively high rate of transition of electrons from the s band to lower states in the d band. In other words the narrow d band contributes a large number of possible transitions for the propagating electrons in the s band and hence increases the probability of interactions of the electrons with the scattering centers. In ordinary metals the d band is filled and such transitions are not possible.

The term ρ_0 for disordered alloys has been calculated by Nordheim [47] using the Bloch theory. The result is that ρ_0 is proportional to $x(1-x)$ where x is the concentration of solute or solvent. The normal effect of long-range ordering is to reduce ρ_0 simply because the structure becomes more periodic. This is illustrated by the work of Johansson and Linde [48] shown in Figure 5. Curve (a) shows the effect of alloying without ordering and the

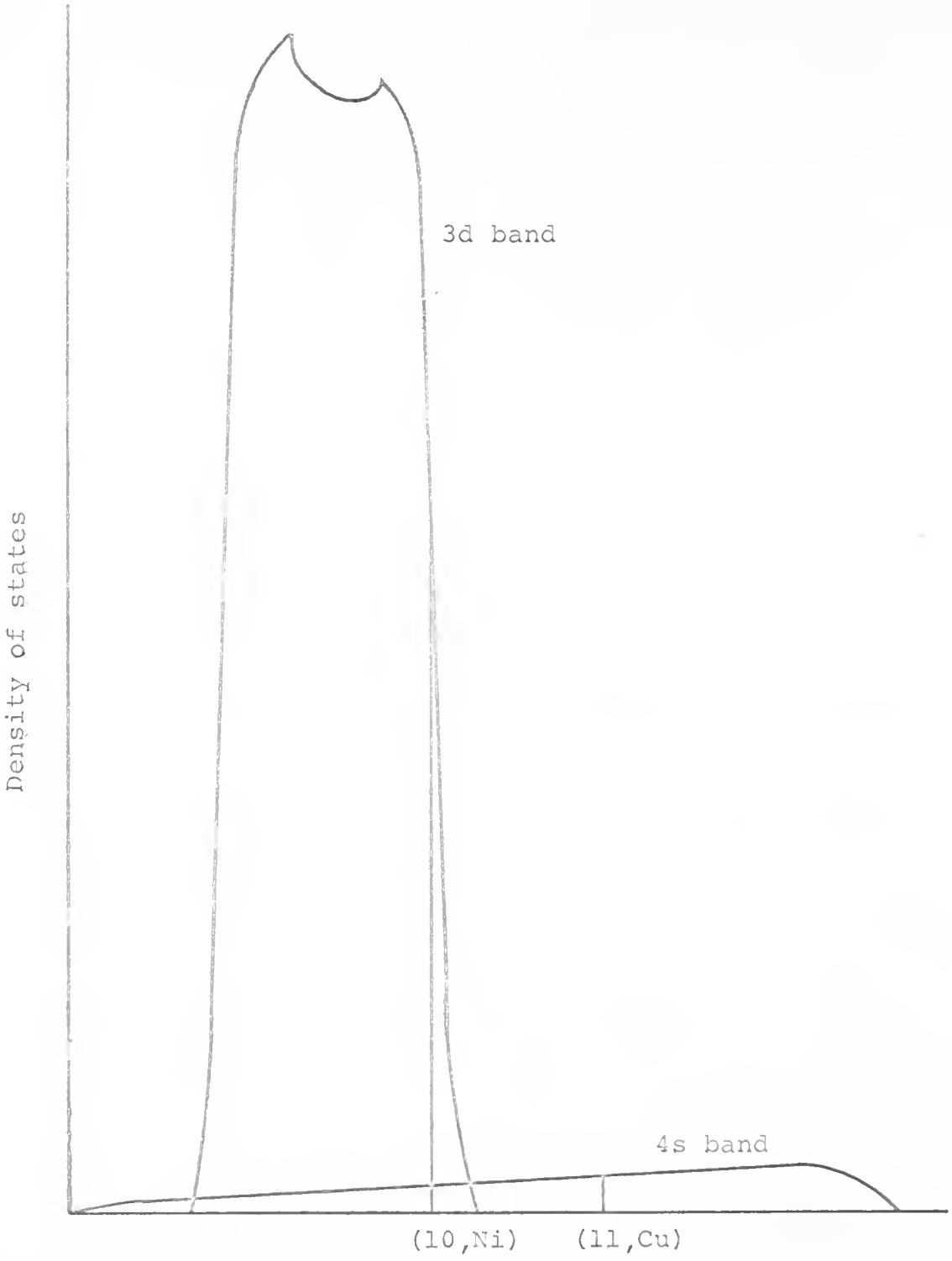

Fig. 4--Schematic view of wide s band overlapping narrow d band in transition metals (after Bardeen).

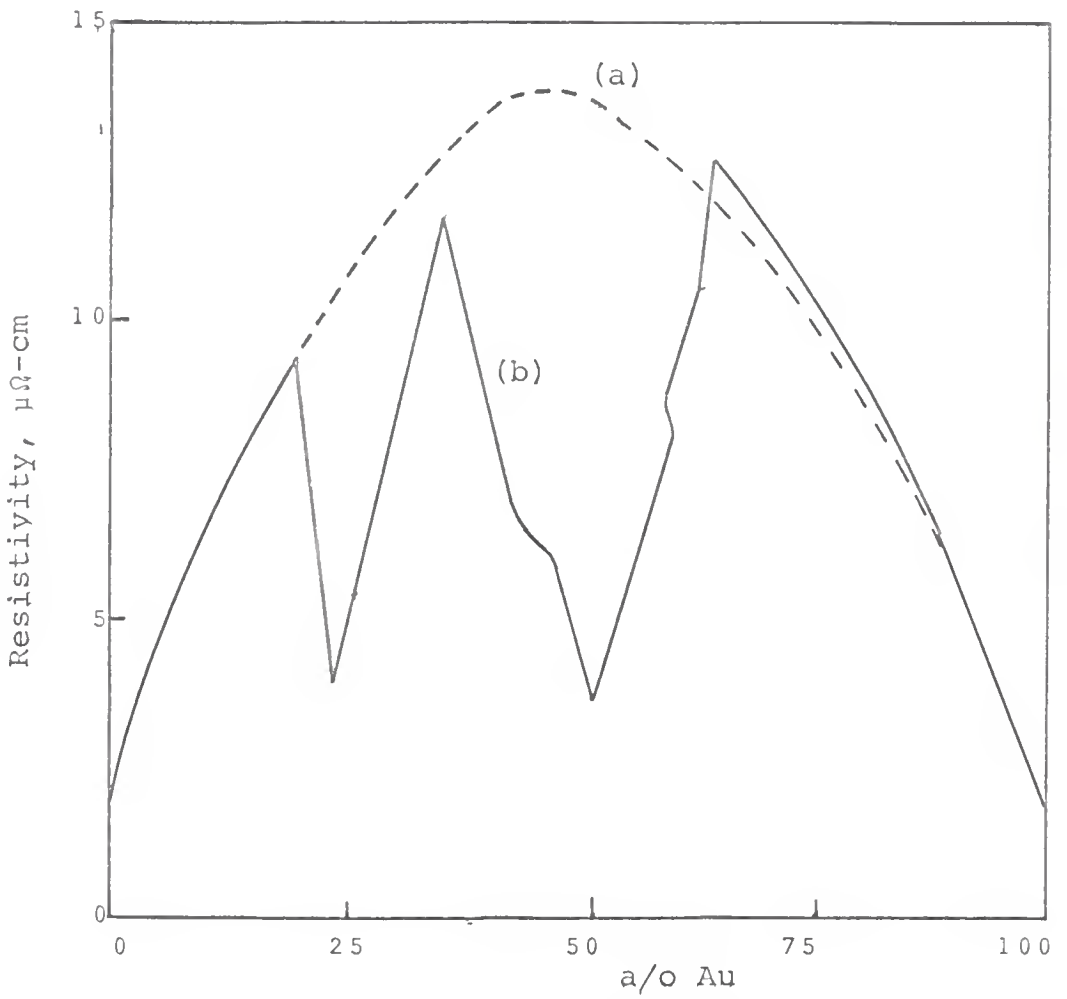

Fig. 5--Resistivity vs. composition for Cu-Au alloys in ordered and disordered states (after Bardeen).

result is in agreement with the prediction of Nordheim. Curve (b) shows the effects of long-range order at the compositions Cu_3Au and CuAu. As expected, there is a sharp decrease in ρ_0. An expression predicting the effect of long-range order on ρ_0 has been derived by Krivoglaz and Smirnov [41] using the many-electron quantum theory. Their approach was to determine the probability of the transition of a system of electrons from one state to another as a result of the perturbation produced by an imperfectly-ordered arrangement of atoms. One very important assumption is that the number of conduction electrons is independent of composition and of the order parameters; consequently, this treatment determines only the effect or rearrangement of scattering centers. The result is:

$$\rho_0 = \text{const.}[x(1-x) - 3/16\ \eta^2] \qquad (6)$$

where η is the long-range-order parameter. Since η increases as the degree of order increases (it varies between 0 and 1 for the stochiometric composition), this expression correctly predicts that long-range order decreases the resistivity. For a random solution, i.e., $\eta = 0$, this equation reduces to that of Nordheim.

Krivoglaz and Smirnov have also developed an expression for the effect of short-range order on ρ, again

based on the assumption that the number of conduction electrons remains unchanged. They found that when only the first coordination shell is considered, short-range order should decrease ρ_0 just as does long-range order. There are some important restrictions on this derivation however. The treatment of Krivoglaz and Smirnov assumes that there is "correlation" and nothing more is said concerning its nature. Correlation simply means that there is a statistically greater than random preference for unlike neighbors in the first shell. The various possible forms that this correlation might take could have significantly different effects. These will be discussed in a later section. The total effect of short-range order becomes more confusing when correlation is considered beyond the first coordination shell. This point is illustrated by the data of Damask [37] in which it is found that the residual resistivity of Cu_3Au above the critical temperature decreases up to 485°C and then begins to increase. It is not clear whether this complex behavior is due to electronic effects or whether it can be attributed purely to the complexity of "correlation" between neighboring scattering centers.

One further example should serve to point out the differences between electronic and lattice contributions

to the total resistivity. In some alloy systems involving a transition element with a non-transition element it is found that a plot of ρ_0 vs. %x is assymetric as shown in Figure 6. The resistivity does not follow the parabolic shape predicted by Nordheim with a maximum at 50 a/o solute. Instead the maximum is displaced toward the Pd-rich side. Mott offered the explanation that in alloys above 40 a/o Pd the d shell is not complete. In accordance with the previous discussion of the transition elements this leads to a resistivity that is higher than normal.

The effect of precipitates on resistivity is actually a combination of several factors, as might be inferred from the previous discussion. In the very early stages of the precipitation process there is the enhanced scattering of electrons at the Fermi surface because of the presence of small heterogenieties having the same size as the wavelength of the conducting electrons [7,25, 26]. A quantitative expression for the change is resistivity, $\Delta\rho$, caused by the presence of zones has been calculated by Matyas [50]. In addition, coherency strains between the precipitate and the matrix also tend to increase the resistivity. On the other hand, the process of precipitation removes solute atoms from the matrix and puts them into a more periodic arrangement in the precipitate.

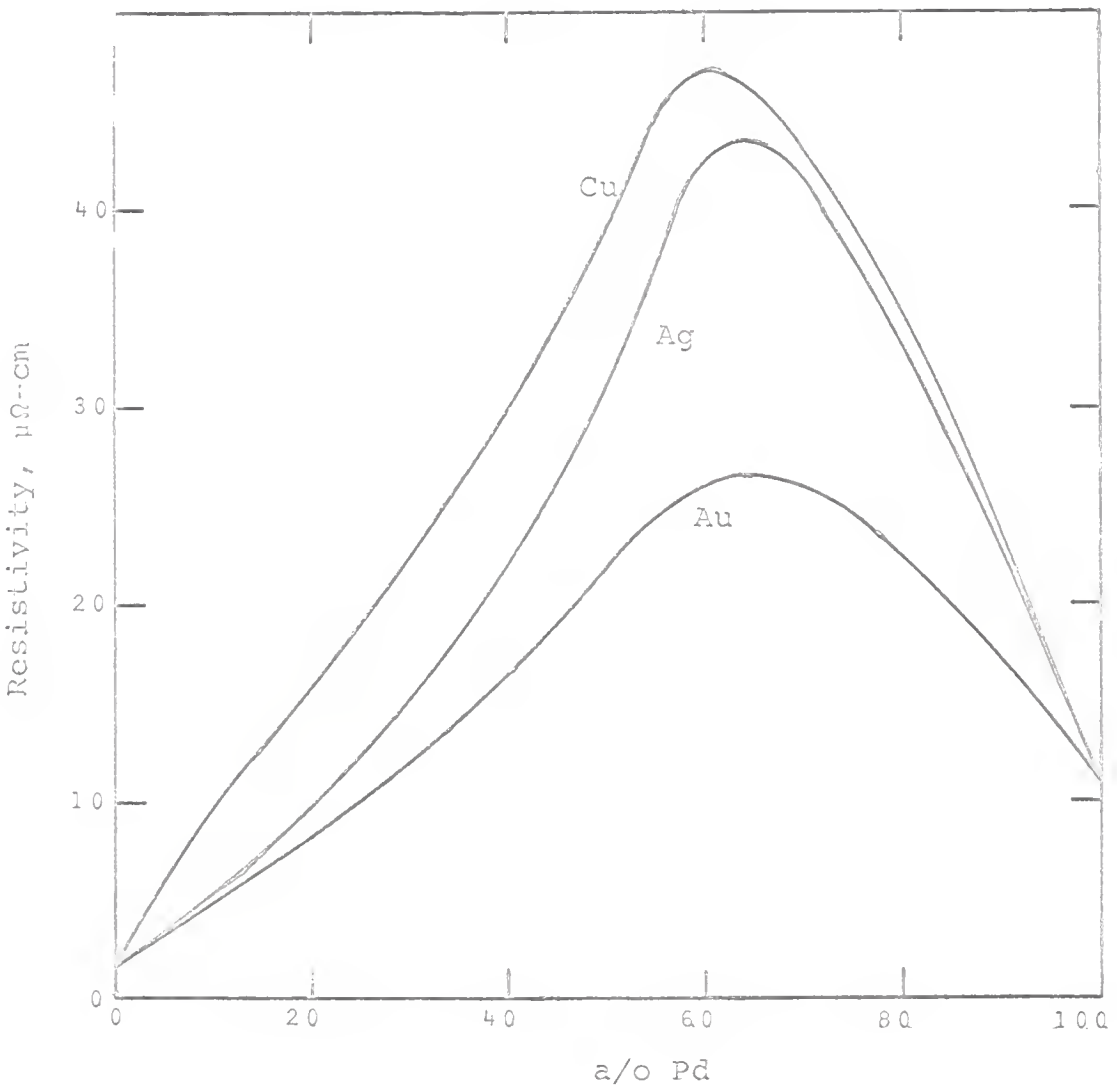

Fig. 6--Plots of resistivity vs. composition for alloys Pd with Cu, Ag, and Au (after Svensson [49]).

This effect tends to reduce the resistivity since the combined resistivity may be considered as a weighted average of that of the matrix and that of the precipitate. The effect of depleting the matrix usually predominates, and one sees an abrupt decrease of resistivity upon precipitation. This has been a classical tool in the determination of equilibrium phase diagrams.

A complete theory of resistivity of metals is, of course, much more detailed and complicated than the simple version presented here. The purpose of this section is simply to give a brief review of the important factors that will be considered in discussing the anomaly of resistivity in the K-state alloys. An attempt has been made to emphasize the difference between the electronic and the lattice contributions to the resistivity. Failure to do so has led to some widely held misconceptions such as the idea that ordering always decreases the resistivity.

1.2 *Diffuse Scattering of X-rays and Ordering*

It has long been known that the diffuse scattering of x-rays can give much information regarding the structure of the crystalline solids. This can be understood without going into the mathematics of the problem by simply recalling the fact that complete interference, which is necessary to give sharp spots at the reciprocal lattice

nodes and zero intensity between the nodes, depends upon perfect crystallinity within the specimen. Any departure from this perfect periodicity results in a broadening of the diffraction peaks and a general increase in the "background" or diffuse scattering between peaks. A good review article dealing with the experimental measurement and the interpretation of diffuse scattering is that of Warren and Averbach [51].

As pointed out in this article, the background intensity can be attributed to one of the following:

1. Scattering by air or other extraneous material in the primary beam
2. Scattering by other wavelengths if the beam is not monochromatic
3. Compton-modified scattering
4. Temperature-diffuse scattering
5. Diffuse scattering due to a structural disorder within the specimen.

By evacuating the air near the specimen and by proper arrangement of slits and baffles the scattering from source 1 can be eliminated. By using a monochromator the scattering from source 2 can be eliminated. The Compton modified scattering, which is the "inelastic" component of the scattering process, can be computed and subtracted once the sources 1 and 2 have been accounted for and the intensity put in absolute or electron units. The

temperature-diffuse scattering can be determined experimentally by making measurements at various temperatures and then extrapolating to absolute zero. Alternately, a calculation may be used in some instances to obtain a satisfactory correction for this factor [52]. More detailed treatments of the effects of temperature-diffuse scattering are given by Walker and Keating [53], and by Paskin [54]. The remaining intensity is truly characteristic of the structure of the specimen. One of the most useful applications of diffuse scattering is to determine local order* in alloys. For this purpose, the intensity must be converted to electron units by comparison with a standard substance whose intensity in electron units can be calculated. An electron unit is the intensity scattered by a single free electron in the given direction, $\vec{S}$, of reciprocal space.

One of the early pieces of work done on the interpretation of local order from diffuse x-ray scattering was by Cowley [56] in a study of Cu_3Au using single crystals. His formulation was later extended by Warren, Averbach,

---

*Following the convention of Flinn [55] the term local order will be used to mean any local departure from randomness in the solid solution. This includes clustering, which is a preference for like nearest neighbors, and short-range order (abbreviated SRO) which is a preference for unlike nearest neighbors.

and Roberts [57] to include the contribution to diffuse scattering due to difference in atomic sizes. This development is outlined here.

Consider an alloy containing A and B atoms arranged in some fashion. The total scattered intensity in electron units is given by:

$$I = \sum_{mm'} \sum f_m f_{m'} \exp[i\vec{k}\cdot(\vec{R}_m - \vec{R}_{m'})] \qquad (7)$$

where $\vec{k} = \frac{2\pi}{\lambda}(\vec{s} - \vec{s}_0)$, $\vec{s}$ and $\vec{s}_0$ being unit vectors in the direction of the scattered and incident beams. f_m and $f_{m'}$ are the atomic scattering factors of atoms located at the tips of vectors $\vec{R}_m$ and $\vec{R}_{m'}$ from some arbitrary origin within the crystal. The following substitutions can be made:

r_i = average distance between two lattice points where one is in the i^{th} coordination shell with respect to the other

$r_{AAi} = r_i(1 + \varepsilon_{AAi})$, where r_{AAi} = distance between two A atoms where one is in the i^{th} shell with respect to the other

$r_{BBi} = r_i(1 + \varepsilon_{BBi})$

$r_{ABi} = r_i(1 + \varepsilon_{ABi})$

$\alpha_i = (1 - P_i/m_A)$ where P_i = probability of finding an A atom at a distance r_i from B atom and m_A is the mole fraction of A atoms

$$\beta_i = \left(\frac{1}{\eta-1}\right)\left\{\left(\frac{m_B}{m_A} + \alpha_i\right)\eta\varepsilon_{BBi} - \left(\frac{m_A}{m_B} + \alpha_i\right)\varepsilon_{AAi}\right\}$$

where $\eta = f_A/f_B = \dfrac{\text{atomic scattering factor of A}}{\text{atomic scattering factor of B}}$.

The intensity can then be written as:

$$I = Nm_Am_B(f_B - f_A)^2\left\{\sum_{ij}\sum\alpha_i\exp(i\vec{k}\cdot\vec{r}_{ij}) + \sum_{ij}\sum\beta_i i\vec{k}\cdot\vec{r}_{ij}\exp(i\vec{k}\cdot\vec{r}_{ij}) + \sum_{mm'}\sum(m_Af_A + m_Bf_B)^2\exp[i\vec{k}\cdot(\vec{R}_m - \vec{R}_{m'})]\right\} \quad (8)$$

where N is the total number of atoms in the primary beam. The last term in the bracket gives that part of the spectrum resulting in sharp diffraction peaks. When this term is dropped, the remaining diffuse intensity from a single crystal can be written as:

$$I = Nm_Am_B(f_B - f_A)^2\left\{\sum_{lmn}\sum\sum\alpha_{lmn}\cos 2\pi(lh_1 + mh_2 + nh_3) - \sum_{lmn}\sum\sum\beta_{lmn}2\pi(lh_1 + mh_2 + nh_3)\sin 2\pi(lh_1 + mh_2 + nh_3)\right\} \quad (9)$$

where h_1, h_2, and h_3 are the fractional reciprocal lattice coordinates. The corresponding equation for polycrystalline specimens is,

$$I = Nm_A m_B (f_B - f_A)^2 \left\{ \Sigma_i c_i \alpha_i (\sin Sr_i)/Sr_i - \Sigma_i c_i \beta_i [(\sin Sr_i)/Sr_i - \cos Sr_i] \right\} \qquad (10)$$

where $S = 4\pi \sin\theta/\lambda$ and c_i is the coordination number of the i^{th} shell.

The actual experimental data consist of a set of intensities (in counts per second) as a function of S. These data are converted to electron units per atom by comparison with a suitable standard as described above. The Compton-modified and temperature-diffuse scattering components, also in electron units (eu) per atom, are determined and subtracted. The remaining intensity-distribution function is that given by equation (9) or (10). It represents the diffuse intensity of the specimen on a per atom basis attributable only to the particular way in which the A and B atoms are arranged in the solid solution. To solve the problem of what that arrangement is, one must first invert equation (9) or (10), depending upon whether the single crystal or powder method is used, and then determine the parameters α and β.

The further analysis involves assuming various models to determine which atomic arrangement best fits the derived parameters. For cases in which the size-effect terms are negligible the α's can be obtained directly from

single-crystal data by Fourier inversion. The powder data can be put into a form which also makes a Fourier inversion possible. The problem becomes more involved when the β's cannot be neglected. A suitable technique has been developed by Borie and Sparks [58] for separating and determining the α and β coefficients from single-crystal data. For the powder method a technique has been developed by Flinn, Averbach and Rudman [59] for separation of the α and β terms; however, this method is subject to a certain amount of false detail and a complete separation is difficult to obtain. The powder method also suffers from the fact that there is inherently less detail in these data. The intensity at each θ setting is an integrated measurement over the surface of a sphere in reciprocal space with a radius of $\sin \theta/\lambda$. It is the general concensus of opinion among experts in the field that data obtained by the powder method should be used only for a qualitative picture of the local order; any quantitative interpretations should be based upon single-crystal data.

Before discussing some of the limitations of the Warren-Cowley development, a good insight into the effects of local order on the diffuse intensity can be gained by looking at the predicted curves of equation (10) for powder samples. These effects are summarized in Figure 7. For a

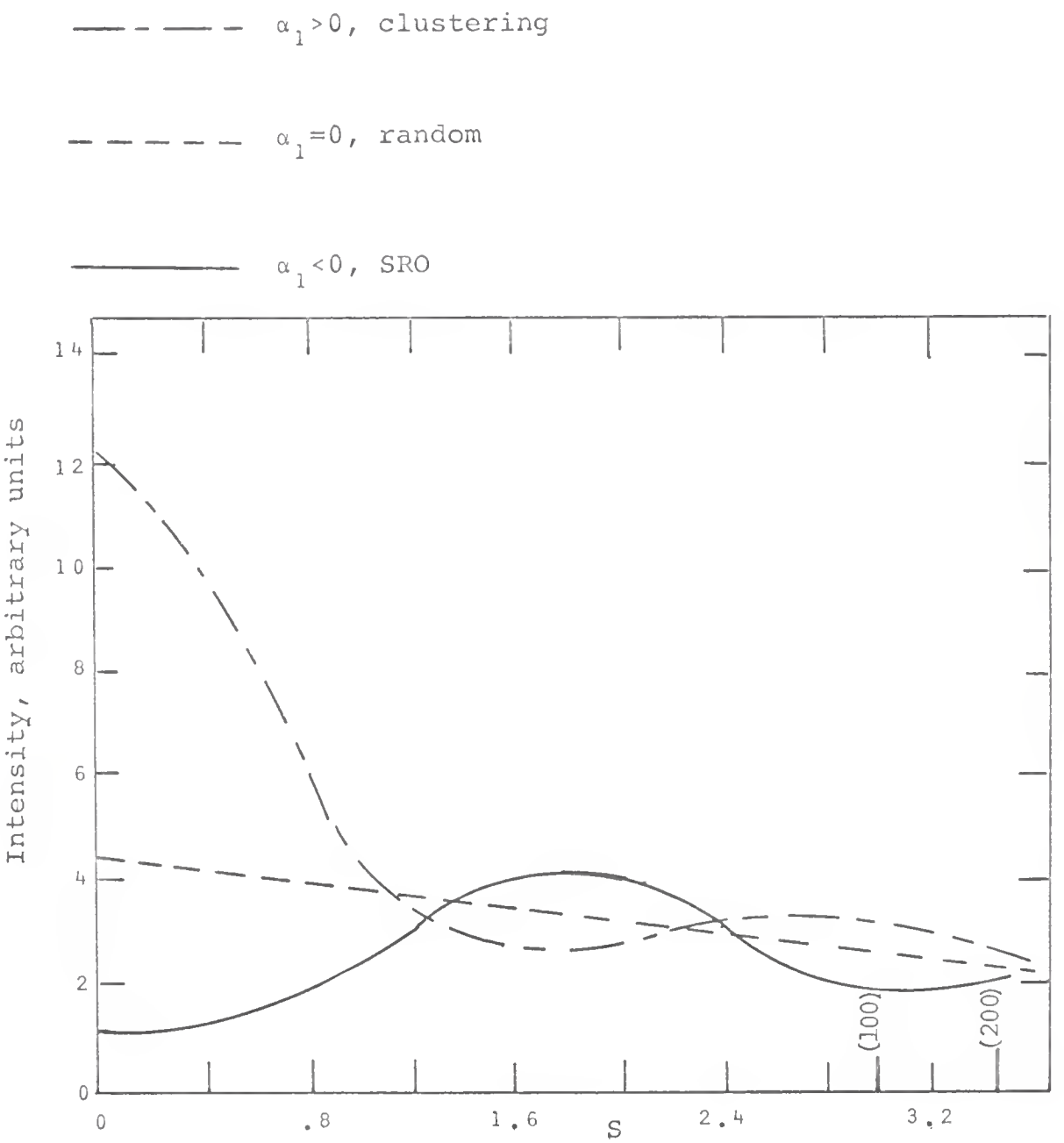

Fig. 7--Typical x-ray diffuse powder patterns corresponding to clustering, randomness, and SRO in metallic solid solutions (after Warren *et al.*).

specimen exhibiting a completely random distribution of the solute atoms, the α_i are equal to zero and the intensity decreases monotomically (Laue monotonic scattering). For alloys in which $\alpha_1 > 0$ we find maxima near the origin and at other reciprocal-lattice nodes. This behavior is to be expected when one considers the fact that $\alpha_1 > 0$ implies a preference for like neighbors, i.e., clustering, which in turn would be expected to produce the well known small-angle-scattering effect. Good examples of systems in which such a diffuse-scattering distribution has been obtained are Al-Zn [51], and Al-Ag [60]. In these cases analysis of the data does show that $\alpha_1 > 0$ as expected. For $\alpha_1 > 0$ the curve typically shows a maximum at $Sr_1 \simeq 4.5$. This represents a condition in which there is a greater-than-random occurrence of unlike nearest neighbors. The exact shape of the curve will depend on the higher order α_i parameters as well as on the values of the β's, but in general a specimen exhibiting a preference for unlike nearest neighbors will exhibit a curve, with a maximum at $Sr_1 \simeq 4.5$.

Several points should be noted in connection with the Warren-Cowley development. First, the equations are not restricted to the description of local order but also reflect the effects of long-range order (abbreviated LRO). As pointed out by Spruiell [31], if LRO is present the α's

will have definite values which depend upon the degree of this type of order. The convergence of the series will depend upon the size of the antiphase domains, and the series itself will describe the sharp superstructure reflections characteristic of LRO. One may visualize the diffuse scattering of SRO as representing the extreme broadening of the superlattice peaks. As the degree of order increases, these peaks increase in sharpness so that there is a general transition from the diffuse maximum to the sharp superlattice lines. This view aids in visualizing the distribution of diffuse intensity from non-random alloys, although, as Warren points out, one cannot in general regard SRO as simply small domains of LRO. In the derivation of equations (9) and (10) the preference for like or unlike neighbors is regarded only in a statistical sense. This will be discussed in greater detail later.

Another important feature of the Warren-Cowley development is that the distance between a given pair of atoms is assumed to be only a function of the species involved and not a function of the distribution of atoms separating the pair in question. One would expect, however, that not all tenth-nearest A-B pairs, for example, would have the same separation. Huang [61] used a different

approach in analyzing the size-effect contribution. His model assumes that the lattice is an elastic medium with centers of distortion at the sites of the solute atoms. His theory predicts that because of the size effect, there will be a reduction of the integrated intensity of the primary reflections and a concentration of diffuse scattering in the vicinity of these peaks. Borie has shown [62] that both the effects predicted by Warren and those predicted by Huang ought to be observed. The predictions of his more general approach can be summarized as follows:

1. The diffuse scattering caused by local order and by size effect are both present, as predicted by Warren.

2. The diffuse scattering predicted by Huang is also present. It is concentrated near the Bragg maxima and along a line from each maximum through the origin of reciprocal space. Temperature-diffuse scattering also increases in the vicinity of the Bragg peaks as shown by Warren [52].

3. The integrated intensities of the Bragg peaks are reduced as a result of the lattice distortions produced by the size effect. This effect is in complete analogy with the reduction in intensity caused by the dynamic displacement of atoms as a result of thermal vibrations. The size-effect displacements are, of course, static, but the effect is similar.

4. The size-effect distortions cause a broadening in the diffuse short-range order peaks and a decrease in the apparent α terms. Once again the analogy with thermal vibrations is complete. The treatment by Walker and Keating [53] shows that the effect of thermal vibration is also to broaden the short-range order peaks and to reduce the α's.

The interpretation of the diffuse-scattering intensity in terms of the best model for the type of local order present has to a large extent been speculative. The reason is that no unique solution can be obtained. It is well known in x-ray structure determination that the exact atomic arrangement within a crystal cannot be determined from the intensity distribution alone. The situation is no different when considering the diffuse intensity. The usual approach is to assume a reasonable model based upon some knowledge of the phase diagram, and then to modify this model in a trial and error fashion until the best fit for the observed α's is obtained. There may, however, be many models which will fit the same set of α coefficients.

It is significant that almost every instance of SRO can be explained by assuming that it consists of small and imperfect domains of some form of LRO existing in the given alloy system. This coincidence is surprising since Warren has pointed out that there is nothing in his development that calls for such a model. In his treatment SRO is considered only as a statistical departure from the random probability of unlike neighbors in the first, second, third, and higher coordination shells and no domain structure is assumed.

A good example of SRO that can be interpreted as small domains of LRO is found in the alloy CuAu [63].

CuAu orders by forming alternate layers of copper and gold atoms on {100} planes with a slight accompanying tetragonal shrinkage. This shrinkage should result in a slight shift of the superlattice reflections such as (001) and (003) outward from the origin. In specimens quenched from above the critical temperature, T_c, the diffuse SRO peaks occur approximately as though they were produced by a broadening of the (100) and (300) reflections, and they are actually shifted outward as expected. The primary reflections, however, are not shifted since the overall symmetry of the lattice is cubic as a result of the averaging of small slightly tetragonal domains of ordered CuAu. The domains are so small that diffuse maxima are produced rather than sharp superlattice lines. The diffuse maxima are shifted outward in accordance with the slight tetragonal shrinkage of the lattice. Sato *et al.* [64] used electron diffraction to observe very diffuse superlattice spots in CuAu as much as 50°C above T_c.

CuPt is another example of an alloy in which the SRO appears to be best explained by assuming it to be composed of small domains of LRO. Analysis of powder data by Walker [65] on specimens held above T_c showed the unusual result that α_1 and α_3 are zero whereas α_2 is negative and α_4 is positive. This result can be understood by

examining the structure of fully-ordered CuPt, which consists of alternate {111} layers of Cu and Pt atoms. For such a structure there are six Cu and six Pt atoms in the first coordination shell of any given atom, hence α_1 is zero. The same is true for all the odd-numbered shells. For α_2 all the neighbors are unlike atoms, and for α_4 all the neighbors are like atoms, hence α_2 is negative and α_4 is positive. In view of the similarity of the α coefficients calculated from the data obtained, T_c, it is reasonable to assume that SRO in CuPt consists of small domains of CuPt-type LRO.

A recent article by Gehlen and Cohen [66] concerning the determination of SRO models by a Monte Carlo computer technique offers further evidence for the small-domain concept, at least for the case of Cu_3Au. The technique is one of obtaining the best fit to the first three α coefficients by a trial-and-error computer calculation of the rearrangement of a three-dimensional array of atoms. For Cu_3Au above T_c, the calculated structure consists of small ordered domains embedded in a random matrix. It was found that the same final configuration was reached regardless of whether the starting matrix was completely ordered or completely disordered. This result gave the authors confidence in the method although they could not prove analytically that this method is unique.

It is common to expect clustering ($\alpha_1 > 0$) for those solid solutions that ultimately decompose at a lower temperature (or at a slightly enriched composition) into two terminal phases and to expect SRO ($\alpha_1 < 0$) for those solid solutions that transform into an ordered phase. Although this idea is to some extent intuitive, it is supported by the observed behavior in a number of systems. For example the CuAu, Cu_3Au, and CuPt systems mentioned above exhibit SRO at an elevated temperature and LRO at a lower temperature. Examples of clustering in systems which later decompose into G.P. zones have been previously cited [51,60]. In the Au-Ni system, on the other hand, it is doubtful that this type of behavior occurs. The miscibility gap in this system indicates that one should find clustering at temperatures above those at which decomposition takes place. According to the quasi-chemical approach [67] a positive heat of mixing, characteristic of Au-Ni, should be observed for a solution exhibiting clustering. However the surprising result of Flinn *et al.* [68] from analysis of powder data is that $\alpha_1 < 0$, indicating a preference for unlike neighbors. This system has been re-studied by Münster and Sagel [69] who find a positive α_1 in agreement with the quasi-chemical theory. In this case the disagreement might be resolved if precise single-crystal data were available.

It appears that SRO (and/or clustering) is the rule rather than the exception in solid solutions. Some insight into the driving force for these departures from randomness are provided by the theories of Friedel [70], Flinn [55], and Rudman [71]. The theories of Friedel and Flinn are based on electronic structure whereas in the more intuitively appealing theory of Rudman, elastic strain energy is visualized as the driving force that produces a local rearrangement of atoms. So far all the alloys mentioned have been face-centered cubic. Evidence has also been found for short-range order in body-centered cubic and close-packed hexagonal systems. What may be even more surprising at first glance, is the fact that SRO has even been found in systems which exhibit complete solid solubility, e.g., Au-Pd [72].

In summary, it is clear that the usefulness of diffuse scattering of x-rays for studying local order in solid solutions has been adequately demonstrated. Although data from polycrystalline specimens may be used for a qualitative picture of the nature of the local order, single-crystal data are definitely desirable for quantitative results. It is a popular concept that SRO is simply small domains of LRO. While there is evidence that this is a good model in some systems, there is nothing in

the scattering theory or in the thermodynamic theory of solutions that justifies this model. Until convincing evidence for such a model can be presented for the particular system in question, it is best to consider SRO as simply a greater-than-random preference for unlike nearest neighbors. Since the particular configuration assumed by the atoms represents the state of minimum energy, it is reasonable to assume that it should reflect the decompositional tendencies of the system at lower temperatures, but it has not yet been proven that this is universally true. This point can be further emphasized by using the Au-Pd system as an example. This system is completely isomorphous according to current data, and yet it shows a definite SRO. The fact that a unique solution to the diffuse-intensity data cannot be obtained means that other experimental data are needed to support the presumed model. Field-ion microscopy offers some hope for a means of direct observation since there is evidence that it can be used to detect a small region of a domain structure.

1.3 *Explanations of K-state Phenomena*

Several papers have dealt with possible explanations of the K-state in various systems. Now that a brief discussion has been given on the theory of resistivity, the peculiarities of the transition elements, and the concepts

of local order, this background can be employed in an analysis of some of these theories.

In the previous discussion of resistivity of metals emphasis was placed on the distinction between purely electronic effects and those effects caused by a change in scattering because of a redistribution of ion cores and defects within the lattice. It has been suggested that subtle changes in the electronic structure of a solid solution can accompany SRO. This view has been supported by Köster and Rocholl [16] in their work on Ni-Cr. They concluded that the K-state is related to a change in the density and mobility of electrons and holes in the upper energy bands as a result of SRO. This conclusion was based on measurements of resistivity, Hall constant, thermoelectric power and magnetic susceptibility. No particular model for the SRO was assumed. The assumption was made that SRO has the same effect as adding more solute atoms because in both cases the number of unlike nearest neighbors increases. Even though a certain amount of correlation will exist between scattering centers as a result of SRO and may decrease the resistivity according to Krivoglaz as discussed before, it was assumed that the change in the electronic structure of the alloy upon ordering has the larger effect.

The significance of the particular model assumed for SRO is seen when one considers the theory of Gibson [73]. In this treatment it is assumed that SRO consists of small domains of LRO. The relative position of the Fermi surface with respect to the first Brillouin-zone boundary of the random lattice and the superlattice determines whether SRO should produce an increase or decrease in the resistivity. This idea has been discussed by Muto [74], Slater [75], and Nicholas [76] in terms of the "superzone" concept. Upon forming a superstructure from a random alloy, the symmetry of the lattice is changed; e.g., in the transformation from β to β′ brass the Bravais lattice goes from body-centered cubic to simple cubic merely as a result of ordering. With changing symmetry the Brillouin-zone construction in K-space changes and in turn produces a change in the effective number of conduction electrons. In particular, if the Fermi surface lies well inside the Brillouin-zone boundary of the disordered alloy and close to the Brillouin-zone boundary of the ordered alloy, then SRO will decrease the number of conduction electrons and thereby increase the resistivity. This of course, corresponds to a K-effect. It is important to bear in mind that for this theory the idea that SRO consists of small domain is important, but the presence of a transition element is not. In fact, in

certain Ag-Pd alloys which show a K-effect (9.5 a/o and 41.3 a/o Pd) Chen and Nicholson [6] found that neither cold work nor heating changes the magnetic susceptibility. They concluded therefore, that although the transition element Pd is present, the 4d shell is completely filled.

Logie *et al.* [77] attributed the K-state in the Au-Pd system to local lattice distortions rather than to SRO. It will be recalled that the high resistivity of the transition elements is caused by the high probability of transitions of the conduction electrons from the s to the d band upon scattering. According to Logie's theory the s-d scattering is enhanced by local lattice distortions around dislocations. The argument is supported by a rough estimate of the expected change in resistivity based on the approximate density-of-states curve for the 4d shell of Pd. The authors were able to predict from a simple model that the d shell of Pd becomes filled at about 55 a/o Au and that the maximum decrease in resistivity due to deformation should occur at about 50 a/o Au. The maximum decrease in resistivity does in fact occur at about 50 a/o Au. At least two arguments can be used against this theory. First of all, a decrease in resistivity with deformation is still found in alloys as rich as 80 a/o Au, well beyond the concentration at which the

d shell is completely filled. Furthermore, the authors have assumed that since no superlattices have been found in Au-Pd, SRO or clustering does not occur. As we have already noted, Copeland and Nicholson [72] have found SRO in Au - 40 a/o Pd by x-ray diffuse scattering. Further support, however, for the idea that s-d scattering is the prime cause of the K-state is the fact that the K-state has even been reported in pure Cr [78]. On the other hand, the research on Cu-Au [35,36,37], Cu-Al [38], and Cu-Zn [38] indicates that such effects can be produced in non-transition element alloys.

The idea that local lattice distortions, rather than SRO is responsible for the K-state is supported also by Jaumot and Sawatzky [79] and by Aarts and Houston-MacMillan [80]. The reasons are not quite the same as those of Logie *et al.*, however, Jaumot and Sawatzky in their study of Cu-Pd assumed that the number of conduction electrons is increased by cold work. This is presumably accomplished by a shift in the centers of gravity of the s, p, and d bands as a result of local dilations of the lattice. A change in s-d scattering was deemed unlikely largely on the basis that the alloys are diamagnetic, indicating a filled d shell. A similar conclusion was reached by Chen and Nicholson [6] regarding the filled d

shell in Ag-Pd. They agreed that a change in s-d scattering is not the primary consideration. On the other hand, they felt that SRO is a more likely explanation than local distortions. The explanation of Aarts and Houston-MacMillan for Ag-Pd is similar to that of Jaumot and Sawatzky. A more recent paper on Ag-Pd by Westerlund and Nicholson [81] lends support to the suggestion that SRO rather than local lattice distortions causes the K-state. This conclusion is based on the fact that there is a relatively large decrease in the Hall constant upon cold work. The authors pointed out that this decrease in the Hall constant reflects a large increase in the number of effective electrons. It is difficult to see how this factor alone favors the idea of SRO over that of local lattice distortions.

A treatment of the effect of SRO and of clustering on resistivity has been given by Dehlinger [82]. He considered only the effect of redistribution of solute atoms as scattering centers and not the effect of any changes in electronic structure. The surprising conclusion is that SRO can cause an increase in resistivity over the value characteristic of the random distribution. This conclusion was reached upon considering Damask's data [37] along with the calculations of Gibson [73]. Using known

parameters of SRO for Cu_3Au at 405 and 460°C Gibson's calculations showed that ρ *decreases* with increasing temperature in this range in agreement with the data of Damask. Gibson's calculations also predicted that the presence of SRO would increase the resistivity above the value for a random solid solution. The equation for the residual resistivity due to SRO is:

$$\rho = K\frac{C_A C_B}{N}\iint \left| V_A - V_B \right|^2 \sum\sum\sum_{lmn} \alpha_{lmn} e^{(\uparrow-\uparrow')V_{lmn}} d\uparrow d\uparrow' \quad (\underline{11})$$

where $\uparrow$ and $\uparrow'$ represent the wave vectors of an electron before and after a transition is made because of the perturbations of the potential from different atoms A and B. The integration is taken over the Fermi surface, which is assumed to be spherical and independent of the degree of SRO. In this formulation SRO is considered only statistically regardless of whether or not it is truly a domain structure. As pointed out by Krivoglaz, however, the value obtained by a calculation of this type depends on the range over which the α_{lmn} parameters are considered. Until definite models for SRO can be found this type of calculation is at present reliable for quantitatively predicting changes in ρ. It does, however, show that SRO can cause an increase in ρ simply on the basis of the redistribution of scattering centers, contrary to the

generally accepted notion that SRO will always decrease ρ because it represents a greater degree of periodicity. Physically it is difficult to see why this should be true except in the case of very small domains. It has been argued by Bennet [83] that antiphase domains boundaries will scatter conduction electrons. It is easy therefore to see that this type of SRO could lead to a maximum in ρ corresponding to a certain domain size. This conclusion has in fact been implied by Davies [5] in his explanation of the K-state. In general, however, it would seem that the fundamental changes in electronic structure which accompany SRO will have a larger effect than scattering by domain boundaries.

Müller and Muth [10] have offered further support for the theory that subtle changes in electronic structures are responsible for the K-state. After summarizing the properties which generally accompany the K-state, they concluded that it is accompanied by a lowering of the Fermi level with a transition of s electrons to d states. They also proposed that for Ni-Cr and Ni-Cr-Fe alloys an increase in covalent bonding of the d electrons is responsible for the lattice contraction, the increase in hardness and elastic modulus and the decrease in magnetic susceptibility. They assumed that SRO is responsible for these effects.

As far as the author is aware, only two other explanations for the K-state have been offered. One is the possibility of the effect of preferred orientation. It would be extremely difficult to rule this out in all cases. However, it is possible to produce a K-effect in some alloys by simply quenching and annealing. Under these conditions very little change in preferred orientation would be expected. The final explanation to be considered, due to Taylor and Hinton [12], is that the creation of an ordered structure will create new reflecting planes for the electrons at the Fermi level. They calculated that for the Ni_3Cr superlattice the d spacing of the {100} planes is roughly the right magnitude for the Bragg reflection of the valence electrons, assuming that each Ni atom contributes 0.6 electrons and each Cr atom contributes 1.0 electrons. Hence, if one assumes that SRO consists of small domains of Ni_3Cr, this idea can be used to explain the increased resistivity. This explanation is open to the following criticism. If the lattice were perfectly ordered, the resistivity at absolute zero would be zero. The reflecting superlattice planes would still be present but the resistivity would be zero. In other words it appears that the net effect of Bragg reflection of electrons should be zero.

In summary it appears that most of the current suggestions as to the cause of the K-state phenomenon favor the idea that certain fundamental changes in the electronic structure of these alloys occur. Some of the theories which have been previously cited attirubte these changes in electronic structure to SRO, whereas others attribute the changes to local lattice distortions. Since most of the alloys which are capable of forming the K-state contain a transition element, significance has frequently been attached to the presence of a vacant d shell. There is evidence, however, of the K-state in alloys that presumably have a filled d shell. It has also been suggested for some alloys that heterogenieties in the solid solution such as clustering, G.P. zones, or concentration of solute atoms at dislocations are responsible for the anomalous properties of the K-state.

1.4 *Field-Ion Microscopy*

The field-ion microscope was used in this study in an effort to determine the nature of the SRO that occurs in the Ni-Mo system since, as will be shown later, this has a direct bearing on the explanation of the K-state. Field-ion microscopy is the only technique available at present by which individual atoms can be resolved and photographed. Although the problem of interpreting field-

ion micrographs is in its very early stages, there is much promise in this method for studying local order.

The field-ion microscope was first introduced to the public in 1951 [84] by Müller. A general review of the principles and techniques of field-ion microscopy are given in a later review article [85], also by Müller. Individual atoms are imaged by the technique shown in Figure 8. The specimen is polished to a small-radius tip of a few hundred atom diameters and is placed at a high positive potential (3-30 KV) with respect to a fluorescent screen below. The high potential and the small radius of the tip cause an extremely high field at the specimen surface. This intense field, which may be as high as 5×10^8 volts per cm, polarizes certain atoms at the specimen surface, by causing the electron cloud to be pulled back, thus exposing the positive ion cores. When a precooled imaging gas such as He or Ne is allowed to flow over the tip at a very low pressure, the gas atoms are at first polarized and attracted to the surface of the tip by the high positive potential. Once at the surface and in the vicinity of the polarized metal atoms, the gas atoms are ionized by electronic tunneling and are accelarated radially to the screen. On hitting the screen, the gas atoms produce images of polarized atoms which caused the ionization.

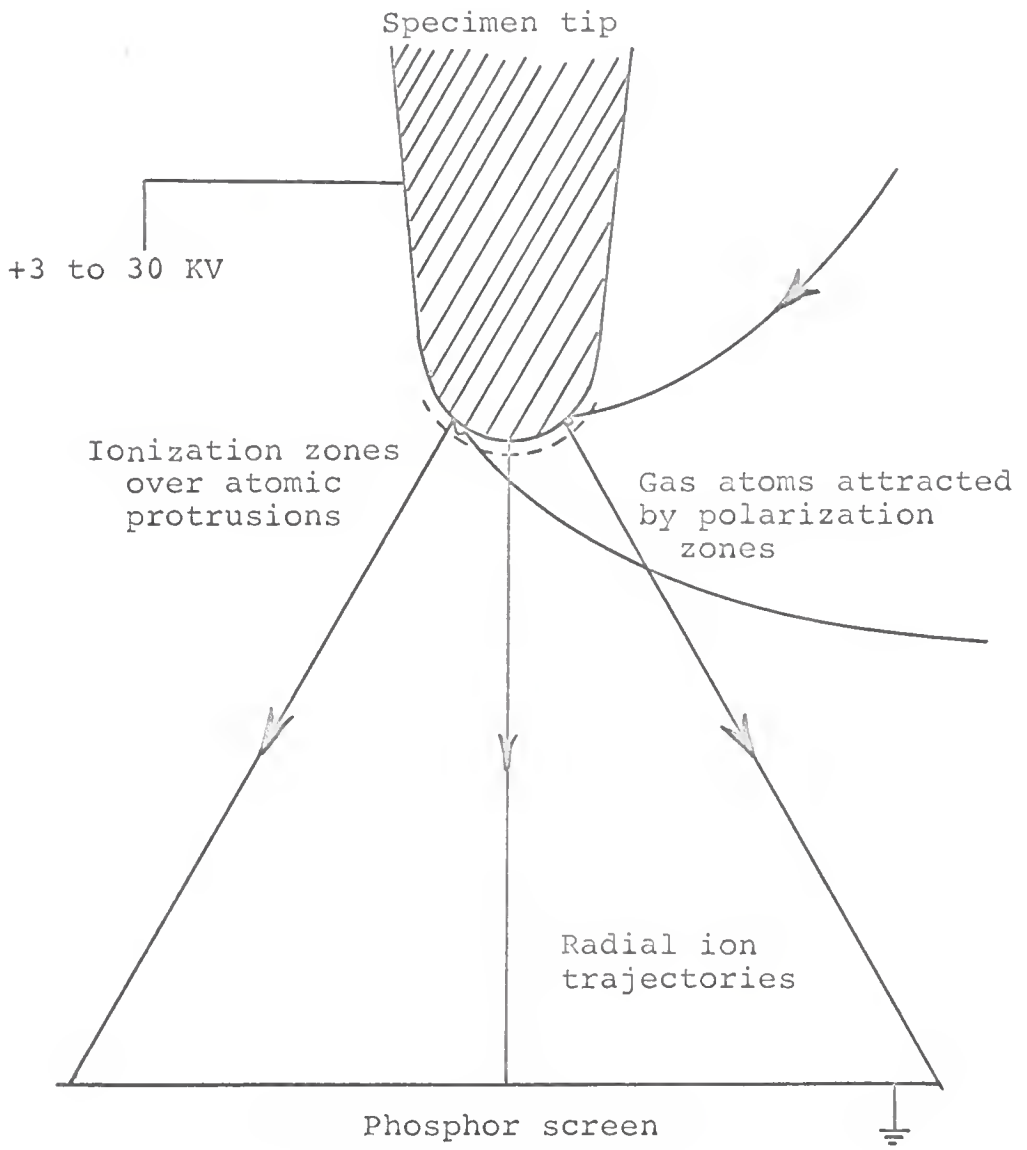

Fig. 8--Schematic illustration of the field-ion microscope (after Brandon).

The resolution of the field-ion microscope is such that individual atoms are distinguishable as points of light. The resolution improves as the tip is cooled to lower temperatures with a corresponding decrease in the magnitude of the atomic vibrations. Only certain atoms produce an image, however. This is because on an atomic scale the curvature of the tip is only approximate; the surface is actually composed of layers or planes of atoms. The criterion for imaging has not yet been completely established, but it is clear that the ability of a given atom to be polarized by the imposed field is a factor, and this in turn is related to how tightly it is bound at the surface. Therefore those atoms which occupy "corner" positions in a layer are the ones which image preferentially. The planes appear as rings of atoms and the symmetry of the crystalline lattice is quite apparent. An example of a field-ion micrograph from tungsten is given in Figure 9.

The application of field-ion microscopy to the study of LRO has been demonstrated by Ralph and Brandon [86, 87] in a Co - 50 a/o Pt specimen. It was found that ordered alloys produced sharp images in which the crystallographic poles were well defined, whereas disordered alloys formed images which were very "spotty" and appeared almost as a random array of points rather than well defined rings.

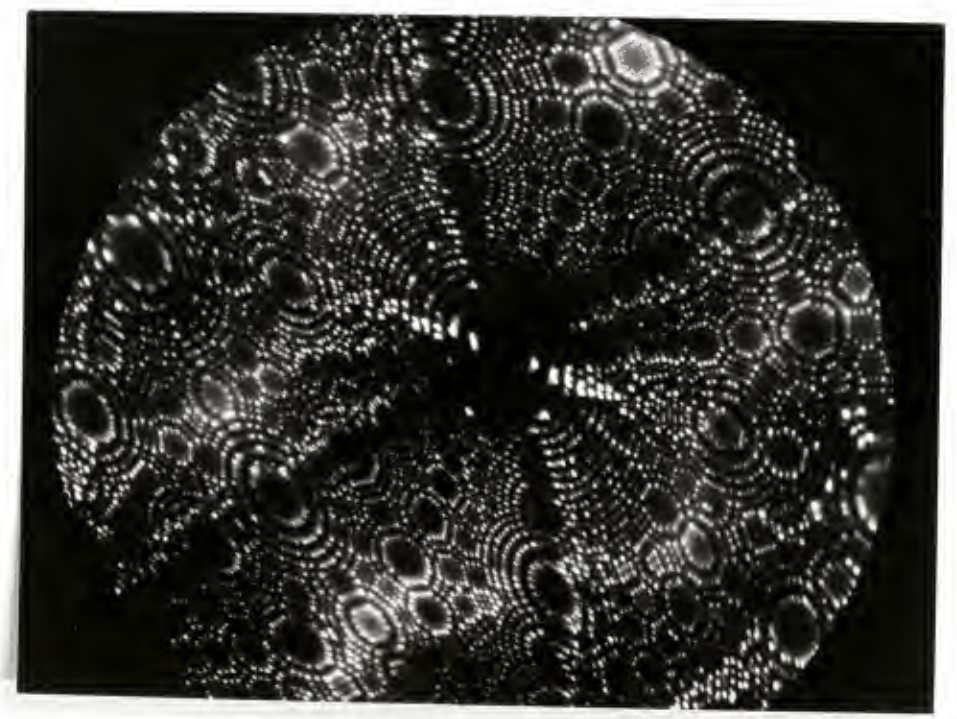

Fig. 9--A field-ion micrograph of tungsten (courtesy of R. W. Newman).

This behavior was attributed to the fact that in a disordered alloy the atoms possess a random distribution of binding energies. This leads to an irregular field evaporation of the various atoms, and causes an irregular image. The greater the degree of order, therefore, the more regular and complete is the corresponding field-ion image.

Short-range order has also been studied in the Co-Pt system. This work was done by Southworth and Ralph [88] employing the principle discussed above. These investigators observed small domains of LRO embedded in a disordered matrix above the critical temperature in CoPt. On the micrograph a domain of LRO appeared as a small, comparatively regular region against a random background. This micrograph is reproduced in Figure 10 where the domain is designated by the letter A. The interpretaion by Southworth and Ralph was that SRO in CoPt consists of small domains of LRO. As far as the author is aware, this is the only direct experimental evidence supporting the small-domain concept of SRO. The present investigation was undertaken to determine whether similar ordered domains could be found in Ni-Mo alloys containing SRO.

In the study of ordering with field-ion microscopy the ability to distinguish antiphase boundaries is important.

Fig. 10--A field-ion micrograph of CoPt showing a domain of SRO above the critical temperature (after Southworth and Ralph).

There has been very little work done on the interpretation of crystallographic features from field-ion micrographs, since this part of the science is in its early stages. Consequently it is not known exactly how an antiphase boundary should appear on such a micrograph. The appearance depends sensitively on the particular system and on the type of boundary in question. A good example is again the system Co-Pt [88]. This system orders by forming alternate layers of Co and Pt atoms on {002} planes. An antiphase boundary of the type in which the "C" axes of the adjacent domains are parallel can be distinguished as a line of bright atoms and vacant sites cutting across certain poles. For such a boundary, since the "C" axes of the two domains are parallel there is no misfit between adjacent domains even though ordering is accompanied by a tetragonal distortion. Apparently the boundary is visible because of preferential field evaporation along the line of its intersection with the surface. A rotational type of domain boundary occurs when the two domains have their tetragonal "C" axes at right angles. Such a boundary is clearly visible as a line along which the rings of the crystallographic poles are sheared slightly. This shearing is due to the fact that a certain amount of misfit occurs along this type of boundary.

There are two other features of a domain boundary that might contribute to its visibility in a field-ion micrograph. Even though the boundary is distorted, it is an interface, i.e., a region in which the stacking sequence has been interrupted. Consequently the imaging properties in the region of this interface should be affected to some extent since the interface represents a region of perturbation of the lattice potential. On this basis alone one would expect the boundary to appear as a bright or dark line. If a slight distortion is present within the boundary its visibility should be enhanced since the distortion represents an additional perturbation of the lattice.

Regardless of which of the above factors contribute to the visibility of a domain boundary it should appear as a line across which there is no rotation of the crystallographic poles. This is the criterion that distinguishes a domain boundary from a grain boundary, a subgrain boundary, or a twin boundary.

1.5 *Small-Angle X-ray Scattering*

Small-angle x-ray scattering measurements were used in the present work as a means for examining the early stages of precipitation of the β phase. This work was complimented by electron-transmission microscopic studies. The small-angle scattering technique can be used to study

the growth of particles which are in the size range of approximately 10 to 1,000 Å; hence, it effectively compliments electron-microscopic techniques in many cases. With proper analysis one can determine such quantities as the size of the particles, the surface area per particle, and the density of particles in the system.

The theory of small-angle scattering is discussed in great detail in a book by Guinier and Fournet [89]. The phenomenon is based on the fact that any dispersion of particles or voids within a matrix will produce a measurable scattering intensity near $2\theta = 0$ since all particles, whether they are crystalline or not, will produce a {000} diffraction node. This node, in the ideal case, is a very sharp peak, though it cannot be observed because it cannot be separated from the primary beam. If the particles are in the size range 10-1,000 Å, however, this {000} node will broaden sufficiently to be detected without interference from the primary beam, provided that a suitable experimental technique is used. Hence the small-angle scattering phenomenon is actually a special case of line broadening due to particle size. Measurements are generally made in the range $2\theta = 0.5\text{-}6°$.

The most common application of small-angle scattering measurements is to determine particle sizes through a

quantity known as the radius of gyration. The square of the radius of gyration is defined as the second moment of the mass of the particle divided by its volume. For spherical particles the true radius and the radius of gyration are equivalent. Guinier [116] has shown that in a system in which the distribution of precipitates is random and dilute, the small-angle scattering intensity can be written as:

$$I = K\exp\left[-\frac{4\pi^2\varepsilon^2R^2}{3\lambda^2}\right] \qquad (12)$$

where R = radius of gyration of the particle

$\varepsilon = 2\theta$ expressed in radians

λ = wavelength of incident radiation

K = a constant which contains geometric factors, incident beam intensity, density of particles, etc.

This equation is known as the Guinier approximation. Within the range for which it is valid a plot of log I vs. ε^2 yields a straight line. From the slope of this line the radius of gyration of the particles can be determined.

CHAPTER II

REVIEWS OF PREVIOUS WORK ON NICKEL-MOLYBDENUM ALLOYS

2.1 *The Nickel-Molybdenum Phase Diagram*

Most of the basic features of the Ni-Mo binary phase diagram have been established. In Figure 11 the general form of the complete diagram is shown. It is taken from Hansen's *Constitution of Binary Alloys* [90]. The region between 12 and 50 a/o Mo has recently been reinvestigated [91,92]. This part of the diagram is shown in Figure 12. The main differences between this and the previous diagram are an increase in solubility of Mo in Ni at the peritectoid reaction, $\alpha + \gamma \rightarrow \beta$, and a decrease in the solubility of Mo in Ni below this reaction.

The earliest published work on the Ni-Mo system was by Grube and Schlecht [93] in which they reported the results of Baar, Dreibholz, and Köster and Schmidt along with their own. Baar and Dreibholz used thermal analysis and optical microscopy in a study of the high-temperature region of the diagram including the solidus and liquidus lines. Köster and Schmidt found that alloys containing greater than 18 w/o Mo showed an increase in hardness upon aging. According to their work the aging began at 600°C and the maximum effect was observed at approximately 800°C. Grube and Schlecht

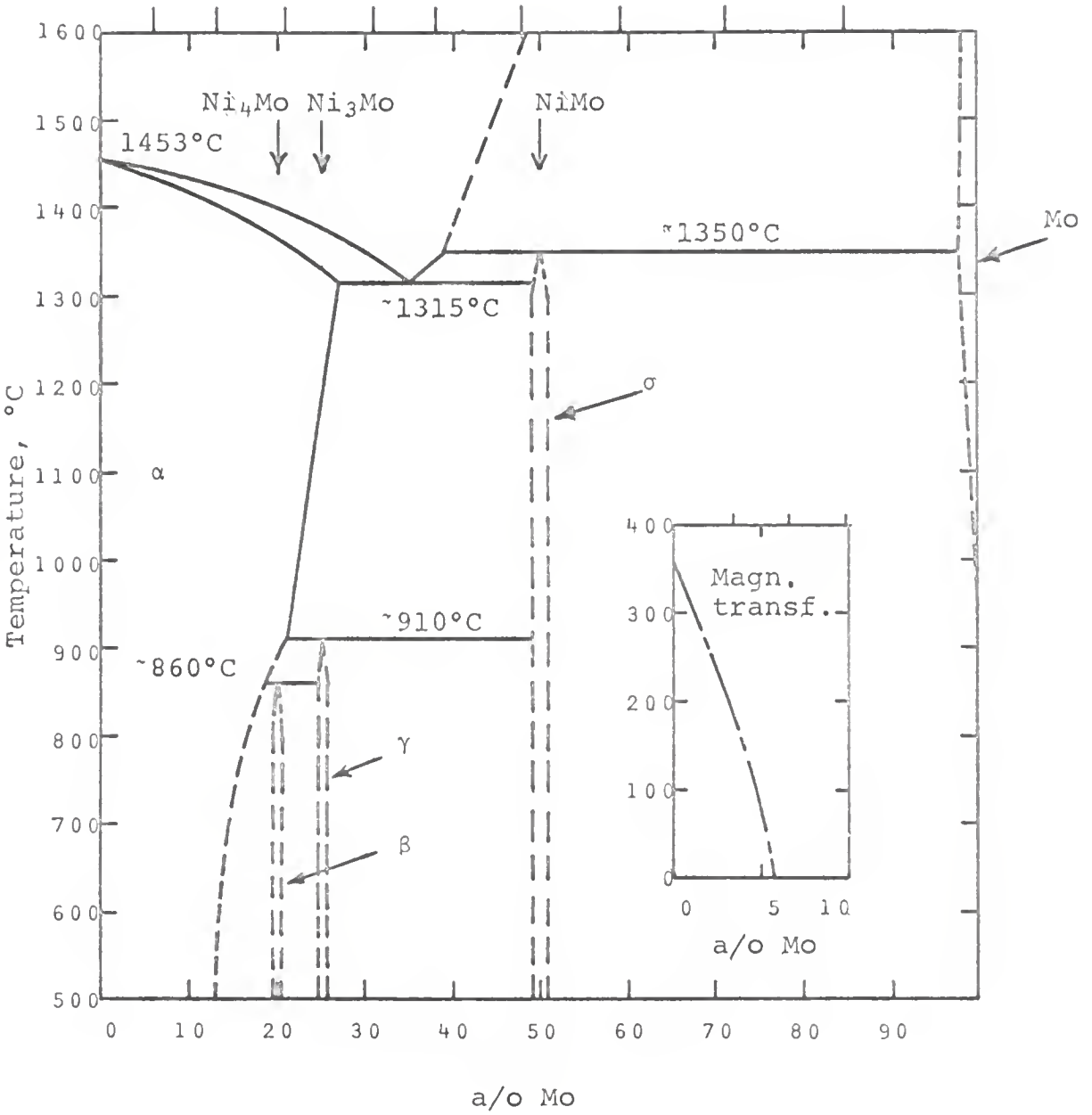

Fig. 11--A binary phase diagram of the Ni-Mo system (after Hansen).

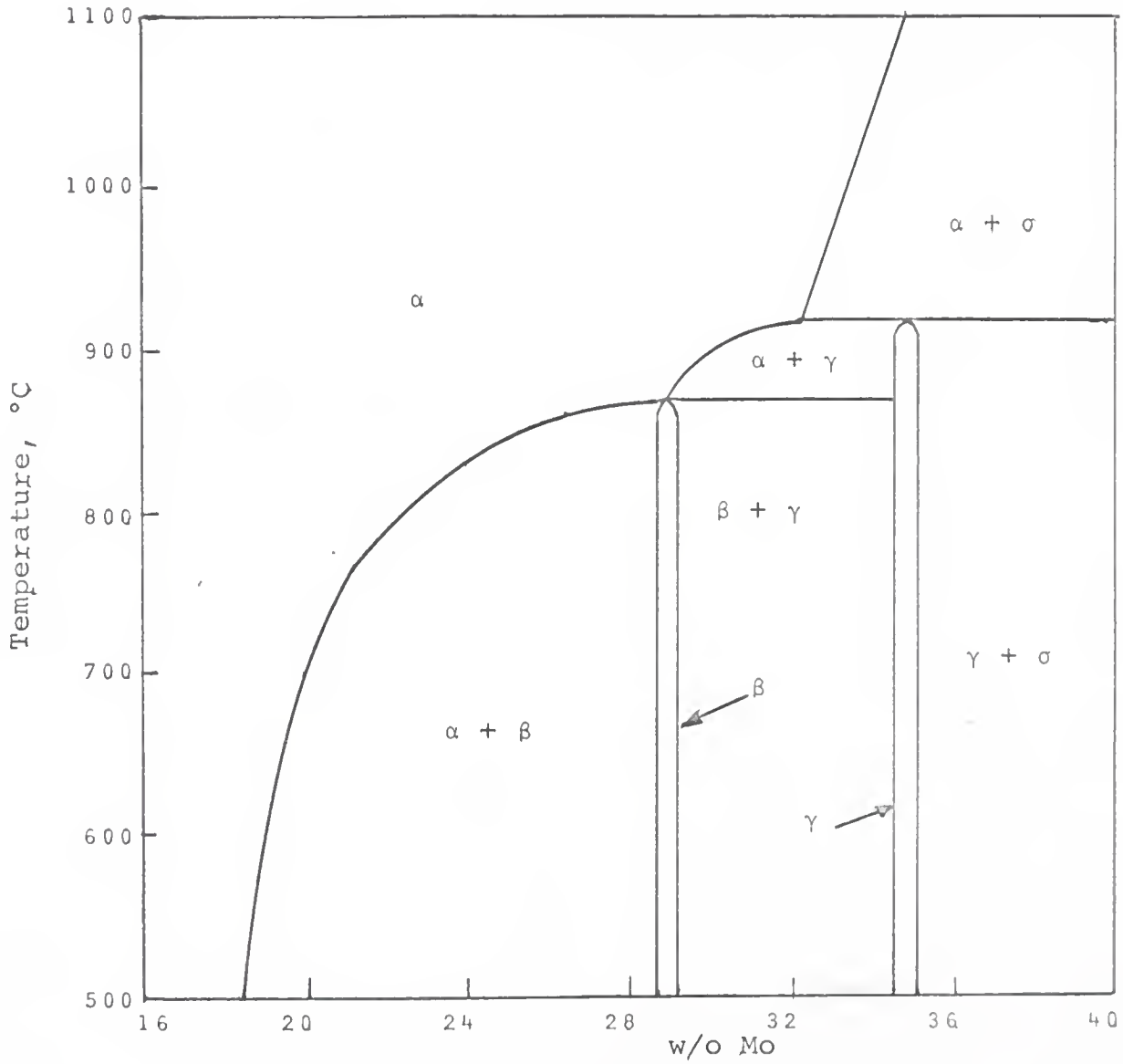

Fig. 12--A partial binary phase diagram of the Ni-Mo system (after Guthrie and Stansbury).

used resistivity, metallography, hardness, and x-ray diffraction in an attempt to complete the phase diagram but were only partially successful. They were able to identify the β phase, which corresponds to the composition Ni_4Mo, as a tetragonal phase; however, there was considerable uncertainty in the low-temperature region of their proposed diagram between 31 and 62 w/o Mo.

The work of Grube and Schlect was continued by Grube and Winkler [94]. They were able to confirm the existence of the previously questionable γ phase corresponding to the composition Ni_3Mo. They identified this phase as having a close-packed hexagonal structure with a c/a ratio of 1.65. The γ phase has since been identified by Saito and Beck [95] as an orthorhombic phase of the Cu_3Ti type, having the following lattice parameters: $a_0 = 5.064$ Å; $b_0 = 4.224$ Å; $c_0 = 4.448$ Å. According to Saito and Beck there is reasonably good agreement between the observed and the theoretical x-ray intensities for the γ phase if one assumes the orthorhombic structure. Despite the disagreement on the structure of the γ phase, the complete diagram proposed by Grube and Winkler has proven to be essentially correct. There have been changes in solubility limits and reaction temperatures however.

The work of Grube and Winkler was largely confirmed by Ellinger [96] who used x-ray diffraction, metallography,

and hardness data. Ellinger proposed a complete phase diagram which is very little different from that of Grube and Winkler except for the reaction involving the evolution of the β phase. According to Ellinger the β phase precipitates by means of the peritectoid reaction: $\alpha + \gamma \rightarrow \beta$. According to the diagram of Grube and Winkler the α phase can transform directly to the β phase; however, this may be regarded as a special case of the above peritectoid reaction in which the compositions of the α and β phases are the same. This apparent difference is therefore only a question of the solubility of Mo in the α phase at the peritectoid temperature. The crystal structure of the β phase was also identified by Ellinger as close-packed hexagonal in agreement with Grube and Winkler; however, Saito and Beck identified this phase as orthorhombic as already noted. The most recent work in this area of the phase diagram is by Guthrie and Stansbury [91] and Stoffel and Stansbury [92]. Their work is shown in Figure 12, and it is in agreement with that of Grube and Winkler with regard to the evolution of the β phase.

The crystal structure of the β phase, which was originally identified by Grube and Schlect as face-centered tetragonal, has since been revised by Harker [97]. Harker identified the Bravais lattice as body-centered tetragonal

and the space group as C_{4h}^{5} - $I\frac{4}{m}$. This structure has since been confirmed by Guthrie and Stansbury [91], who also showed that the β structure can be derived from the α by the process of ordering accompanied by a tetragonal distortion. The evolution of the β phase from the α phase will be discussed in more detail later. The solubility limits of Mo in Ni established by Guthrie and Stansbury are in reasonable agreement with the work of Mikheev in this region [98]. Riddle [99] made dilatometric measurements and determined that the temperature of the peritectoid reaction α + γ→β is 865°C. This result is also in good agreement with the work of Guthrie and Stansbury.

The crystal structure of the phase NiMo has not been completely established; however, it appears to have tetragonal symmetry. This conclusion is based on the work of Smiryagin *et al.* [100], Bagaryatskii and Ivanovskaya [101], Shoemaker *et al.* [102], and Obrowski [103].

2.2 *The α to β Transformation*

The crystal structure of the β phase, corresponding to the composition Ni_4Mo is shown in Figure 13. This structure, which is body-centered tetragonal, was first derived by Harker [97] and later confirmed by Guthrie and Stansbury [91]. Guthrie and Stansbury also showed that this structure can be derived from the FCC α structure by

the process of ordering accompanied by a tetragonal distortion. The relationship between these two structures is also shown in Figure 13. The nature of the ordering is such that the Mo atoms are arranged as far apart as possible within the lattice. The unit cell of the β phase contains 8 Ni and 2 Mo atoms. The coordinates of the Mo atoms are 0,0,0; 1/2,1/2,1/2; and the coordinates of the Ni atoms are x,y,0; $\bar{x},\bar{y},0$; $\bar{y},x,0$; $y,\bar{x},0$; x+1/2, y+1/2,1/2; $\bar{x}$+1/2,$\bar{y}$,+1/2,1/2; $\bar{y}$,+1/2,x+1/2,1/2; y+1/2, $\bar{x}$+1/2,1/2 where x = 0.2 and y = 0.4. Harker's values for the lattice parameters of the unit cell are a_0 = 5.720 Å, c_0 = 3.564 Å, c/a = 0.6231. The volume of the cell is 2-1/2 times the volume of the distorted unit cell of the FCC lattice from which it is derived. Accompanying the transformation are shrinkages of approximately 0.5% and 1.0% in the tetragonal a_0 and c_0 directions, respectively.

There is good evidence that the β phase actually does form by ordering of the α phase. It can be shown that for such a process there are 30 possible ways by which the β phase may nucleate, but due to the multiplicity of the lattice this results in only six different orientations. Spruiell [31] has shown by oscillating single crystal x-ray diffraction patterns that the predicted orientation relationships between the α and β phases are

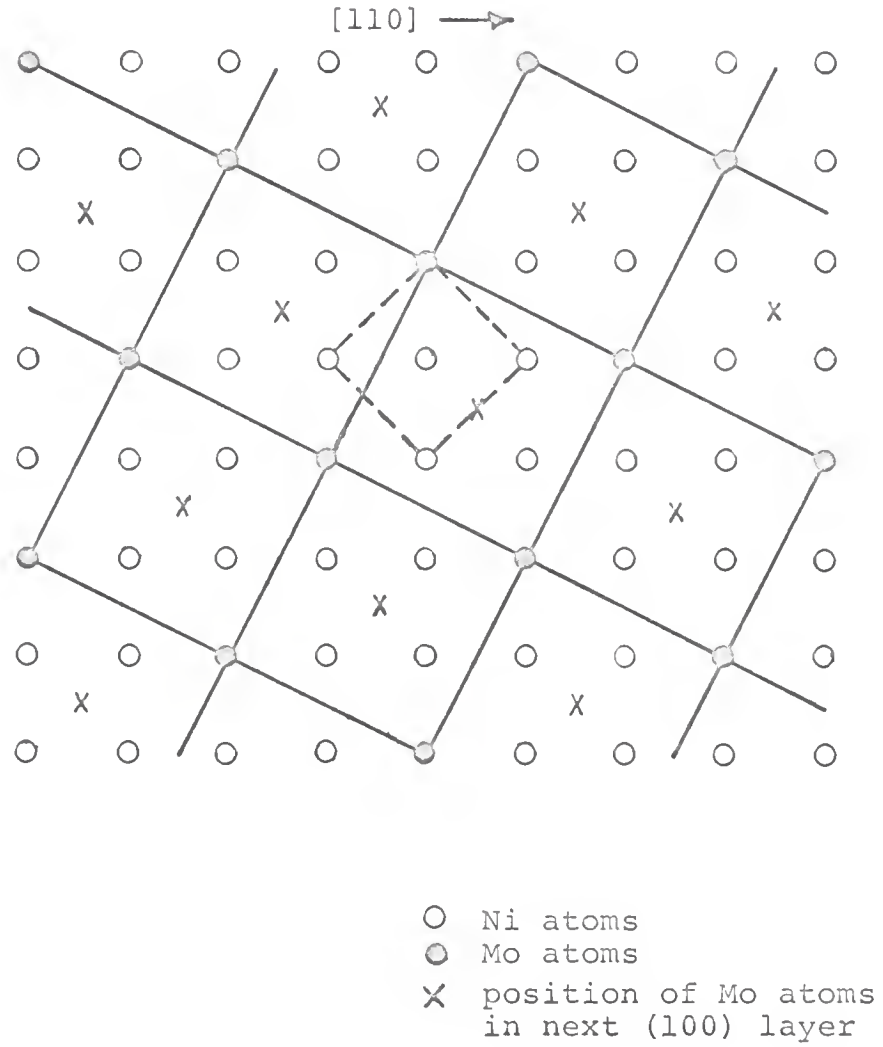

Fig. 13--Schematic representation of the ordered Ni_4Mo (β) phase (after Guthrie and Stansbury).

always found. Further evidence that the β phase is derived by ordering of the α phase is provided by the x-ray powder data of Guthrie and Stansbury [87]. During the transformation α to β, the primary α refections split into triplets, with the exception of the {111} and {222} planes. One of the peaks of the triplet is a nearby superlattice reflection of the β phase. The other two peaks are due to a splitting of the original primary peak since the α and β phases have slightly different lattice parameters. During the early states of the α to β transformation the Debye pattern shows the formation of a face-centered tetragonal lattice. As the transformation proceeds, the weak superlattice lines appear, indicating the presence of the fully-ordered body-centered tetragonal β phase. This picture correlates with the hardness data of Guthrie and Stansbury in the following way: there is a rapid initial increase in hardness during the α to β transformation followed by a decrease and then another increase. Guthrie and Stansbury interpret the initial increase as being due to local tetragonal distortions of the α lattice at the beginning of the transformation. The absence of the well-defined superlattice lines indicates that the degree of order at this stage of the transformation is very imperfect. As the degree of order increases, coherency strains increase to a

certain point and then coherency is lost. This loss of coherency is accompanied by a decrease in hardness. As the domains of the β phase continue to grow in size and perfection and to impinge upon one another the hardness again rises.

Metallographically the β phase is observed to grow from the α phase in a variety of forms. It sometimes takes the form of a very finely-dispersed second phase, but quite often it develops as a pronounced Widmanstäten structure. Both Ellinger [96] and Guthrie and Stansbury [91] found that the finely-divided precipitate occurred frequently in two-phase alloys that are near the solvus line of the α phase whereas the pronounced Widmanstäten structure occurred predominantly in alloys near the Ni_4Mo composition. Both forms of the precipitate formed preferentially near, but not within, grain boundaries, and very little coalescence of this dispersed phase was observed even after several hundred hours of annealing. With optical microscopy it is difficult if not impossible to distinguish between a structure containing precipitated β in primary α and one containing pure β that has transformed from the α phase. This is because both structures may form a highly developed Widmanstäten pattern. In the case of the exact Ni_4Mo composition this striated structure

remains even after all the α phase has transformed. The observed etching effects were attributed by Guthrie and Stansbury to the high degree of strain that accompanies the transformation and the mismatch, i.e. lattice strain, at the interface between impinging domains. They also assumed that the β phase precipitates as platelets. Since only three directions were ever observed for the striations which appeared in the primary α grains, they further assumed that the platelets formed on {100} habit planes within the α matrix. Spruiell [31] has since shown that the observed striations were parallel to {111} planes. There was some doubt, however, about whether these were slip traces or actually β platelets. No confirmation of a {111} habit plane has yet been derived from electron-microscopic data.

Alloys within the α and β region of the phase diagram have been found by several investigators to respond readily to age-hardening treatments. Studies of this type have been performed by Ellinger [96], Guthrie [104], Block [105], and Guthrie and Stansbury [91]. Although the agreement of the data is not particularly good, the investigators all agree that large hardness increases can be produced within a few tenths of an hour by annealing in the temperature range of approximately

600°C to 850°C. Both Ellinger and Guthrie and Stansbury observed a definite two-stage hardening process during isothermal annealing, and the latter even observed a peak hardness during the first stage as previously noted. The beginning of the second stage of hardening was found to vary with the annealing temperature and the composition, but in general it occurred after a time of several hours, sometimes taking as much as 50-100 hours. The hardening is assumed by Spruiell [31] to be mainly due to the strains induced in the lattice as the β domains grow in size and perfection.

Hardness measurements were used by Block [105] to study the kinetics of the isothermal α to β transformation in alloys containing 27, 28, and 29 w/o Mo. From these data he constructed a time-temperature transformation curve that had a "C" shape typical of many solid-state phase transformations. The maximum rate of hardening was found to occur at 800°C. Lampe and Stansbury [106] later used resistivity measurements to study the kinetics of the α to β transformation in an alloy with the Ni_4Mo composition. They also constructed a TTT curve from their data and found it to have a "C" shape. The "nose" of the curve was found to lie within the temperature range 710°C-775°C, and in this region the start of the transformation was too rapid

to be observed. It was also found that above approximately 860°C and below approximately 620°C the transformation had not begun even after 1,000 hours. This curve is reproduced in Figure 14.

Since the α to β transformation proceeds isothermally, it is assumed to occur by a nucleation-and-growth process whereby uphill diffusion of Ni and Mo atoms is the rate-determining factor. No evidence has yet been presented that would indicate a shear-type transformation, nor is there any evidence to indicate that an intermediate metastable phase (or phases) forms during the transformation. If the α to β transformation is indeed a direct homogeneous ordering process, as the orientation relationship between the two phases indicates, then it follows that at some stage of the process the β phase exists in a coherent, or at least partially-coherent, "zone" state. Due to the tetragonal lattice contraction upon ordering and the high degree of strain that accompanies the growth of these zones there will be a tendency for the zones to lose coherency with the matrix. The β phase may therefore prefer to nucleate at imperfections such as dislocations. Evidence will be presented later in support of this idea. The question of whether the transformation actually occurs by a nucleation-and-growth process or by spinodal decomposition cannot be answered from current data.

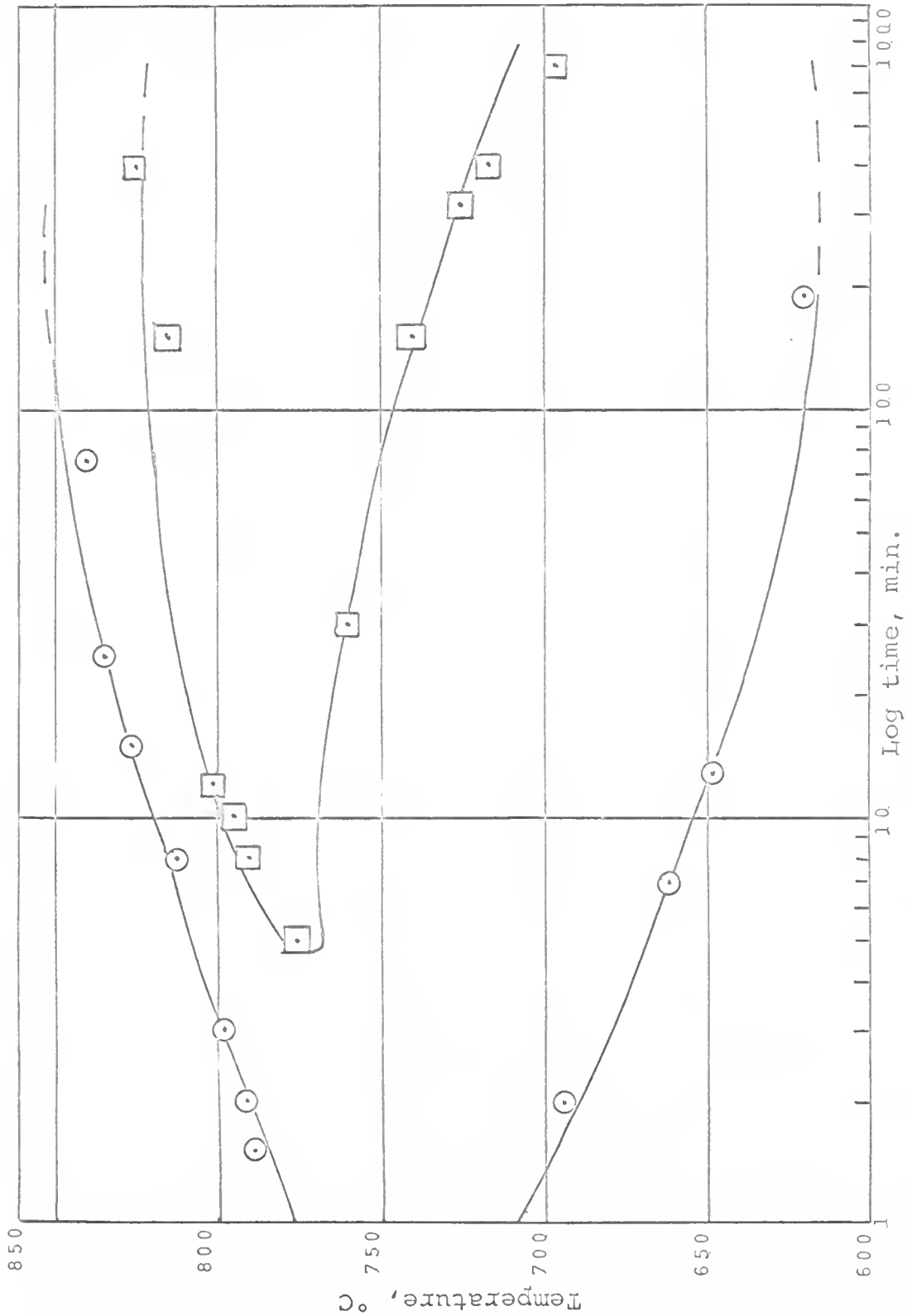

Fig. 14--Time-temperature-transformation curve for the α to β transformation in Ni-29.1 w/o Mo (after Lampe and Stansbury).

2.3 *The K-state in Ni-Mo Alloys*

Thomas [1] in his study of K-state alloys predicted the occurrence of a K-effect in Ni-Mo alloys. This conclusion was based upon two facts: (1) Grube and Schlecht [93] had observed an "S" shaped resistence versus temperature curve for 18-21 w/o Mo alloys, indicating the presence or an anomaly. (2) The system Ni-Cr exhibits a strong K-effect and Cr and Mo are both in group VI-B of the periodic table. Anomalies were later found in the Young's modulus of Ni-Mo alloys by Kritskaya *et al.* [107] and Polotskii and Benieva [108]. These investigators found that alloys in the composition range 5-19.5 w/o Mo exhibited an increased modulus after certain appropriate annealing conditions. One of these conditions was annealing at 400°C after quenching from 1,000°C, corresponding to one of the onditions under which the anomalous resistivity rise can also be produced in K-state alloys. Sukhovarov *et al.* [30] later verified the existence of a K-state in Ni-10 a/o Mo alloys using electrical resistivity and calorimetry measurements. Subsequent work by Kudryavtseva *et al.* [28] and by Popov *et al.* [29] yielded similar results. The experiments of references [28,29,30] were directed primarily toward a study of the kinetics of formation of the K-state in Ni-Mo alloys, and although it was assumed

that SRO was responsible, no direct evidence from x-ray diffuse scattering was obtained.

Spruiell [31] later did a study of SRO in the Ni-Mo system by x-ray diffuse-scattering measurements on single crystals containing 10.7 and 20 a/o Mo. He found a definite SRO in both alloys after quenching from temperatures in the range 900-1,200°C. He also found that annealing the 10.7 a/o Mo alloy in the temperature range 400°C to 500°C sharpened the diffuse intensity maxima, indicating an increase in the degree of SRO. This temperature range corresponds to that in which the K-state can be produced, although Spruiell did not correlate his data with resistivity studies. Another significant study made by Spruiell was the investigation of the change in the diffuse intensity of a quenched 20 a/o Mo specimen upon annealing at 650°C. The diffuse maxima caused by the SRO existing at the quenching temperature were observed to gradually split into doublets and to sharpen considerably. The diffuse intensity appeared to be gradually approaching the sharp intensity distribution of the fully ordered Ni_4Mo structure.

Based on the diffuse-scattering data from the 10.7 a/o and 20 a/o Mo alloys, Spruiell concluded that SRO in dilute Ni-Mo alloys is similar in structure to the

Ni_4Mo type of LRO. In Figures 15 and 16 his models for SRO in these alloys are shown. The several layers of atoms in these figures are successive {002} planes with planes 1, 2, and 3 lying above plane 0 and 1′, 2′, and 3′ lying below plane 0. The dark circles represent Mo atoms, the light circles Ni atoms, and the crossed circles "statistical-average atoms" which are 66.8% Ni. The number of atoms included in each of the figures in the minimum number required to obtain a reasonable fit to the derived SRO parameters. In both the 10.7 and the 20 a/o Mo alloys, the SRO may be interpreted as small, imperfect domains of Ni_4Mo-type LRO.

Baer [109] did a similar x-ray diffuse scattering study on single crystals of Ni_4W, which has the same type of LRO as Ni_4Mo, and concluded that a domain structure of Ni_4Mo LRO is not the proper model for SRO in Ni-W. Baer's model consists of double layers of {420} planes which are alternately nickel-poor and nickel-rich as compared to the random solid solution. He extended this idea to the Ni-Mo system. Baer did an earlier study of the K-state in Ni-W and Ni-Mo [27] in which he compared resistivity measurements with diffuse x-ray scattering on Ni-W polycrystals. He was able to correlate SRO with the K-state in Ni-W but because of the low diffuse intensity

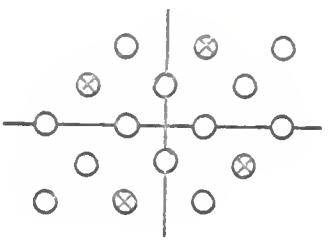

Plane 0

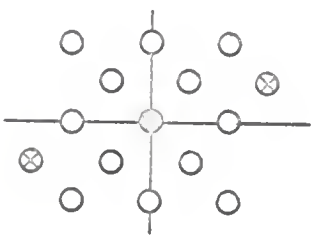

Plane 1 or 1′

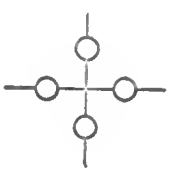

Plane 2 or 2′

Plane 3 or 3′

Fig. 15--Spruiell's model of the SRO existing in a Ni-10.7 a/o Mo alloy quenched from 1000°C into iced brine (after Spruiell).

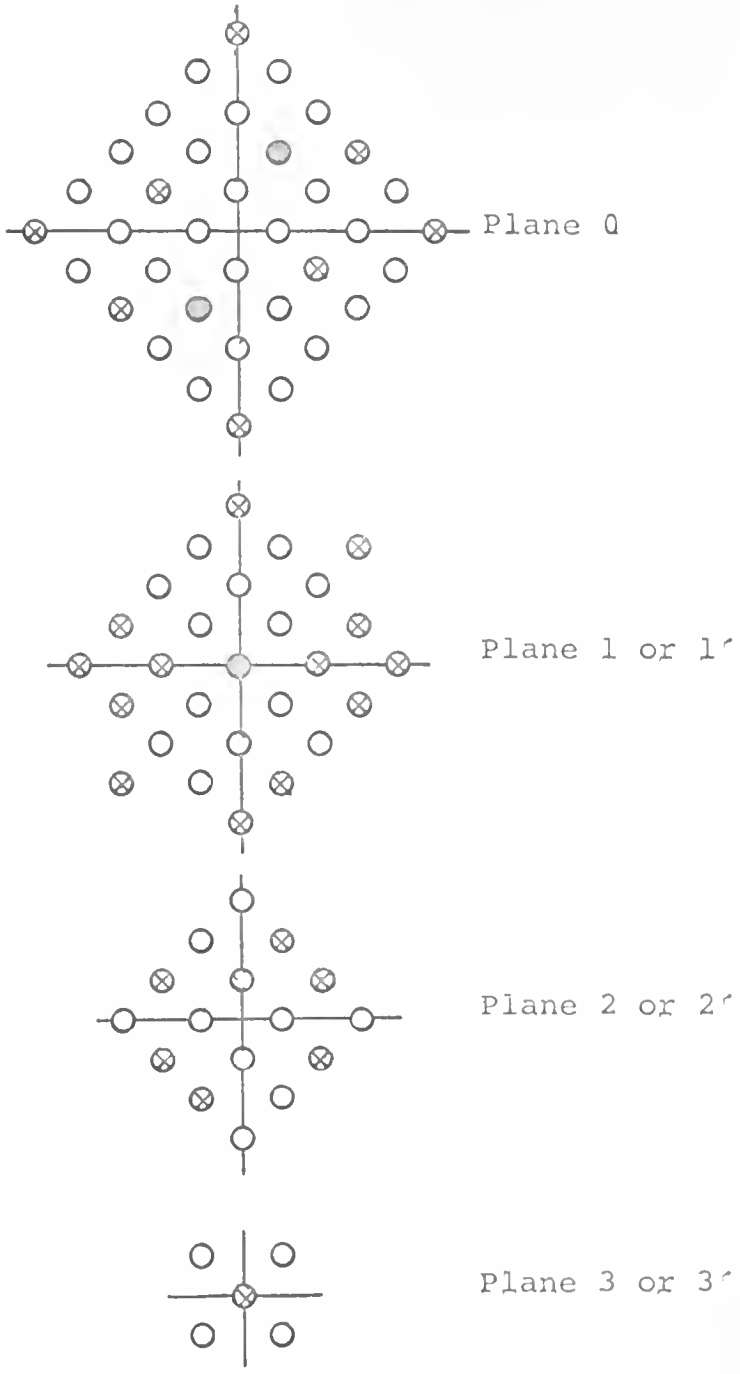

Fig. 16--Spruiell's model for the SRO existing in Ni_4Mo quenched from 1000°C into iced brine (after Spruiell).

of Ni-Mo alloys (due to the small difference in atomic scattering factors) no such correlation was made.

McManus [32] has also demonstrated the presence of SRO in Ni_4Mo alloys quenched from above the critical temperature. He used polycrystalline specimens and derived the SRO parameter α_1 from these powder data. The diffuse-scattering curve had the typical shape of a system in which the atoms prefer unlike neighbors (Figure 7). This result is in agreement with the work of Spruiell [31] in which the proposed atomic model contained no Mo-Mo nearest neighbors. The actual value of the α_1 parameter derived by McManus was -0.13 whereas the maximum possible value is -0.250. Again no correlation was made between the observed SRO and the K-state. Of importance, however, is the fact that the size-effect parameter, β_1, was essentially zero. This means that one can ignore the scattering contribution due to atomic-size difference in Ni-Mo alloys when correlating SRO with property changes.

The work of Popov *et al.* [29] on the kinetics of K-state formation in Ni-Mo alloys gave interesting data on the migration of atomic defects in FCC Ni and its alloys. By isochronal annealing of 10 a/o wire specimens which had been cold-worked or quenched from an elevated temperature, these investigators found two stages of K-state

formation, one at approximately 100°C and the other at about 300°C. These stages correspond to the two stages of recovery of point defects in cold-worked and quenched Ni, the activation energy for the lower stage being about 22 K-cal/mole and that of the second stage about 36 K-cal/mole [110,111]. These two stages were attributed [112] to the annealing out of interstitial atoms and vacancies. Popov *et al.* also found that the activation energy for the low-temperature stage of K-state formation in Ni-Mo was about 22 K-cal/mole. They reasoned that if the K-state were due to SRO, the low-temperature stage could not be caused by the migration of interstitials for two reasons: (1) In order for SRO to take place by interstitial migration both Mo and Ni atoms would have to move by this mechanism. Due to the large size difference between Ni and Mo atoms, (Goldschmidt diameters of 1.24 Å and 1.40 Å) it is unlikely that Mo atoms would move by an interstitial mechanism. (2) If this stage were due to interstitial migration then the motion of the larger Mo atoms would be the rate-controlling step; consequently, the measured activation energy should be much higher than the 22 K-cal/mole since this is also the activation energy found in pure Ni. For the high-temperature stage, they found an activation energy of about 66 K-cal/mole as compared to 36 K-cal/mole

for pure Ni. They assumed that this stage is indeed due to the migration of vacancies as assumed by other investigators [110,111]. They assumed that the disagreement in activation energies is caused by the binding energy between Mo atoms and vacancies. By comparing the initial rate of K-state formation for specimens quenched from various temperatures and annealed in the range of the high-temperature stage, they evaluated the energy of formation of vacancies for Ni - 10 a/o Mo. By comparison with the activation energy for migration of vacancies in the high-temperature stage, they evaluated the binding energy between vacancies and Mo atoms as being approximately 20 K-cal/mole. These calculations were based on the assumption that the K-state in Ni-Mo is caused by SRO. As further evidence of the validity of this assumption it was noted by the authors that these two stages are also observed in K-state formation in Ni-Cr [113], and for that system the activation energy for the high-temperature stage is almost identical to that for pure Ni. Furthermore, the atomic sizes of Ni and Cr are almost the same. This is, at least, strong evidence that the K-state formation is diffusion controlled in Ni-Mo and in Ni-Cr even though it does not definitely prove that SRO is a necessary condition.

Interesting anomalies in the specific heat of Ni-Mo alloys were found by Stansbury, Brooks and Arledge [9]. They found that the specific heat versus temperature curve for Ni - 15 w/o Mo underwent a rapid rise in the temperature range 500-600°C, indicating that changes in the structure of the solid solution were taking place. By comparing the integrated energies under the ideal and the real curves, they found that the energy expended in the process corresponding to the anomaly was about 5.5 joules/gm. The authors attributed this effect to the partial destruction of SRO as the temperature was increased. They found a similar effect in Ni-Cr, which is another K-state alloy thought to exhibit SRO, whereas pure Ni did not show this effect (Figure 17). They concluded that the anomaly in Ni-Mo and also in the Ni-Cr alloys was due to the destruction of SRO. Since the equilibrium degree of SRO should decrease with increasing temperature one would expect that SRO would be continuously destroyed as the temperature increased. Therefore, one should see a higher than normal value of the specific heat over the entire temperature range studied. The fact that this effect is not observed implies that the equilibrium state of SRO does not keep pace with the changing temperature until about 500°C is reached. This means that one should expect

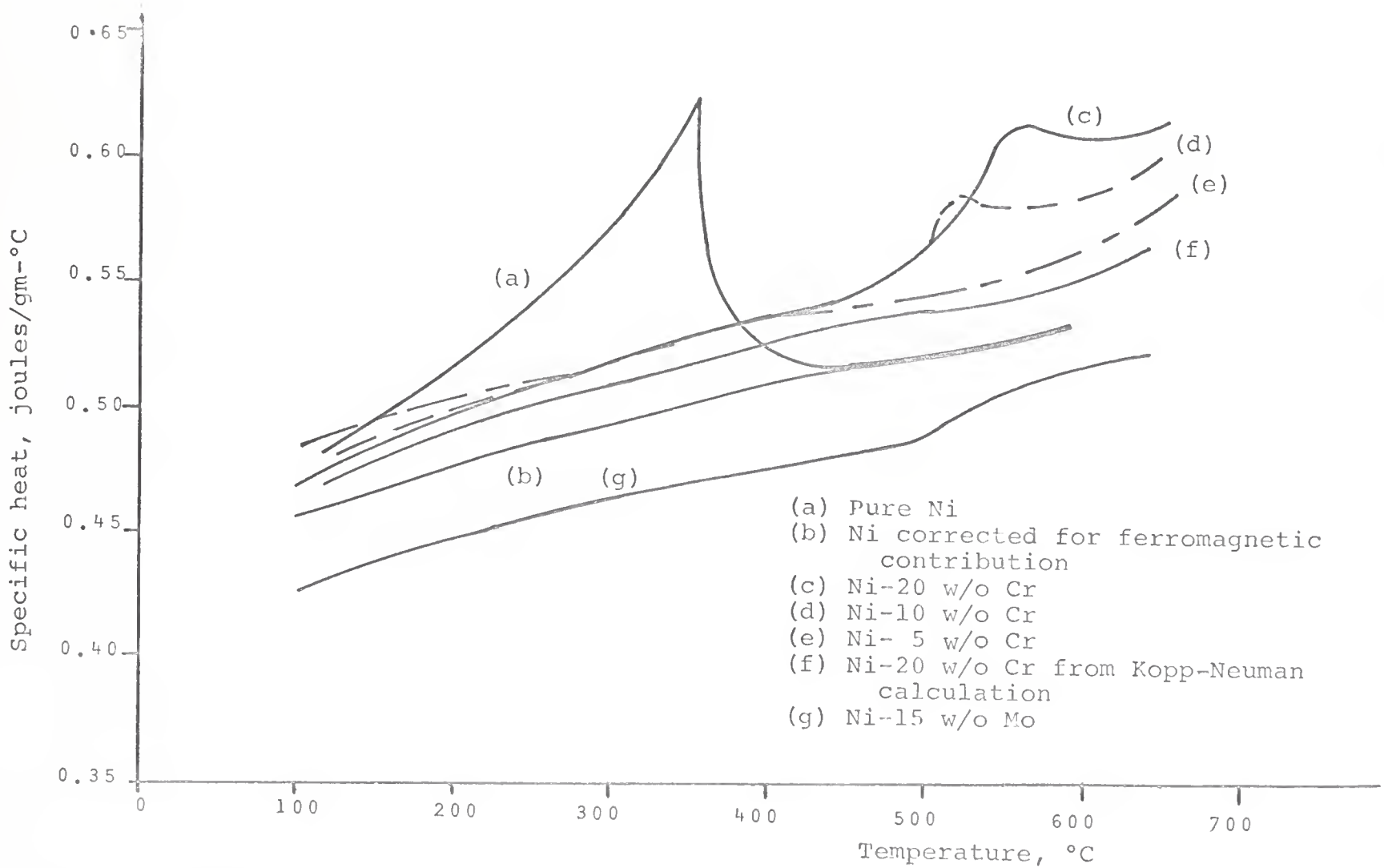

Fig. 17--Curves of specific heat vs. temperature for Ni, Ni-Cr, and Ni-Mo alloys (after Stansbury, Brooks, and Arledge).

the state of SRO existing in a slowly-quenched specimen to correspond roughly to the equilibrium state at about 500°C. The reason for this behavior can be found in the balance between the thermodynamic driving force and the kinetics. This is the same balance of factors that causes a diffusion controlled phase transformation to follow the usual "C" shape in its TTT curve. The specific-heat data of Stansbury *et al.* [9] are in agreement with the resistivity data of Sukhovarov *et al.* [30] shown in Figure 18. In a plot of % change in ρ versus T for different annealing temperatures after quenching from 950°C, they found a maximum response at around 500°C also.

In summary, it is clear that the occurrence of the K-state in dilute Ni-Mo alloys has been well established. In addition to the resistivity anomaly, the K-state in Ni-Mo is associated with an increase in the elastic modulus and an increase in the specific heat. It is also known that SRO exists in the α phase of the Ni-Mo system but a satisfactory correlation between SRO and the K-state in this system has not been established.

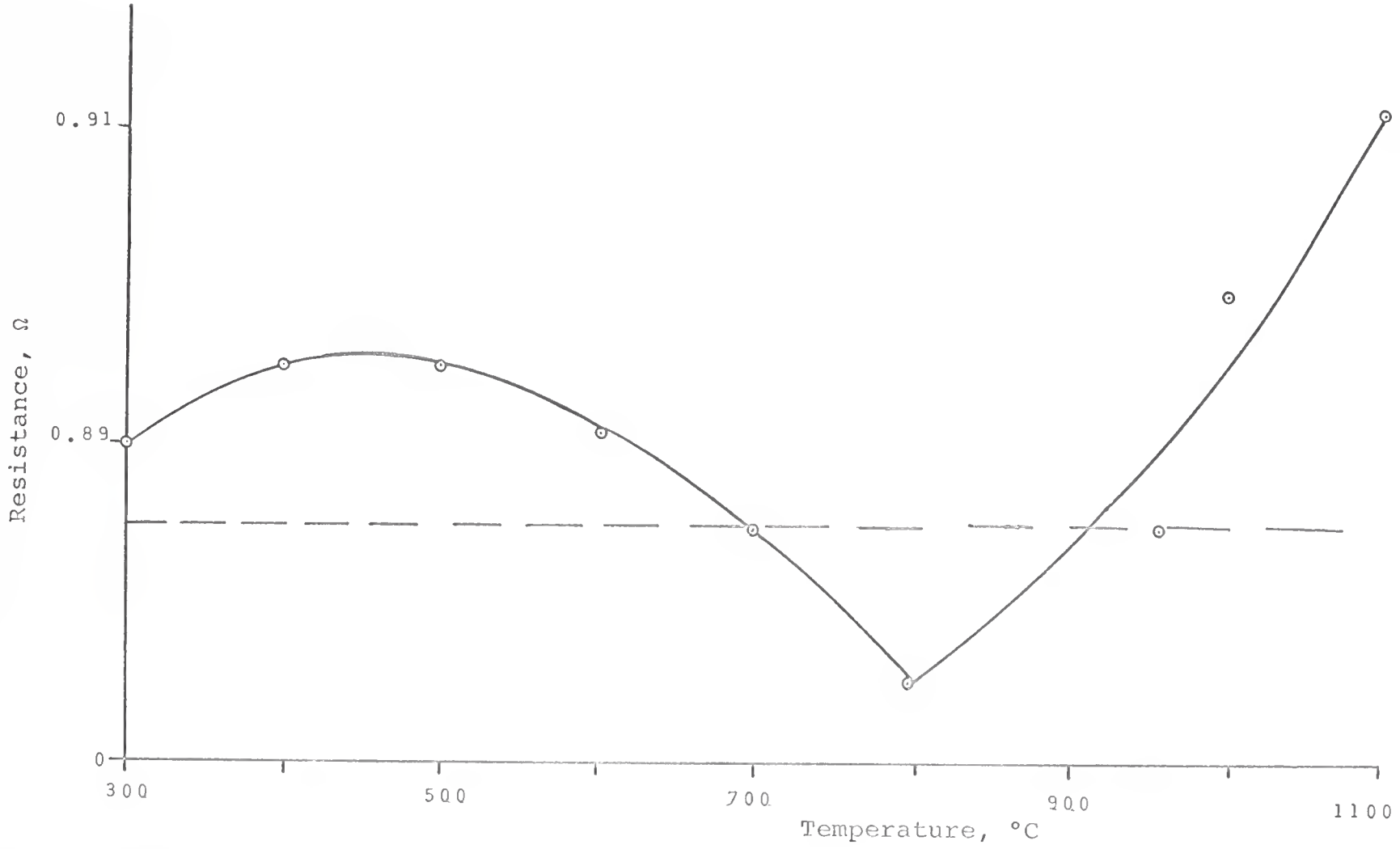

Fig. 18--Plot of electrical resistance vs. annealing temperature for a Ni-10 a/o Mo alloy quenched from 950°C (after Sukhovarov *et al.*).

CHAPTER III

EXPERIMENTAL EQUIPMENT AND PROCEDURES

3.1 *Preparation of Alloys*

Ni-Mo alloys of compositions 10.5 a/o, 14.0 a/o, and 20.0 a/o Mo were used in this research. These alloys were kindly supplied by Professors J. E. Spruiell and P. V. Guthrie of the Department of Metallurgical and Materials Engineering, University of Tennessee. The base metals were 99.95% purity Ni from the International Nickel Company and 99.8% purity Mo from the Climax Molybdenum Company. The alloys were prepared by induction melting under a partial pressure of hydrogen and chill casting into a cold copper mold [91]. Approximately 250 grams of weighed stock was melted in a graphite-lined alumina crucible which was surrounded by a hydrogen atmosphere during melting. The melt was superheated 300-400°C to promote homogeneity, and prior to casting a partial vacuum of 25 inches of mercury was obtained. The melt was chill cast into a cold copper mold to produce ingots of the approximate dimensions 3/4 inches x 1/2 inch x 3 inches. The ingots were then homogenized for 100 hours at 1,250°C. The 14.0 a/o alloy had been hot rolled to approximately 50% reduction of area at temperatures between 1,000 and

1,100°C. The 10.5 a/o and 20 a/o alloys were received in the as-cast and homogenized condition. The treatment given these alloys by the author consisted of annealing and cold-rolling them to a convenient thickness of 1.5 to 2.0 mm. The annealing was done in dry hydrogen at 1,000°C.

From this stock four different types of specimens were prepared for various purposes. The mechanical and thermal histories of these specimens are given in Table I. The specimens with an "R" prefix were used for resistivity measurements on a precision Kelvin bridge and they had dimensions of roughly 5 x 0.7 x 0.17 cm. The specimens with an "F" prefix were in the form of foils approximately 0.005 cm thick. They were used for small-angle x-ray scattering, electron-microscopic and resistivity studies. Specimens with an "X" prefix were used for x-ray diffuse-scattering and resistivity measurements. These specimens were in the forms of rectangular strips approximately 5 x 1.8 x 0.05 cm. Specimens with a "W" prefix were in the form of very fine wires 0.013-0.020 cm in diameter. These were used for field-ion microscopic studies. The strips and foils were prepared by alternately annealing and cold rolling. The wires were prepared by annealing and cold drawing. Each of the different experimental techniques will be described in a separate section and

TABLE 1

TREATMENT AND STUDIES MADE FOR EACH SPECIMEN

Specimen Number	Composition	Treatment	Studies Made
R-1	10.5 a/o Mo	Annealed 24 hours at 1,000°C and water-quenched; cold-rolled to 29.2% reduction of area; annealed for 200 hours at 500° C	Resistivity
R-2	14.0 a/o Mo	Annealed 24 hours at 1,000°C and water-quenched; cold-rolled to 33.5% reduction of area; annealed 10.5 hours at 400°C, 7.5 hours at 450°C, 94 hours at 475°C, 12.5 hours at 500°C	Resistivity
R-3	10.5 a/o Mo	Annealed 24 hours at 1,000°C and water-quenched; annealed 153.5 hours at 500° C	Resistivity
R-4	14.0 a/o Mo	Annealed 24 hours at 1,000°C and water-quenched; annealed 153.5 hours at 500°C	Resistivity
X-1	10.5 a/o Mo	Water-quenched from 1,000°C; cold-rolled to 70% reduction of area; annealed 201 hours at 500°C; annealed 24 hours at 1,000°C and water-quenched	Resistivity and x-ray diffuse scattering

TABLE 1--*Continued*

TREATMENT AND STUDIES MADE FOR EACH SPECIMEN

Specimen Number	Composition	Treatment	Studies Made
X-2	14.0 a/o Mo	Water-quenched from 1,000°C; cold-rolled to 65% reduction of area; annealed 246 hours at 500°C, 3.75 hours at 330°C, 5 hours at 650°C, 1.5 hours at 750°C, annealed 24 hours at 1,000°C and water-quenched	Resistivity and x-ray diffuse scattering
F-1	14.0 a/o Mo	Annealed 36 hours at 1,000°C and water-quenched; annealed 175 minutes at 630°C, 125 minutes at 650°C	Resistivity
F-2	14.0 a/o Mo	Annealed 24 hours at 1,000°C and water-quenched; cold-rolled to 20% reduction of area; annealed 210 minutes at 630°C, 125 minutes at 650°C	Resistivity and small-angle x-ray scattering
F-3	14.0 a/o Mo	Annealed 24 hours at 1,000°C and water-quenched; cold-rolled to 20% reduction of area; annealed 5 hours at 650°C	Electron microscopy and small-angle x-ray scattering

TABLE 1--*Continued*

TREATMENT AND STUDIES MADE FOR EACH SPECIMEN

Specimen Number	Composition	Treatment	Studies Made
F-4	14.0 a/o Mo	Annealed 24 hours at 1,000°C and water-quenched; cold-rolled to 20% reduction of area; annealed 140.5 hours at 500°C, 10.5 hours at 650°C	Resistivity and small-angle x-ray scattering
F-5	14.0 a/o Mo	Water-quenched from 1,000°C; cold-rolled to 20% reduction of area; annealed in hot stage of electron microscope	Electron microscopy
F-6	14.0 a/o Mo	Annealed 15 hours at 1,000°C and water-quenched; annealed in hot stage of electron microscope	Electron microscopy
W-1	14.0 a/o Mo	Annealed 1 hour at 850°C and water-quenched	Field-ion microscopy
W-2	14.0 a/o Mo	Annealed 1 hour at 850°C and water-quenched; annealed 2.5 hours at 700°C	Field-ion microscopy
W-3	20.0 a/o Mo	Water-quenched from 950°C; annealed 110 minutes at 750°C	Field-ion microscopy

more information will be given about the technique itself and about the specimens used.

Preliminary x-ray studies on the 10.5 a/o alloy showed the presence of "superlattice" lines corresponding in position to those of the ordered β phase. According to the phase diagram this alloy is completely within the α-phase region at all temperatures up to the melting point. It was concluded that either the assumed composition of the alloy was incorrect or else the ingot was inhomogeneous. A precision lattice parameter determination was made to verify the composition of the alloy. The x-ray data were obtained with a General Electric XRD-5 diffractometer and the calculations were made on an IBM 7090 computer using a Fortran program supplied by M. H. Mueller of Argonne National Laboratory. The lattice parameter of the alloy was measured to a precision of 0.01% and compared to the lattice spacing vs. composition data of Guthrie and Stansbury [91]. Within the accuracy that could be obtained from the graph, the composition of the alloy was exactly 10.5 a/o Mo as expected. The ingot was then re-homogenized for 100 hours at 1,000°C. After this treatment the superlattice lines disappeared and metallographic examination showed that the alloy was homogeneous and free from any evidence of coring. It was assumed therefore that either

the alloy was not completely homogeneous in the as-received condition or else some surface absorption of oxygen or other impurity had been responsible for the appearance of the β phase which would not otherwise have been stable in the binary Ni-Mo system. The 100-hour homogenizing treatment was performed in an evacuated Vycor tube.

3.2 *Heat Treatment of Specimens*

During this research, annealing treatments were performed on the various alloys for two reasons. One reason was to recrystallize the work piece so that it could be further cold-rolled, cold-drawn, or machined to the proper shape. For such work the alloys were annealed in the temperature range 800-1,000°C in dry hydrogen or in an evacuated Vycor cylinder. The other reason for annealing the alloys was to study various aspects of the K-state after appropriate heat treatments. For this purpose the specimens were sealed in evacuated Vycor cylinders. To further protect them against oxidation, Zr chips were placed in the tube and the specimens were wrapped in Ta foil.

The pumping station used for sealing the specimens in the evacuated Vycor cylinders is shown in Figure 19. This system was composed of an oil diffusion pump, a roughing pump, and a liquid-nitrogen cold trap between

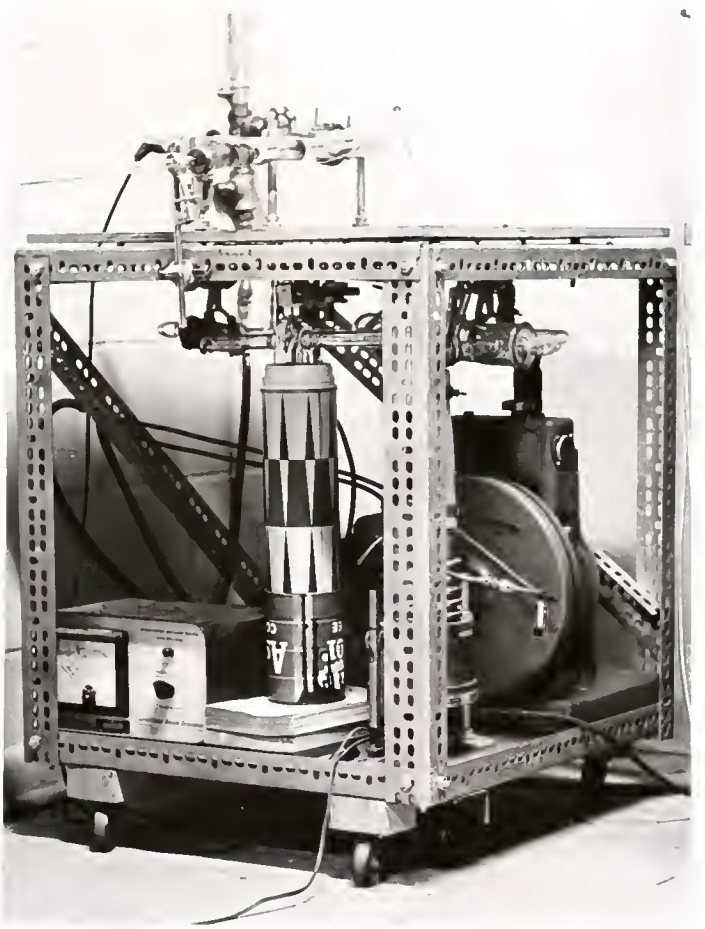

Fig. 19--Photograph of the pumping station used to seal specimens in evacuated Vycor capsules for heat treatment.

the diffusion pump and the specimen. The system was capable of evacuating the capsule to a pressure of 10^{-5} torr. The purpose of the cold trap was to increase the pumping rate by condensing volatile impurities and to prevent back-streaming of the hot diffusion-pump oil to the specimen. The sealing-off procedure was as follows: The specimen and the Ta foil were completely degreased, rinsed in distilled water, and allowed to dry thoroughly in air. These materials along with the Zr chips were loaded into a clean Vycor capsule which was then necked down with a gas-oxygen torch. The Vycor tube was connected to the vacuum system with heavy-wall Tygon tubing, evacuated to a pressure of 1 to 3 x 10^{-5} torr, and sealed off in the neck area with the gas oxygen torch. The Zr chips used in the process had been previously outgassed in vacuum at 1,000°C until the pressure dropped to 10^{-6} torr.

After each heat treatment the specimens were quenched in room-temperature water by rapidly removing the Vycor cylinder from the furnace, immersing it in water, and crushing the cylinder the instant it came into contact with the water. With few exceptions the specimens heat-treated and quenched in this manner exhibited a bright clean surface with no evidence of oxidation. Occasionally a specimen showed a slight tarnish, but this was easily

removed with a light electropolish. This slight tarnish probably occurred during the quench.

3.3 *Metallography Procedure*

During this study several specimens were examined by optical microscopy to determine whether or not they were homogeneous. For this purpose the specimens were rough-polished in the following sequence: 320 grit SiC paper; 400 grit SiC paper; 600 grit SiC; 600 grit SiC powder on billiard cloth. Final polishing was done with 0.3-micron alumina powder on a nylon cloth and with 0.06-micron alumina powder on Buehler AB microcloth. The specimens were etched by swabbing with two separate solutions. Solution I consisted of three parts 20% (by volume) HCl to one part of 30% H_2O_2. Solution II consisted of one part of 10% (by weight) chromic acid to one part of 50% (by volume) HCl. Both solutions were applied hot. Solution I was applied to reveal the grain structure. To reveal the β phase, solution I was applied lightly and then solution II was applied.

3.4 *Resistivity Measurements*

Resistivity measurements for this study were made with a precision Kelvin bridge using specimens in the forms of strips and foils. A schematic view of the apparatus

is shown in Figure 20. It consists of d.c. power source, a variable slide-wire resistor, a ratio box, a galvanometer to indicate the null point, a double-pole switch, a contact switch, and low-resistance leads and clips.

The Kelvin bridge technique is similar in principle to the Wheatstone-bridge method of measuring resistances. The Wheatstone bridge, however, cannot be used for specimens whose resistance is lower than about 0.1Ω because the resistance of the specimen leads and contacts then becomes an appreciable fraction of the resistance of the specimen. This problem is overcome in the Kelvin bridge technique by making two essential changes. The circuit is designed so that the current leads and the gage leads are separate, and the contact resistance is minimized by placing the gage leads in series with high resistances in the ratio arms. The precision of the bridge itself is on the order of 0.04% for values as low as 0.000025Ω.

The actual precision obtained in this work was about 0.2% at resistance values of roughly 0.005Ω which is considerably less than the precision of the Kelvin bridge. The principal limitation was the error in replacing the sample for successive measurements. Although the contact resistance was minimized by using the Kelvin-bridge method, the limiting factor in precision was the

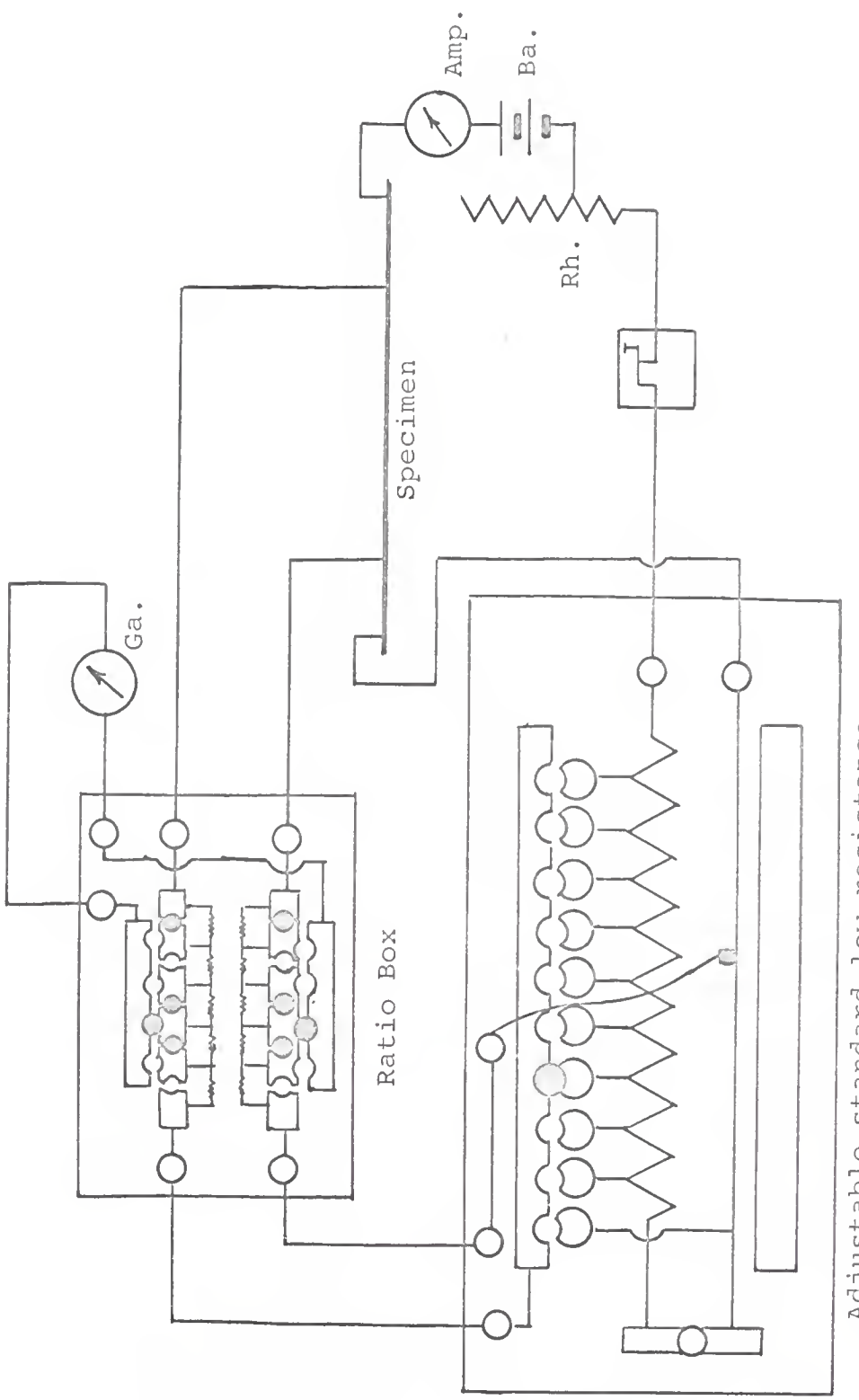

Fig. 20--Schematic View of the precision Kelvin bridge.

variation of the contact resistance from one placement of the specimen to the next. Contact between the specimen and the leads was effected by means of needle-point clips. Small indentations were made in the specimens so that the clips could be replaced in exactly the same position each time.

It was not necessary to make corrections of the resistance for variations in room temperature since, for the alloys investigated, the temperature coefficient of resistivity is much less than the replacement error. This conclusion was verified by placing a specimen in an oil bath and measuring its resistance as the temperature of the bath was varied. It was found that a maximum variation of 0.12% occurred as the temperature of the bath varied from 24.5-43°C. Care was taken not to move the specimen during this experiment, and the oil was stirred continuously to insure a uniform temperature.

3.5 *X-ray Diffuse Scattering Measurements*

Application of the diffuse scattering of x-rays to the study of atomic order in solid solutions has been reviewed in Chapter I, Section 1.2. In the present research the diffuse scattering of x-rays by the powder method was employed to determine the relationship between local order and the resistivity anomaly of the K-state in

Ni-Mo alloys. Diffuse-scattering measurements were made on two specimens, designated X-1 and X-2, after various mechanical and thermal treatments. Specimen X-1 contained 10.5 a/o Mo and specimen X-2 contained 14.0 a/o Mo. Resistivity measurements were also made on these specimens before and after the x-ray scans.

It was pointed out in Section 1.2 that a much care must be used in order to correctly measure the diffuse-scattering spectrum of an alloy and to put these data into electron units. Most of the "background" that is ordinarily observed in a routine diffractometer scan comes from extraneous sources such as scattering from the beam-confining slits and from scattering by the air in the path of the primary beam. Very little of this observed intensity actually originates in the specimen itself. This extraneous scatter must be eliminated by careful adjustment of slits and baffles and by removing the air in the vicinity of the specimen. In addition to these precautions a monochromator must be used either in the primary or in the diffracted beam to eliminate additional background scattering from the specimen caused by the continuous part of the x-ray spectrum. The monochromator is also necessary to permit conversion of the scattered intensity into electron units. If the wavelength of the radiation is well defined, as in

the case of a monochromated beam, the absolute intensity of certain amorphous materials can be theoretically calculated for high angles. By comparing the intensity of the specimen with that obtained from such a standard, one can obtain the intensity of the specimen in electron units. For this study the standard material was polystyrene (C_8H_8) whose intensity at $2\theta = 100°$ with CuKα radiation is 66.2 eu.

The two basic experimental arrangements for x-ray diffuse-scattering measurements are shown in Figure 21. In Figure 21a the monochromator is in the primary beam and causes the primary beam to converge onto the specimen. In Figure 21b the monochromator is in the diffracted beam with the result that a diverging primary beam bathes the specimen. The former technique is usually employed, primarily because the monochromator can be ground with a double curvature to focus the laterally-diverging rays and thereby increase the intensity. This technique is desirable for measurements on single crystals. The latter technique offers a certain advantage, however, in that the diverging primary beam covers a much larger area of the specimen. In cases where large-grain materials are being studied, variations in intensity due to grain size may be the limiting factor. For such work the latter

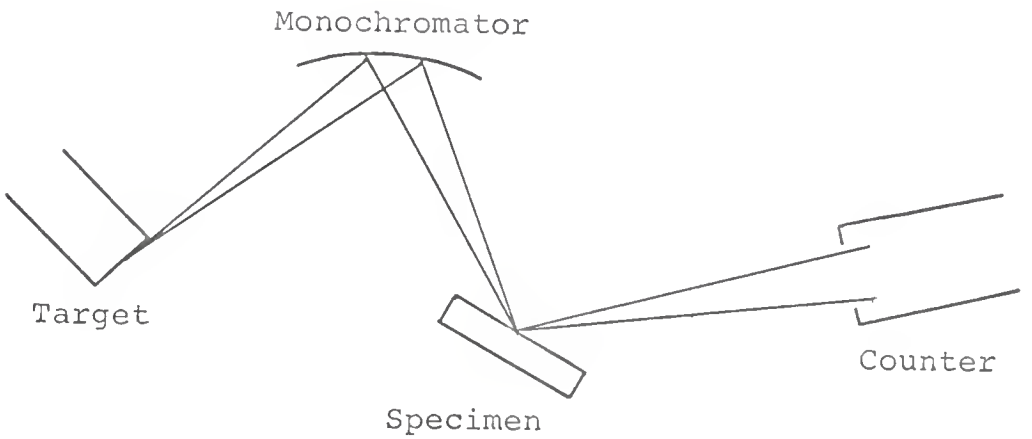

a.

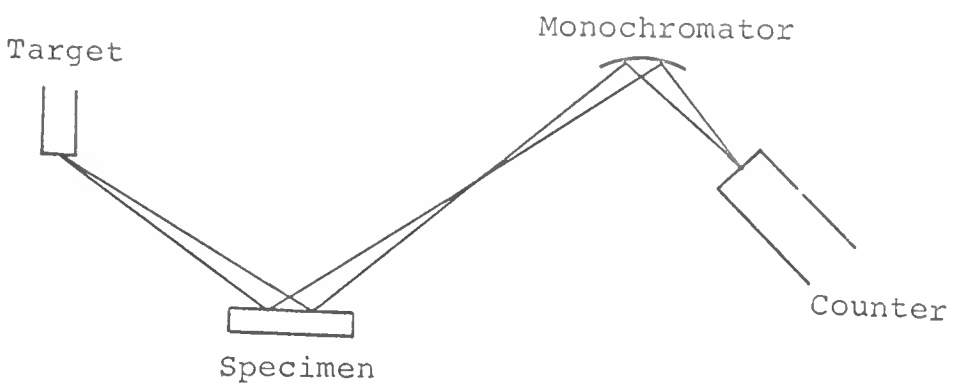

b.

Fig. 21--Schematic illustration of experimental arrangements used for x-ray diffuse-scattering measurements.
a. Monochromator in primary beam
b. Monochromator in diffracted beam

technique is preferable, and for this reason the technique shown in Figure 21b was chosen for the present work.

A schematic view of the complete diffuse scattering apparatus used in this study is shown in Figure 22, and photographs of the actual apparatus are shown in Figure 23. A Norelco diffractometer with a stationary specimen holder was used in conjunction with the AMR-3202 LiF monochromator attachment. Copper $K\alpha$ radiation filtered with Ni was used with an xenon proportional counter and a pulse-height analyzer. Three important modifications of the standard equipment were made. These additions were: (1) an extra beam-confining slit in the primary beam, (2) a vacuum specimen chamber, and (3) an adjustable scatter slit in the diffracted beam.

It was found that without the extra beam-confining slit (S_1 in Figure 22) the "invisible" fringes of the primary beam would completely overshoot the specimen at low angles and would enter the counter directly. This effect produced a very high background and made the data useless at low angles. The width of the slit was determined by closing it until it began to cut into the visible part of the primary beam produced by the 1°-divergence slit. The critical width was determined by means of a fluorescent screen. The beam-confining slit was then re-opened slightly

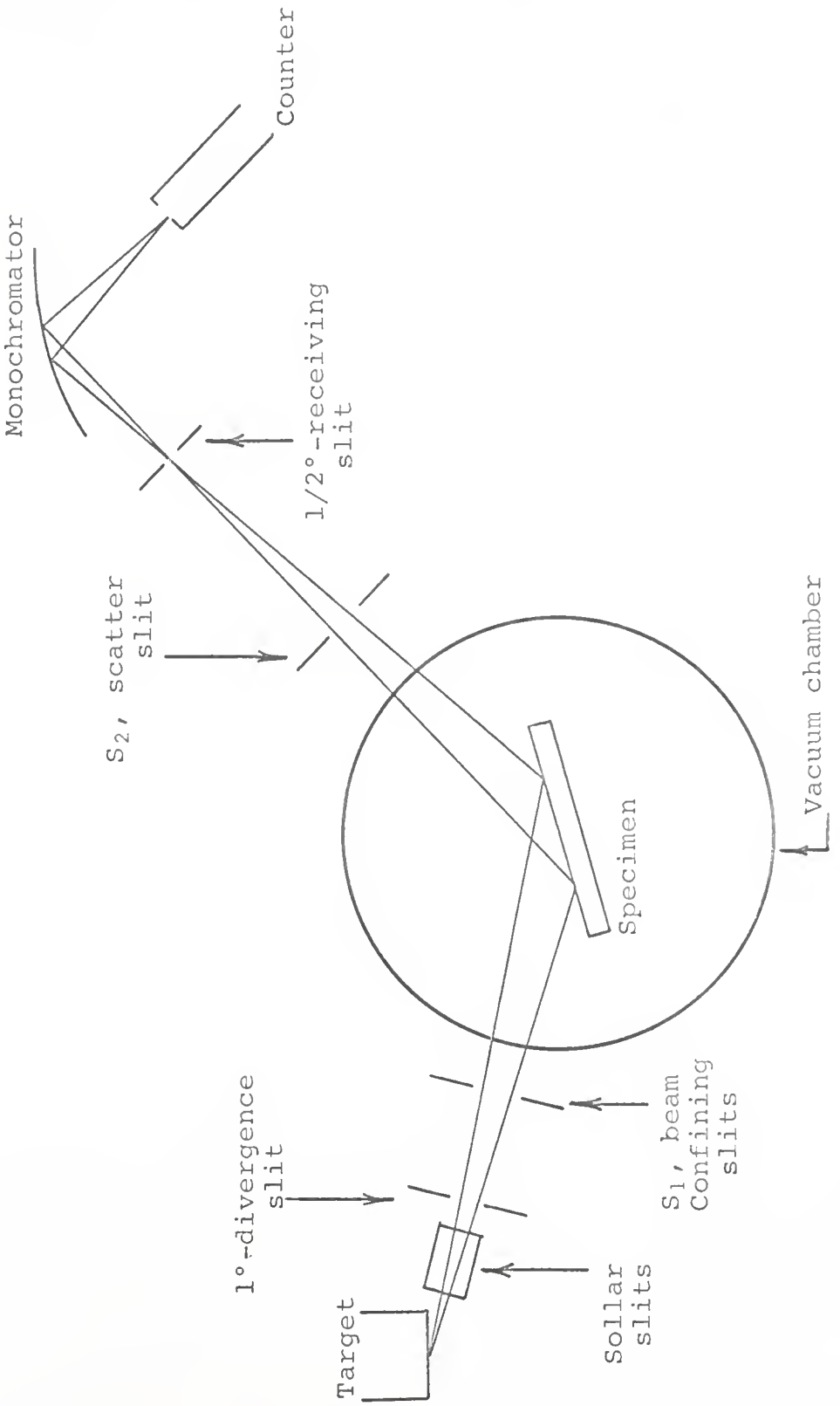

Fig. 22--Schematic drawing of the x-ray diffuse-scattering apparatus used in the present research.

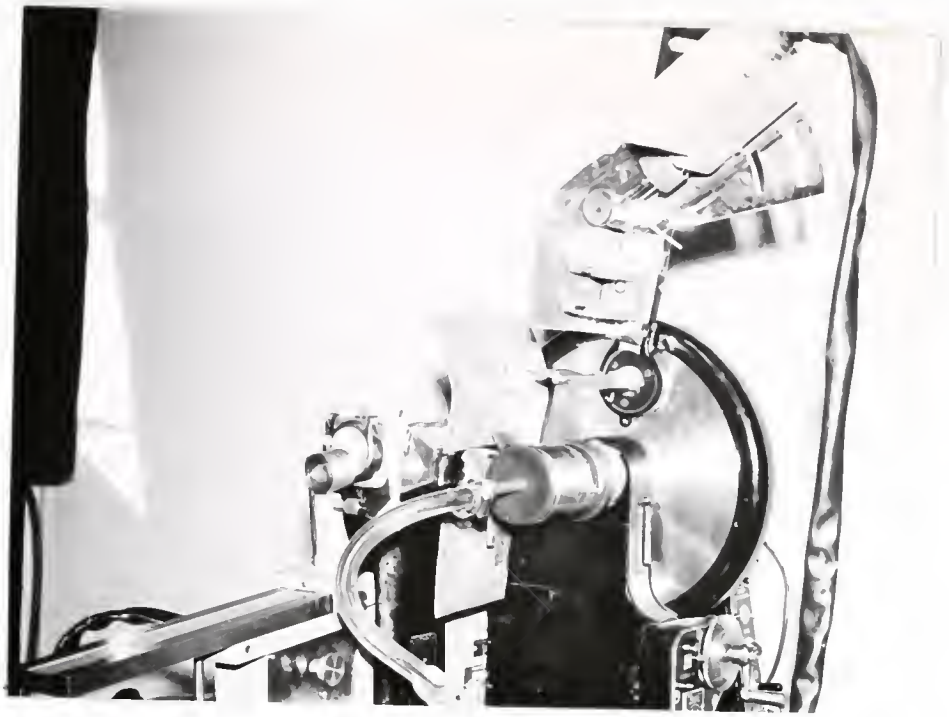

a.

b.

Fig. 23--Photographs of the diffuse-scattering apparatus.
a. Complete view of the apparatus
b. View of the vacuum specimen chamber

to prevent the primary beam from striking it directly. In this way the beam-confining slit was effective in eliminating the diverging invisible fringes of the primary beam as well as the scatter from the 1°-divergence slit.

The purpose of the vacuum specimen chamber was to eliminate scattering produced by the air in the path of the primary beam. Since a large fraction of this scattered radiation is unmodified it can be diffracted by the monochromator and enter the counter. Air scattering becomes very large at low angles as is demonstrated in Figure 24, which is a comparison between the intensity recorded from a pure Ni specimen with and without evacuation of the air in the specimen chamber. It can be seen from this plot that the intensity of the air scattering is several times larger than the intensity from the specimen at low angles.

A photograph of the specimen chamber is shown in Figure 23b. It was found that ordinary one-inch wide cellophane tape served nicely for a window. This tape will support a roughing-pump vacuum, it has good strength, and it has its own adhesive for easy installation. The loss of intensity due to the cellophane window was about 5%; however, this was approximately compensated for by the removal of the absorbing air within the chamber. The

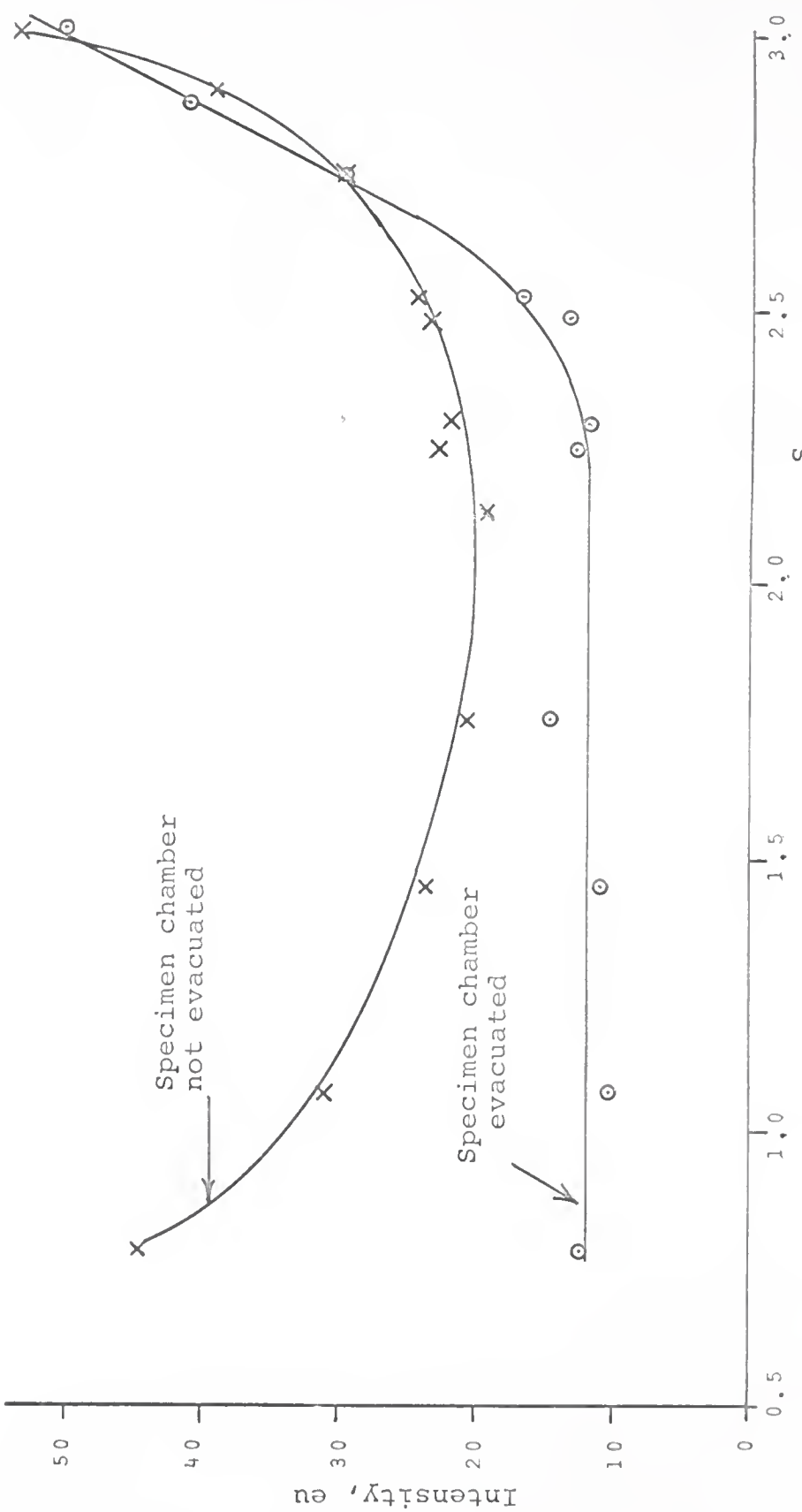

Fig. 24--Measurements of the effect of air scattering on x-ray diffuse-scattering data.

housing for the vacuum chamber was made from a 2-3/8 inch diameter metal cylinder. The cylinder seated against a 5/8-inch thick tapered rubber gasket fashioned from a number 12 rubber stopper.

The third important modification of the standard equipment was the adjustable scatter slit (S_2 in Figure 22). Its purpose was to eliminate from the view of the detector all scattering which originated from points other than those very near the specimen surface. The width of this slit was determined by setting the diffractometer at $2\theta = 28.4°$ to receive the {111} peak of the silicon standard, then reducing the width of the slit until the intensity began to drop. The slit was then re-opened slightly. In this way any scattered intensity from the beam-confining slits and the window of the vacuum chamber could not pass through both S_2 and the receiving slit of the crystal monochromator. The importance of the scatter slit S_2 was clearly demonstrated by the fact that without it the intensity at $2\theta = 11°$ ($S = 0.78$) was approximately 50 eu too high. Measurements could not have been made at low angles without the slit, but as shown in Figure 24 it is not effective in reducing the air scatter at low angles. Air in the immediate vicinity of the specimen surface was responsible for the erroneously-high values

shown in the top curve, and this could be completely eliminated only by evacuating the region around the specimen.

The new AMR LiF monochromators are equipped with a scatter slit to eliminate high background and spurious peaks at low angles in routine work [114]. This scatter slit was not used for the present work since it was desired to have S_2 as close as possible to the specimen, and also because it was important to make this slit adjustable. By adjusting the specimen-to-slit distance and the width of the slit, one can lower the minimum value of θ for which scatter from the beam-confining slits and from the specimen chamber window will begin to effect the measurements. These adjustments can be determined graphically from a scale drawing of the apparatus or they may be determined experimentally as was done in this work.

The specimens used in the diffuse-scattering measurements were in the form of rectangular strips approximately 5 x 1.8 x 0.050 cm. After each heat treatment or rolling operation these specimens were electropolished to remove approximately 0.02 mm from the surface to be examined. The purpose of this operation was to remove any thin oxide or distorted layer that might be present. The electropolishing was done at approximately 0.5 amps per

cm^2 in an electrolyte of 86 cc H_3PO_4, 5 cc H_2SO_4, and 11 gm of CrO_3. A d.c. power supply was used with a stainless-steel cathode. Resistivity measurements were also made on the x-ray specimens before and after each x-ray scan.

The diffuse-scattering spectra of specimens X-1 and X-2 were studied by step scanning in increments of 2°, 1° or 0.5°, depending on which region of the spectrum was being studied. A minimum of 1,000 counts was taken at each setting which represents a maximum counting error of approximately 3%. A high-intensity copper x-ray tube was used at 50 kv and 38 ma with an xenon proportional counter. Before and after each scan the intensity from the polystyrene specimen was counted, and this was used to convert the intensities to electron units. It was found that variations in the primary-beam intensity during the course of a run were insignificant; therefore, the primary beam intensity was not monitored with a separate counter as is sometimes done.

The use of a standard to correct intensities to electron units is necessary because certain constants such as the absolute intensity of the primary beam can only be determined experimentally. The technique for converting to electron units is based on two equations:

$$I_p = K\left[\frac{N}{2\mu}\right]_p P(\theta_p)\ I_p^{eu} \qquad (12)$$

and

$$I_s = K\left[\frac{N}{2\mu}\right]_s P(\theta_s)\ I_s^{eu} \qquad (13)$$

In the above equations I_p^{eu} and I_s^{eu} are intensities in electron units per atom for the polystyrene standard and for the specimen, respectively. I_p and I_s are the experimentally-measured intensities in counts per second. I_p^{eu} can be calculated theoretically for high angles assuming that the atoms scatter independently. I_s^{eu}, the quantity to be calculated from the experimental data, depends among other things on the nature of the atomic arrangement within the alloy, as was discussed in Chapter I, Section 1.2. The term $P(\theta)$ is the polarization factor and is a function of the diffraction angle θ. The term μ is the linear absorption coefficient, and N is the number of scattering centers (atoms or molecules) per unit volume. The term K is a constant that is independent of the Bragg angle. It depends upon such quantities as the intensity of the primary beam and the geometry of the slits. Since the terms N, μ, $P(\theta)$ and I_p^{eu} are known, one can measure I_p and use equation (12) to determine K. Then by measuring I_s one can use the calculated value of K to determine I_s^{eu} from equation (13). A sample calculation is given in the Appendix.

After the intensity from the specimen is put into electron units per atom, the temperature-diffuse scattering and the Compton scattering must be determined and subtracted. The Compton scattering is tabulated in Sagel [115] in electron units per atom for various elements. One way of compensating for the thermal-diffuse scattering is to make two equivalent sets of measurements, one at room temperature or higher and one at liquid-nitrogen temperature. For each 2θ setting the data are extrapolated linearly to absolute zero, and the residual intensity is that which is due to local order. The technique that was employed in the present study was to compensate for both the Compton scattering and the thermal-diffuse scattering by subtracting the absolute intensity obtained from an equivalent set of room-temperature measurements on pure Ni. Since measurements were made only up to $S = 2.99$, the largest difference in Compton scattering between Ni and Mo is 2.4 eu. Since the compositions of the alloys examined were 10.5 and 14.0 a/o Mo, a maximum difference of 0.4 eu exists between the Compton scattering of the alloys and the Compton scattering of pure Ni. This is well within the experimental error of the measurements. The assumption was also made that the temperature-diffuse scattering of pure Ni is not changed significantly by

alloying with Mo. This is equivalent to assuming, that the Debye temperature of pure Ni remains essentially unchanged. Although this is only a rough approximation it is good enough for a qualitative interpretation of the diffuse scattering due to local order. The alternative mentioned above of linearly extrapolating the data to absolute zero involves the assumption that the energy associated with each normal mode of lattice vibration is kT. This technique is obviously only an approximation because the atoms of the crystal do not actually vibrate independently as classical harmonic oscillators.

A major source of error in interpreting the diffuse scattering was the interference from the {111} primary reflection that occurs at $S \approx 3.04$. This reflection is sufficiently broad, except in a well-annealed specimen to interfere to some extent with the diffuse spectrum at $S = 2.0$, which is approximately the position of the SRO maximum. The exact amount of the interference depends on the breadth and the intensity of the {111} peak, which in turn depends on the degree of distortion and of preferred orientation within the sample. Both the distortion and the preferred orientation change with cold work and with annealing; therefore, it is difficult to make comparisons from one x-ray scan to the next unless the variation in

the interference from the {111} peak is taken into account. This was another factor that led to the choice of using pure Ni to account for that portion of the spectrum to be subtracted.

Measurements were made on pure Ni in the cold-rolled condition (approximately 65% reduction of area) and in the recrystallized condition. These two curves are shown in Figure 25. The interference from the {111} peak actually appears greater in the annealed sample; however, this is misleading for the following reason. The intensity at any point within the range of interference is proportional to the intensity at the maximum of the {111} peak. The intensity at the maximum depends upon the degree of preferred orientation, i.e., the number of grains favorably oriented to produce the {111} reflection. In the case of the cold-rolled specimen the {111} peak was broadened, but at the same time the intensity of the {111} maximum was reduced due to the change in texture.

In the theoretical discussion of the diffuse scattering of x-rays given in Chapter I, it was pointed out that temperature-diffuse scattering increases rapidly in the vicinity of a diffraction peak. The analogy between static atomic displacements by cold work or alloying and dynamic atomic displacements produced by thermal vibrations

was also emphasized. These two types of distortion have a similar effect. Warren [52] has shown that temperature-diffuse scattering near the {111} peak in FCC metals begins to increase rapidly at $2\alpha_0 \sin\theta/\lambda \approx 1.0$, which corresponds to $S \approx 1.70$. Due to the similarity between the diffuse scattering produced by cold work and by thermal vibrations, one would expect cold-work to increase the amount of diffuse scattering near the {111} peak and to lower the value of S for which interference from this peak begins. In Figure 25 it can be seen that the point at which the curves for cold-worked and for annealed Ni begin to depart from one another is approximately S = 1.50. In Figure 26 the cold-worked and annealed Ni specimens have been normalized to the same degree of texture by plotting the excess intensity over that at S = 1.50 on a maximum scale of 100.

The method of correcting the diffuse scattering data from the Ni-Mo specimens for Compton scattering, temperature-diffuse scattering, and interference from the {111} peak was as follows: For the cold-worked state, a constant of 12 eu was subtracted below S = 1.50. For the annealed state a constant value of 12 eu was subtracted for all values of S below 2.30. It can be seen from Figures 25 and 26 that these are the approximate points at which interference from the {111} peak begins in each case,

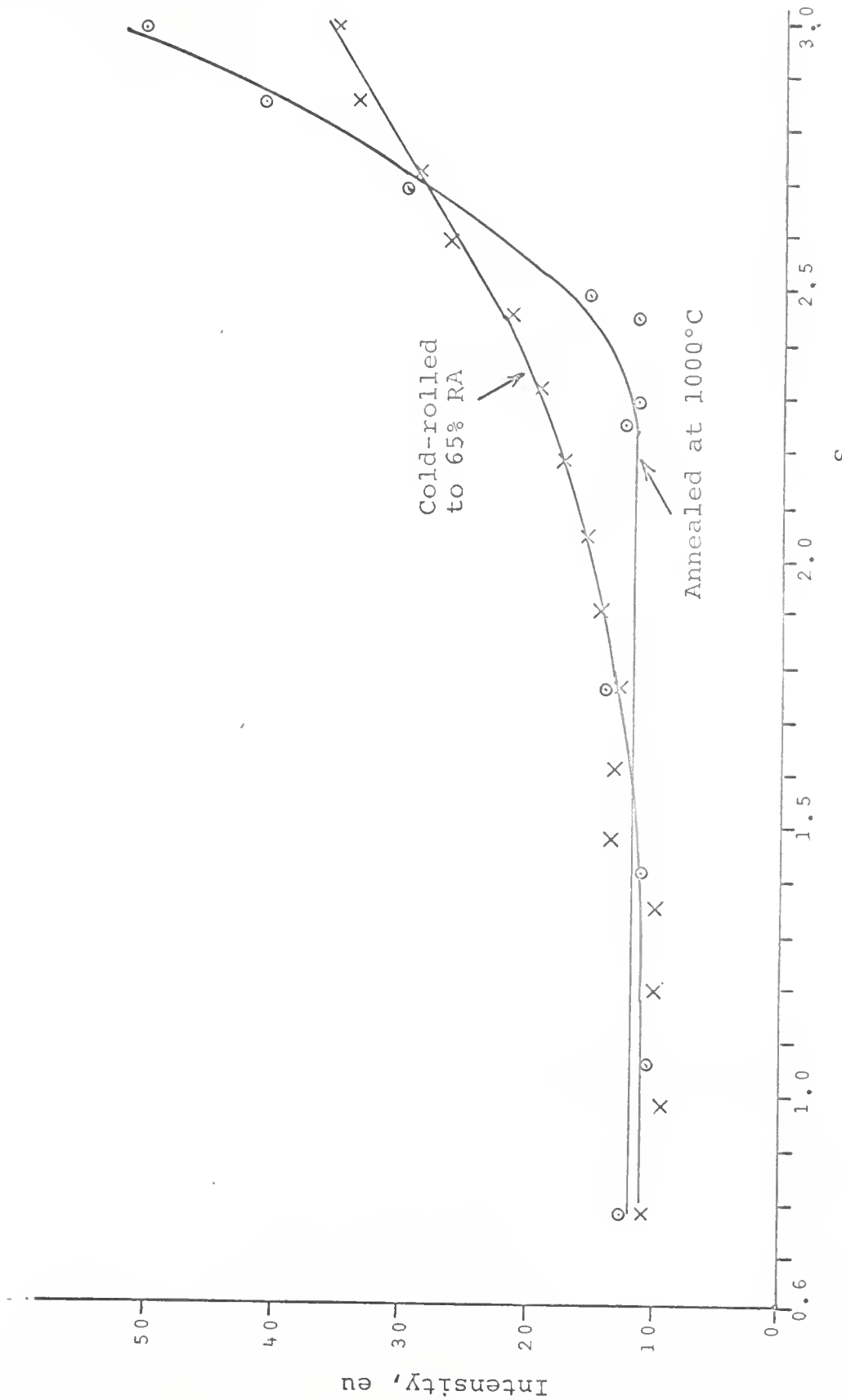

Fig. 25--X-ray diffuse-scattering curves of pure Ni in the cold-rolled and in the annealed conditions.

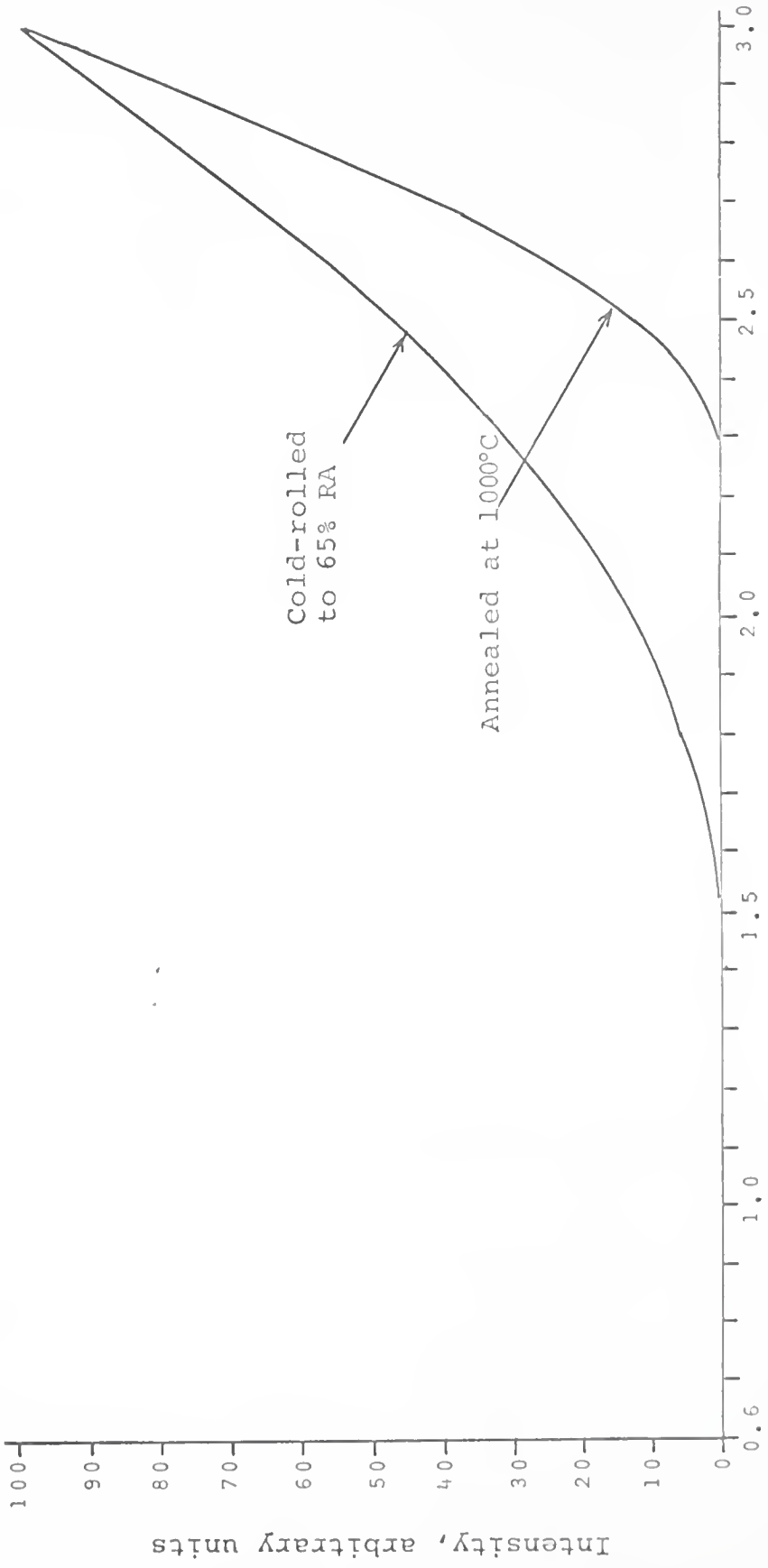

Fig. 26--X-ray diffuse-scattering caused by {111} peak of pure Ni in the cold-rolled and in the annealed condition.

and for s values less than 1.50 or 2.30 respectively the Compton-and temperature-diffuse scattering is approximately constant at 12 eu. The interference from the {111} peak in the cold-worked specimens was determined graphically by smoothly extrapolating the intensity of the {111} peak to a value of 12 eu at s = 1.50. For the annealed state the {111} intensity was extrapolated to a value of 12 eu at S = 2.30.

3.6 *Small-angle X-ray Scattering Measurements*

Small-angle x-ray scattering measurements were made on specimens F-2, F-3, and F-4, all containing 14.0 a/o Mo. These specimens were in the form of foils approximately 0.05 mm thick. These foils were prepared by alternate annealing and cold-rolling until the desired thickness was reached. Resistivity measurements were made on specimen F-2 by the previously described technique to correlate with the small-angle scattering data. Electron-microscopic studies were done on specimen F-3 for the same purpose.

The small-angle x-ray scattering measurements were made on a Norelco diffractometer modified to a Kratky arrangement. This apparatus was built by Professor R. W. Gould of the University of Florida and Professor V. K. Gerold of the Max-Plank Institute für Metallforschung

primarily for the study of pre-precipitation phenomenon. A complete description of this apparatus is given in reference [116], and a schematic drawing is shown in Figure 27. The basic difference between this apparatus and the standard Norelco equipment is the precise collimator and the fine slit arrangement on the diffracted-beam side. The Kratky arrangement permits measurements to be made of the (000) peak with a minimum of interference from the primary beam.

For the small-angle scattering measurements a molybdenum tube was used at 50 kv and 20 ma. The detector system consisted of a scintillation counter and a pulse-height analyzer. A Zr filter was employed on the diffracted-beam side. A certain amount of background was caused by air scattering. Since it is difficult to remove air scattering at low angles by evacuating the region around the specimen, the background was compensated for by comparison with data from a pure Ni specimen of equivalent thickness.

3.7 *Electron-Microscopic Studies*

A Phillips Em-200 electron microscope for the purpose of studying the precipitation of the β phase was used to examine thin foils of the Ni 14.0 a/o Mo alloy in transmission. The purpose of this part of the work

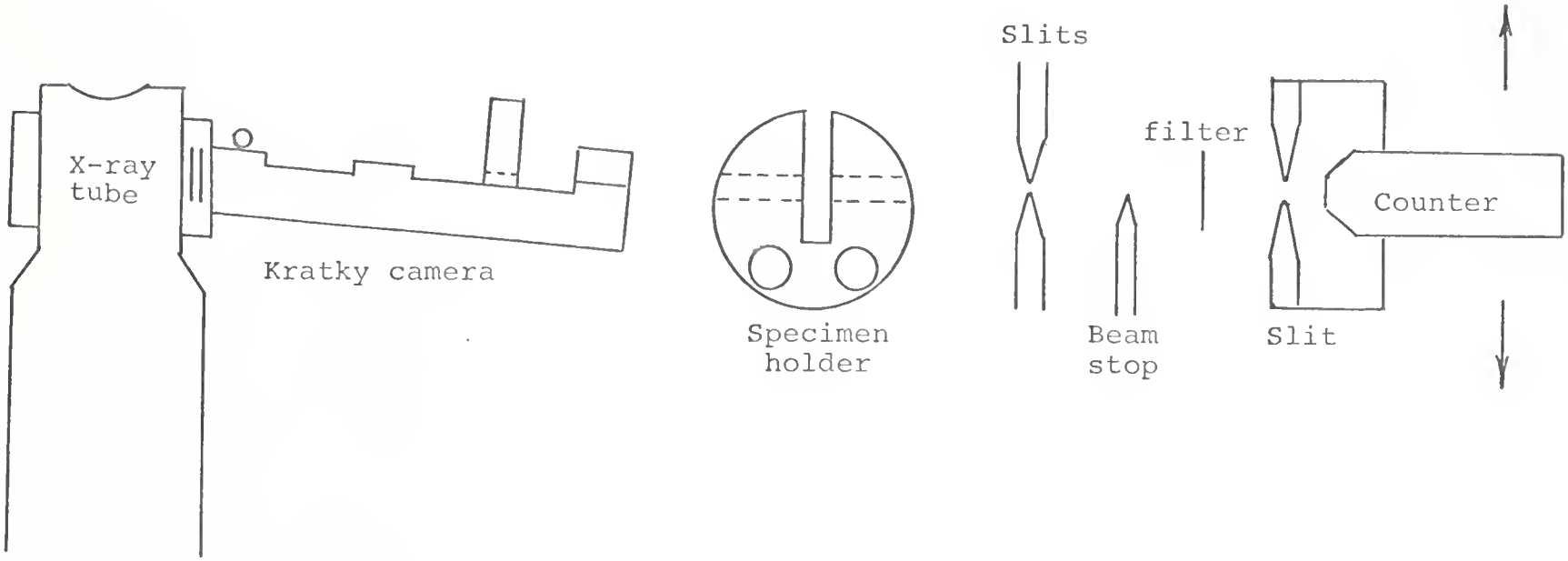

Fig. 27--Schematic illustration of the x-ray small-angle-scattering apparatus (after Gould and Gerold).

was to study the precipitation of the β phase. Thin foils were prepared from specimens F-3, F-5, and F-6, the histories of which are given in Table 1. In some cases the foils were studied by annealing inside the electron microscope by means of a high-temperature specimen holder purchased from the Ladd Company. The information obtained in the electron microscopic study was correlated with the resistivity and small-angle x-ray scattering data.

The "disc" method was used to prepare thin foils for the electron microscope. This technique is a combination of jet machining and preferential electropolishing by the Bollman [117] method using pointed cathodes. Small diameter discs were cut from the foil specimens to be studied. These discs were of the proper diameter to just fit into the microscope specimen holder. The starting thickness was approximately 0.05 mm. These discs were then electropolished in the center by using a small stream of electrolyte until a suitable "dimple" was formed. The disc was then further electropolished preferentially in the center by the Bollman method until the first hole appeared. The specimen was then rinsed in distilled water and ethyl alcohol and placed in the microscope. The same electrolyte that was used to electropolish the x-ray specimens was also used in the preparation of these specimens.

Even though the disc method is one in which reasonable control can be exercised in the preparation of thin metal foils, the percentage yield of usable specimens is still quite low. Only a fraction of the specimens prepared actually possess relatively large areas thin enough to be viewed in transmission.

3.8 *Field-Ion Microscopy*

Wire specimens containing 14.0 a/o and 20.0 a/o Mo were examined in the field-ion microscope [84,85]. The microscope that was used was designed and built by Professor J. J. Hren and graduate assistants R. W. Newman and R. C. Sanwald of the University of Florida. The specimens were examined at liquid-hydrogen temperature by means of a special design of the microscope which included a liquid-hydrogen Cryo-Tip built by Air Products, Inc.

The wire specimens for the field-ion microscope were prepared in the following manner. Small strips were cold-rolled to a thickness of 1 mm. Pieces measuring approximately 1 mm square by 70 mm long were machined from these strips. These pieces were alternately annealed and cold-drawn into wires with a diameter of approximately 0.50 mm. The wires were then electropolished to a final diameter of approximately 0.15 mm, using the same electrolyte which was used to electropolish the x-ray specimens.

It was pointed out in Chapter I, Section 1.4 that the wire specimens must be electropolished to a very small radius tip in order to obtain suitable images in the field-ion microscope. The small radius was obtained by electropolishing the 0.15 mm wires with an a.c. voltage source in an electrolyte of 20% (by volume) HCl. A thin layer of the electrolyte, approximately 2 to 3 mm thick, was allowed to float on a heavier fluid layer of CCl_4. The specimen was connected to one electrode and allowed to penetrate through the electrolyte into the CCl_4 layer. The other electrode consisted of a cylindrical stainless steel shell with a vertical cut made for viewing the specimen. The specimen was polished until the bottom point dropped away. A very light polish was then applied to round-off the tip. The final polish was necessary because the bottom half of the wire actually falls away by fracture when the thickness of the wire in the vicinity of the tip becomes a few atom diameters. The fracturing leaves a heavily cold-worked and irregular tip that must be rounded-off by further polishing. If the final polish is too prolonged, however, the tip becomes too large to produce a suitable image.

Specimen images were obtained by using both He and Ne as the ionizing gas. Voltages in the range 5-30 KV

were used depending on the radius of curvature of the specimen tip. Photographs were taken after successive layers were evaporated under the influence of the high field. On several occasions it was possible to determine the exact number of atomic layers removed between each photograph in a sequence.

CHAPTER IV

EXPERIMENTAL RESULTS AND DISCUSSION

In this chapter of the thesis the experimental results are discussed as they are presented. Some of the peculiar properties of the K-state are shown in the first section in which data on the effect of mechanical and thermal treatments on the resistivity of Ni - 10.5 and Ni - 14.0 a/o Mo alloys are presented. In the next section the correlation between resistivity and SRO is discussed. The x-ray diffuse scattering measurements are presented and interpreted in detail. Following this, a discussion is given on the field-ion microscopic results from which certain conclusions are drawn about the nature of SRO in Ni-Mo alloys. In the final section, the precipitation of the β phase in Ni - 14.0 a/o Mo alloys is discussed. The electron microscopic and small-angle x-ray scattering data are presented in connection with the precipitation process.

4.1 *Effect of Cold-work and Annealing Treatments on the Resistivity of Ni - 10.5 a/o and Ni - 14.0 a/o Mo Alloys*

One of the interesting properties of the K-state is shown in Figure 28. The resistivity for Ni - 10.5 and Ni - 14.0 a/o Mo alloys is plotted as function of the amount

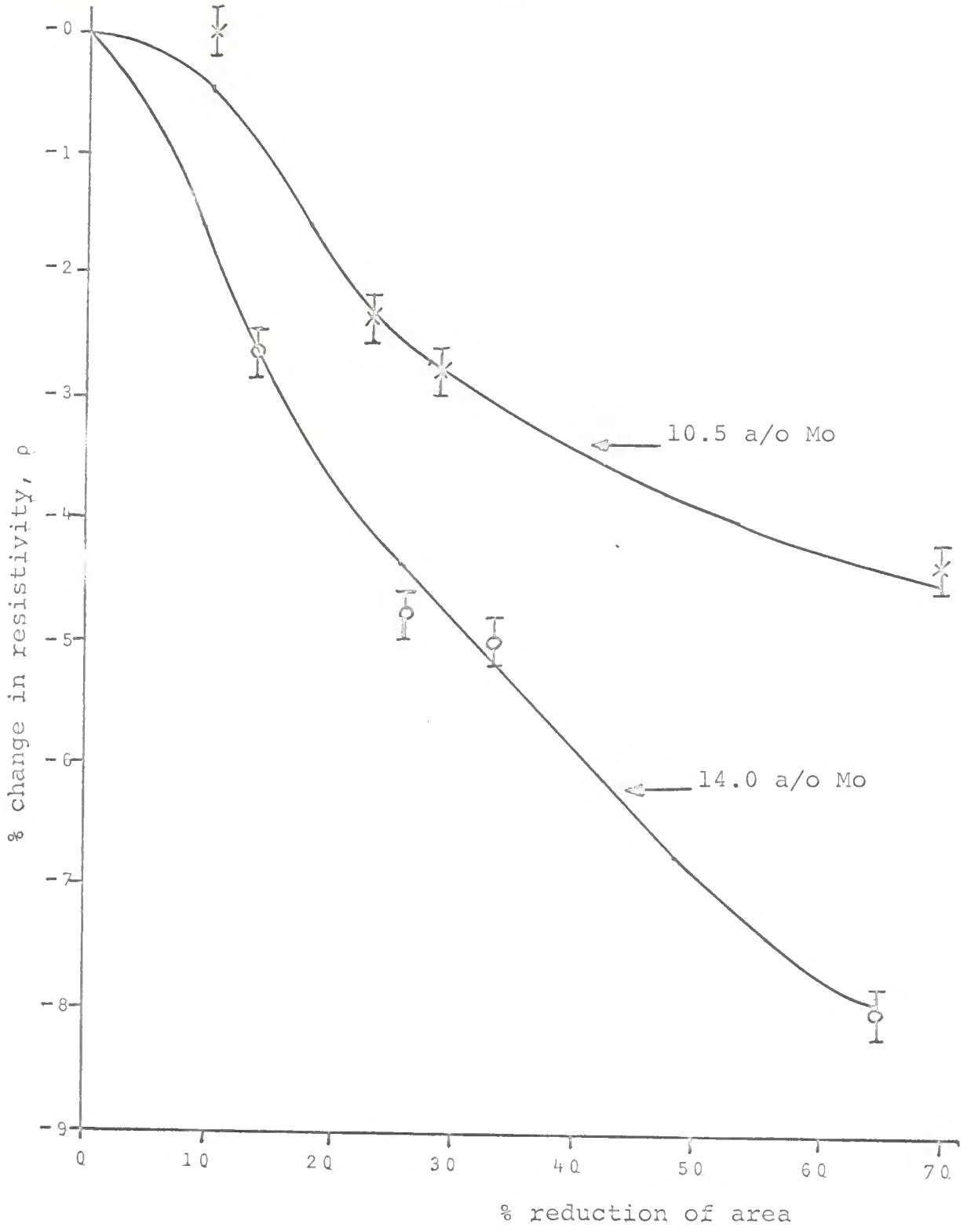

Fig. 28--Effect of cold rolling on the resistivity of the Ni-10.5 a/o Mo alloy and the Ni-14.0 a/o Mo alloy.

of cold rolling. These specimens were in the solution-heat-treated state (annealed for 24 hours at 1,000°C and water-quenched) prior to deformation. It can be seen that cold rolling reduced the resistivity, in contrast to what occurs in normal alloys. It will be shown in the next section, that this reduction of resistivity can be attributed to the destruction of SRO which is quenched-in from 1,000°C. In these alloys, SRO produces a higher resistivity than does the random solid solution. The specimens were not reduced further than indicated in the figure because of the danger of cracking; however, it appears from extrapolation of these curves that the resistivity could be reduced even further by more cold rolling. The decrease in resistivity was more pronounced in the 14.0 a/o alloy because of the fact that a greater degree of SRO is possible in an alloy that has a higher concentration of solute.

In Figure 29 the effect of isothermal annealing of a 10.5 a/o alloy which was initially in the cold-worked state is shown. These data were taken from specimen R-1 which was solution-heat-treated, cold-rolled to 29.2% reduction of area, and then isothermally annealed at 500°C for a total time of 199 hours. At various stages of the annealing process the specimen was quenched and its resistance measured. The zero in this plot corresponds to the solution-heat-treated state. The resistance of the specimen in the

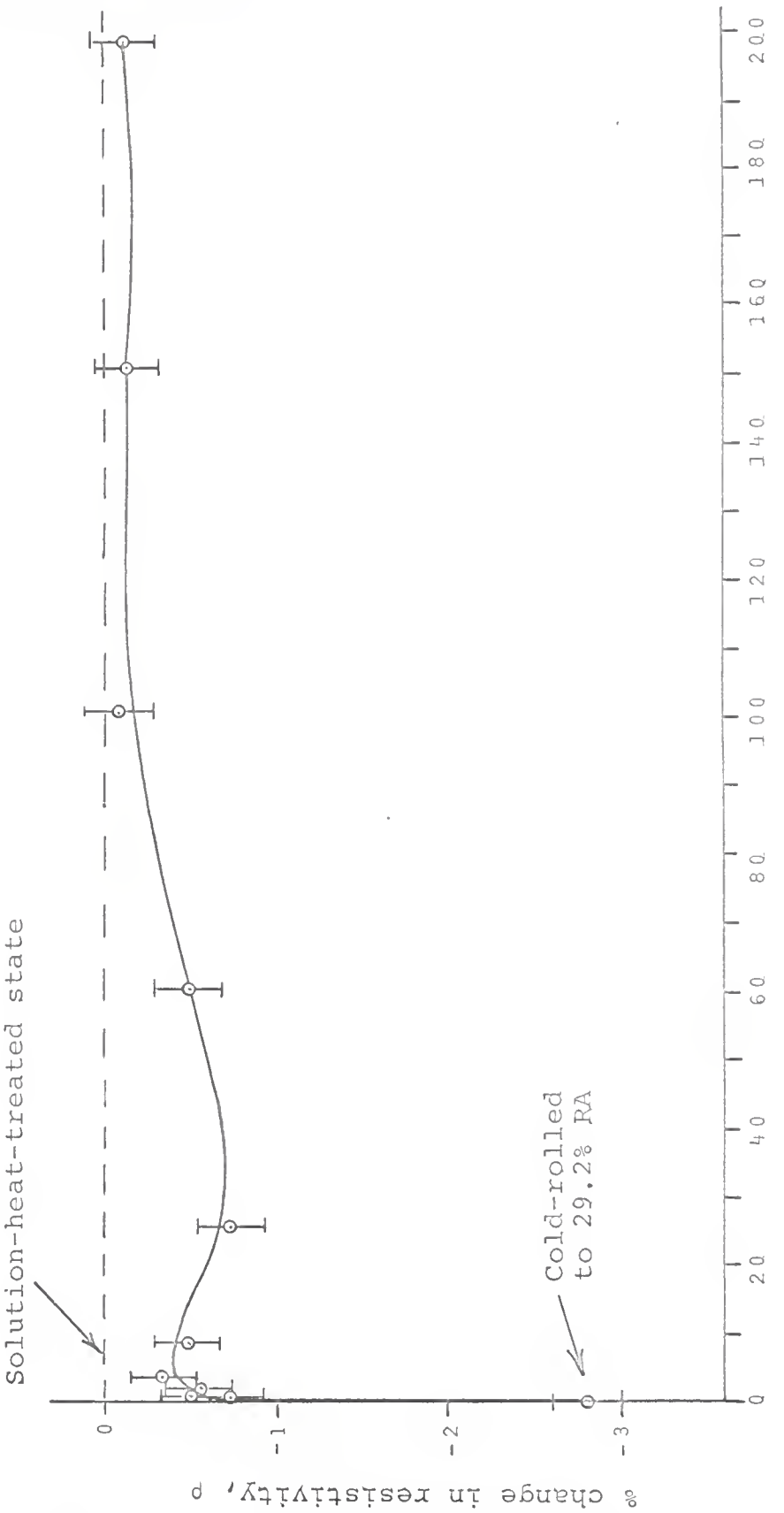

Fig. 29--Change in resistivity of a cold-rolled Ni-10.5 a/o Mo alloy (specimen R-1) on annealing at 500°C.

cold-worked state was lower than that of the solution-heat-treated state due to the partial destruction of SRO, as was discussed in the preceding paragraph. On annealing at 500°C, there was a sudden increase in resistivity above that for the cold-worked state. Again this behavior is contrary to what occurs in normal alloys. It will be shown in the next section that this sudden increase in resistivity is caused by a restoration of the SRO destroyed by cold work. Following this almost instantaneous increase of resistivity there was a slower increase which extended to a time of about eight hours. At this point the curve entered a second stage during which the resistivity underwent a slight decrease. After a time of roughly 40 hours there was another gradual increase which ended after about 100 hours. From this point on the resistivity remained essentially constant.

The rapid initial increase in resistivity is consistent with the establishment of SRO because only short diffusion distances are required. Iida [118] has treated the problem of ordering kinetics both theoretically and experimentally in Ni_3Fe annealed just below the critical temperature of 490°C. He found four distinct stages during the establishment of LRO. The first stage occurred during the time interval 0 to 20 minutes. He attributed this stage to the rapid re-arrangement of the state of imperfections.

The second stage was found to occur during the time interval 20 minutes to 10 hours. He attributed this period to the development of SRO. It has already been noted that the first stage of the curve in Figure 29 appears to be essentially complete after about eight hours, this observation is in qualitative agreement with the conclusion of Iida that SRO is near completion within approximately 10 hours. The rest of the curve may be interpreted in the following way: Following the initial rapid increase in resistivity there was a slow but continuous increase which extended to approximately 100 hours because of a very slight but steady increase in the degree of SRO. This steady increase in resistivity was interrupted during the period 10 to 40 hours by a recovery stage that caused a slight decrease in resistivity. A similar recovery stage was noted by Chen and Nicholson [6] in cold-worked Ag-Pd alloys. They attributed the recovery stage to the annihilation of excess vacancies within the lattice. It seems, however, that part of the recovery could be accounted for by the rearrangement of dislocations.

In Figure 30 the effect of annealing an alloy of 14.0 a/o Mo initially in the cold-rolled state is shown. These data were taken from specimen R-2 in a manner similar to that of R-1 except that the annealing temperature was

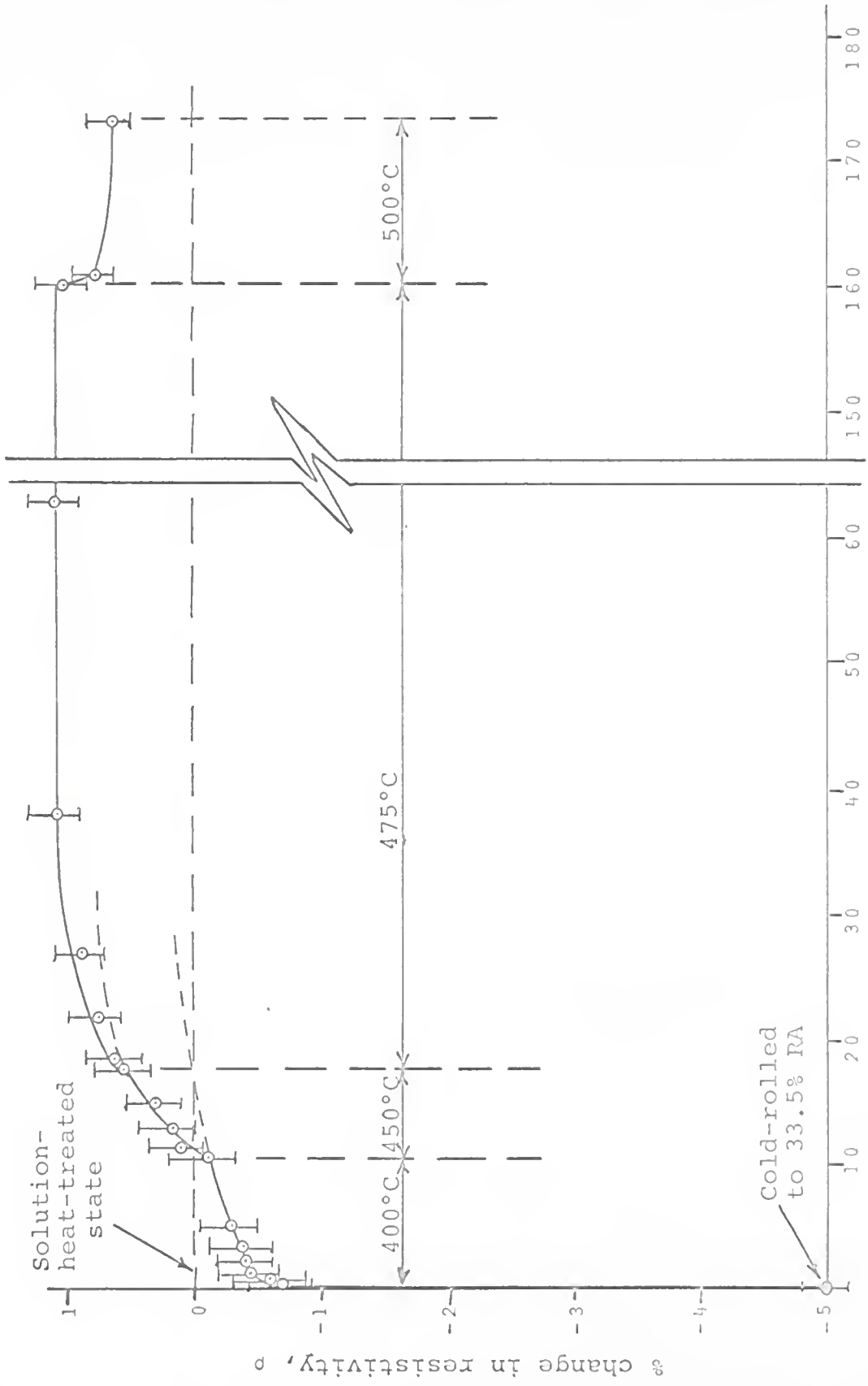

Fig. 30--Change in resistivity of a cold-worked Ni-14.0 a/o Mo alloy (specimen R-2) on annealing.

changed periodically. Once again the resistivity of the cold-worked state was substantially lower than that of the solution heat-treated state due to the partial destruction of SRO. Upon annealing at 400°C there was a rapid initial increase in resistivity followed by a slower exponential increase that continued beyond 10 hours. As the temperature was changed to 450°C a break in the curve occurred when the resistivity suddenly began to increase at a faster rate. A similar break occurred at 18 hours when the annealing temperature was changed to 475°C. The resistivity ceased to change after about 40 hours. After 112 hours at 475°C the temperature was changed to 500°C at which time a slight decrease in resistivity occurred.

Several features of the curve in Figure 30 are worth noting. First of all the abrupt increase in slope with increasing temperature is consistent with the proposal of Popov *et al.* [29] that the K-state in Ni-Mo is associated with the migration of point defects. It will be shown later from the diffuse-scattering data that the increase in resistivity upon annealing a cold-worked 14.0 a/o Mo alloy is also associated with an increase in the amount of SRO. By extrapolating the 400°C and 450°C portions of the curve in Figure 30 one can see that the equilibrium state of SRO was not obtained by annealing at these temperatures because the extrapolated values of resistivity are not in

the correct order. If equilibrium had been obtained, the higher values for resistivity would occur for the lower annealing temperatures since SRO decreases with increasing temperature. It was pointed out in Chapter II, section 2.3 that the equilibrium state of SRO is not readily attained at temperatures below about 500°C according to the data of Stansbury *et al.* [9] and of Sukhovarov *et al.* [30]. It can also be seen from Figure 30 that the resistivity decreased slightly when the temperature was changed from 475°C to 500°C indicating that the equilibrium state of SRO is obtained rather quickly at 500°C.

On annealing at 500°C neither the 10.5 a/o Mo alloy nor the 14.0 a/o Mo alloy showed resistivity values significantly different from those in the solution-heat-treated condition, which presumably represented the state of SRO existing at 1,000°C. One would expect that if the resistivity anomaly were indeed due to SRO, the resistivity at 1,000°C would be lower than that at 500°C. It was also pointed out in Chapter II, Section 2.3 that unless a specimen underwent an extremely rapid quench from 1,000°C, the state of SRO that would exist would represent that of some temperature lower than the quenching temperature. It will be seen later from the x-ray data that in "bulk" pieces, such as the "R" and "X" type specimens, the quench was far from ideal and the degree of order after quenching

from 1,000°C was approximately the same as that for specimens annealed at 500°C. The final value of resistivity at 500°C, therefore, should be approximately the same as that in the solution-heat-treated state. In order to destroy SRO in these specimens it is necessary to cold work them. In Figure 31 the effect of annealing bulk specimens at 500°C without the intermediate cold-working step is shown. These data were taken from specimens R-3 and R-4 which contained 10.5 a/o Mo and 14.0 a/o Mo, respectively. There was very little change in the resistivity at 500°C compared to the initial solution-heat-treated state. The above reasoning can be used to explain why the resistivities of specimens R-1 and R-2 were not significantly different from the solution-heat-treated values.

Another interesting feature of the curves in Figure 31 is the second-stage decrease in resistivity that occurs in specimens R-3 and R-4. In these specimens this stage occurs somewhat earlier than in cold-worked specimen R-1 of Figure 29. The fact that the recovery stage takes longer in the cold-worked specimens lends support to the idea suggested earlier that at least a part of the recovery is caused by the rearrangement of dislocations.

In Figure 32 the effect of annealing on the resistivity of the cold-worked 14.0 a/o Mo alloy is shown. In this case the cold-worked specimen was a foil (specimen F-4)

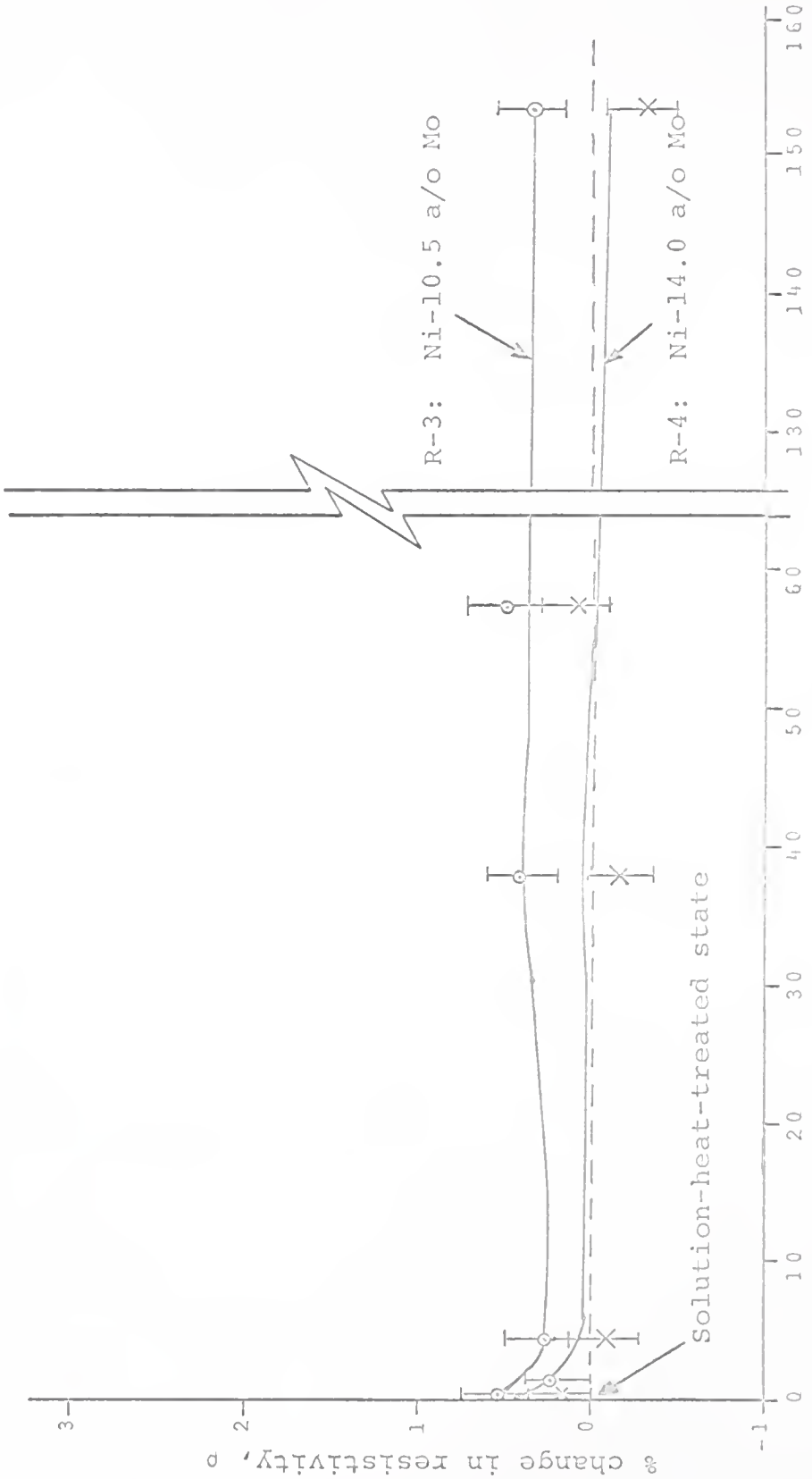

Fig. 31--Change in resistivity of quenched Ni-Mo alloys on annealing at 500°C.

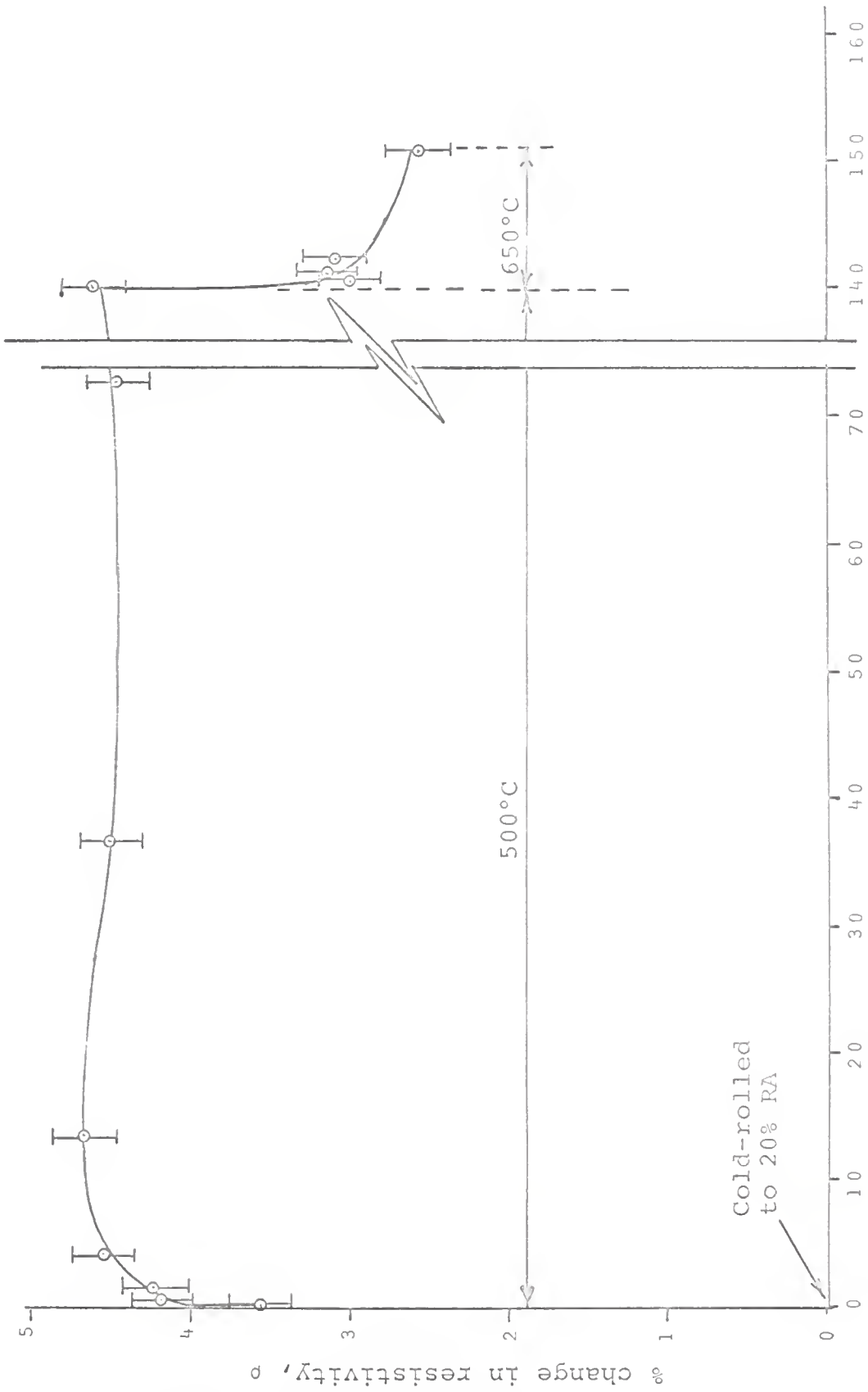

Fig. 32--Change in resistivity of a cold-worked Ni-14.0 a/o Mo alloy (specimen F-4) on annealing.

which had been reduced by cold rolling to a 20% reduction of area. The increase in resistivity above the cold-worked state was slightly less than for specimen R-2 in Figure 30, because of the smaller amount of cold work. The slight decrease in resistivity following the initial rapid increase of Stage I was once again present, but it took a slightly longer time for this stage to occur than in specimen R-1 of Figure 29. This should be expected because specimen R-1 contained less Mo in solution than did specimen F-4, and it is well known that solute atmospheres can impede dislocation motion. After annealing for 140 hours at 500°C, the temperature was changed to 650°C, at which point the β phase began to precipitate, causing a sharp decrease in resistivity.

In Figure 33 an interesting comparison is made between two foil specimens, F-1 and F-2, which were in different conditions prior to annealing. Both specimens contained 14.0 a/o Mo; however, specimen F-2 was quenched from 1,000°C and cold-rolled to 20% reduction of area prior to annealing, whereas specimen F-1 was simply quenched. It can be seen that specimen F-1, shows a significant increase in resistivity on annealing at 630°C. It will be recalled that in the "R"-type specimens mentioned earlier no significant increase was observed for a similar treatment due to the difficulty of quenching-in the lower state of

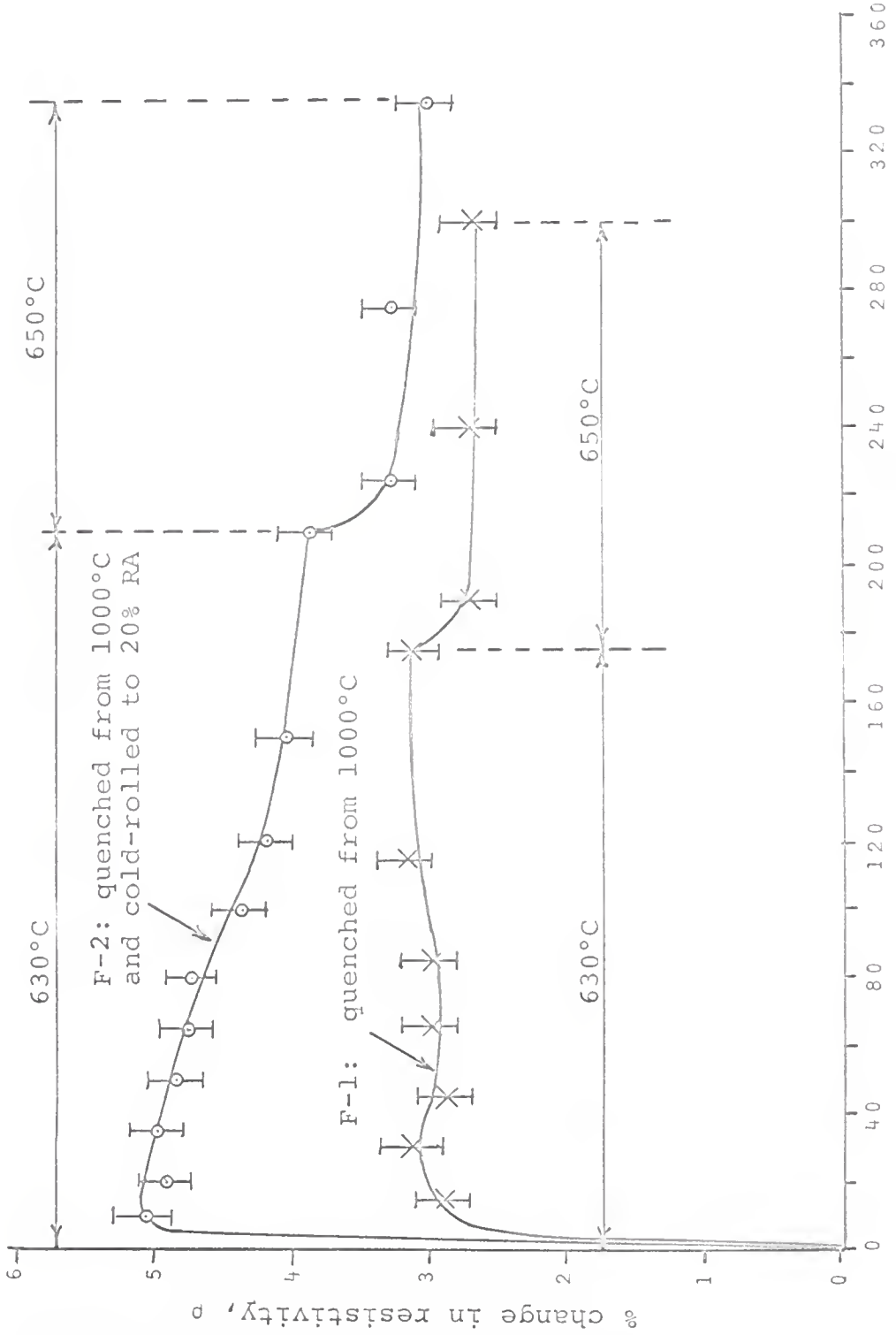

Fig. 33--Change in resistivity of Ni-14.0 a/o Mo alloys on annealing.

SRO at the higher temperature. Specimen F-1 was a foil, however, with a thickness of approximately 0.05 cm. Hence it was possible to quench-in a lower state of SRO because of the factor quenching rate that can be obtained from a thinner specimen.

On comparing the curves for specimens F-1 and F-2 one can see that the most obvious difference is the greater increase in resistivity of F-2 on annealing. This difference can be attributed to the fact that in the initial condition the degree of SRO was less in the cold-worked state than in the as-quenched state. This observation is in agreement with Figure 28 where it was shown that cold rolling reduces the resistivity of a specimen quenched from 1,000°C. Another distinct difference between the two curves in Figure 33 is the manner in which the resistivity of specimen F-2 decreased steadily with prolonged annealing at 630°C while specimen F-1 showed only a temporary slight recovery stage. This decrease in the resistivity of specimen F-2 was probably caused by precipitation of the β phase. When the temperature was increased to 650°C a sharp drop in resistivity occurred in both specimens as a result of the precipitation process.

One would expect that prior deformation should aid precipitation of the β phase since a certain amount of strain is produced by the tetragonal lattice contractions

accompanying ordering. This idea is all the more reasonable when one considers the work of Ellinger [96]. He showed that coarsening of the finely dispersed β phase can be accomplished by an intermediate cold-working step prior to annealing, whereas the β phase remains as a finely dispersed precipitate even after prolonged annealing when the intermediate cold-working step is omitted.

Figures 34 and 35 are electron micrographs which show certain features of the precipitation of the β phase. Figure 34 shows platelets of the β phase which formed after 1 hour at 650°C in foil specimen F-3 which was a companion piece to specimen F-2. Specimen F-3 was also cold-rolled 20% prior to annealing. Plate-like precipitates such as those in Figure 34 were found to occur very sparsely near grain boundaries, where one would expect to find the highest density of dislocation pile-ups. Definite orientations of the β platelets can be seen in this figure. In regions farther away from the grain boundaries dislocation networks such as those shown in Figure 35 were found. In several areas the dislocations appear to be "decorated," and pinned at certain points. It is suggested that nuclei of the β phase had formed at the dislocations and caused these effects. More will be said later about electron-microscopic studies of the precipitation of the β phase.

Fig. 34--Electron transmission micrograph of precipitated platelets of the β phase in Ni-14.0 a/o Mo (specimen F-3) cold-rolled to 20% reduction of area and annealed for 1 hour at 650°C. Magnification x 57,000.

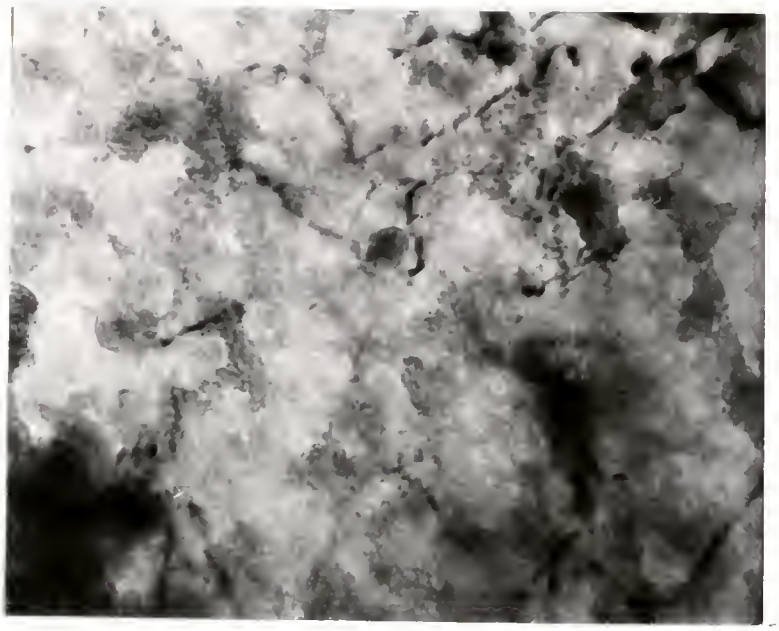

a.

b.

Fig. 35--Electron transmission micrograph of pinned dislocations in the Ni-14.0 a/o Mo alloy (specimen F-3) cold-rolled to 20% reduction of area and annealed for 1 hour at 650°C.

a. Magnification x 215,000
b. Magnification x 96,500

4.2 *Correlation Between SRO and Changes in Resistivity of Ni - 10.5 and Ni - 14.0 a/o Mo Alloys*

It was pointed out earlier that one of the primary purposes of this investigation was to determine whether or not SRO was responsible for the anomalous increase in resistivity associated with the K-state in Ni-Mo alloys. In the previous section in which the resistivity data were discussed, frequent reference was made to the fact the observed increase or decrease in resistivity could be correlated with increases or decreases in the degree of SRO, but no x-ray data were shown. In this section the x-ray data will be presented and it will be shown that SRO is in fact responsible for the K-state in Ni-Mo alloys.

X-ray diffuse-scattering measurements were made on two specimens, X-1 and X-2. These specimens contained 10.5 a/o and 14.0 a/o Mo respectively. In order to be certain that the x-ray data and resistivity data represented identical structural states, resistivity measurements were also made on specimens X-1 and X-2 before and after each x-ray scan. The curves showing the changes in resistivity for these two specimens are shown in Figures 36. Specimen X-1 was initially quenched from 1,000°C and cold-rolled to 70% reduction of area. It was then annealed at 500°C for 201 hours. Following the 500°C anneal, specimen X-1 was solution heat-treated at 1,000°C for 24 hours and

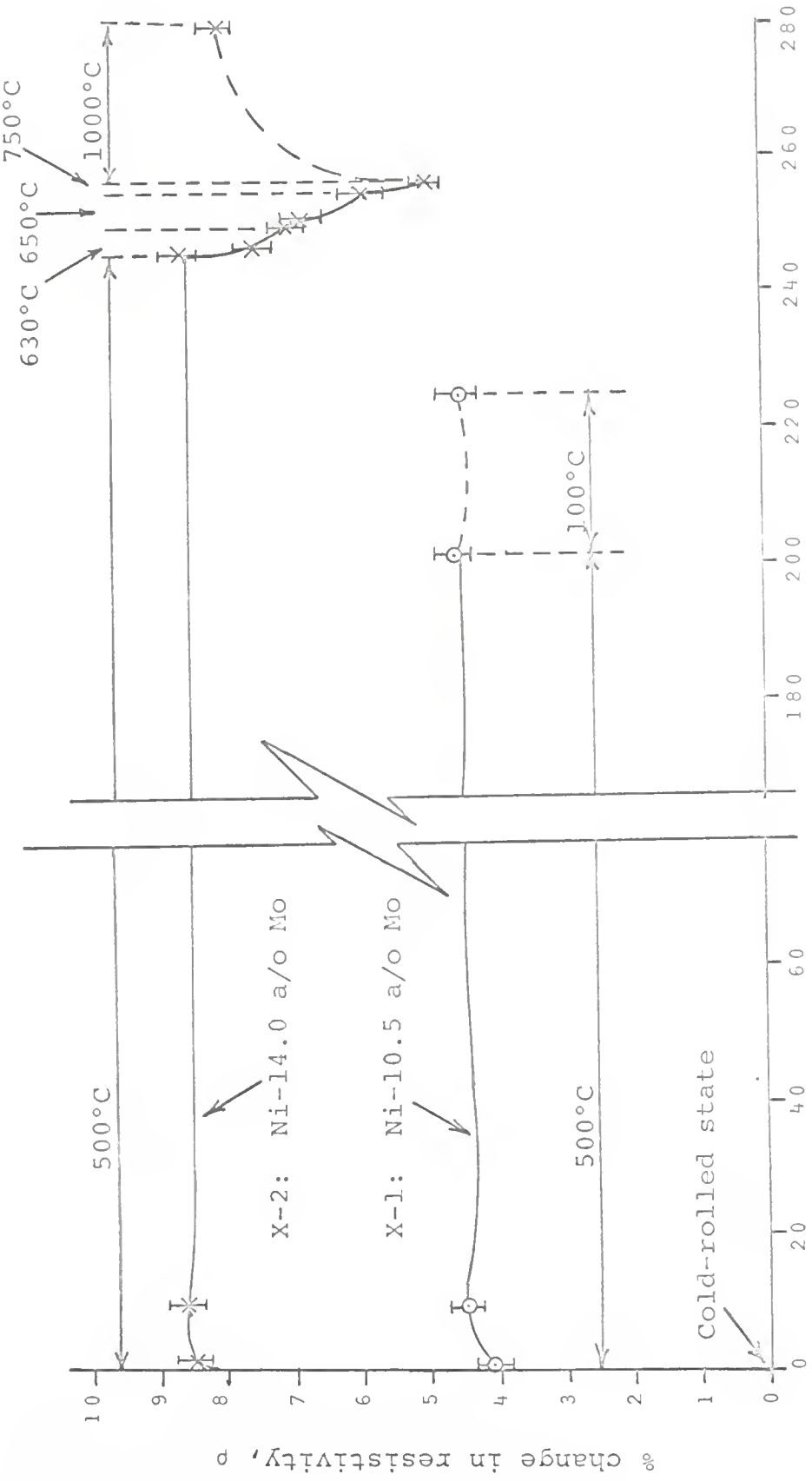

Fig. 36---Change in resistivity of x-ray specimen X-1 and X-2 on annealing.

water quenched. A similar treatment was given specimen X-2 except that between the 500°C anneal and the solution-heat-treatment, three intermediate anneals of 630°C, 650°C, and 750°C were given to cause precipitation of the β phase. For each of the data points shown in Figure 36 a corresponding x-ray diffuse-scattering run was made on the same specimen.

In Figures 37 and 38 the uncorrected diffuse-scattering curves for specimens X-1 and X-2 in the solution-heat-treated state are shown. By comparison with the previous curve for pure Ni (Figure 25) it is apparent that in both the Ni-Mo specimens some kind of local order was present. In Figures 39 and 40 these curves have been corrected for Compton scattering, temperature-diffuse scattering, and interference from the {111} peak according to the method described in Chapter III, Section 3. The corrected curves are characteristic of specimens that exhibit SRO; i.e., exhibit a preference for unlike nearest neighbors ($\alpha_1 < 0$). This preference for unlike neighbors can be seen by comparing with the curves of Figure 7, which are predicted by the Warren-Cowley equations.

The position of the maximum in the diffuse-scattering curves of Ni-Mo alloys was found to occur at approximately S = 2.0. This is approximately the mean positions for the peaks of the (110), (101), and (200) superlattice

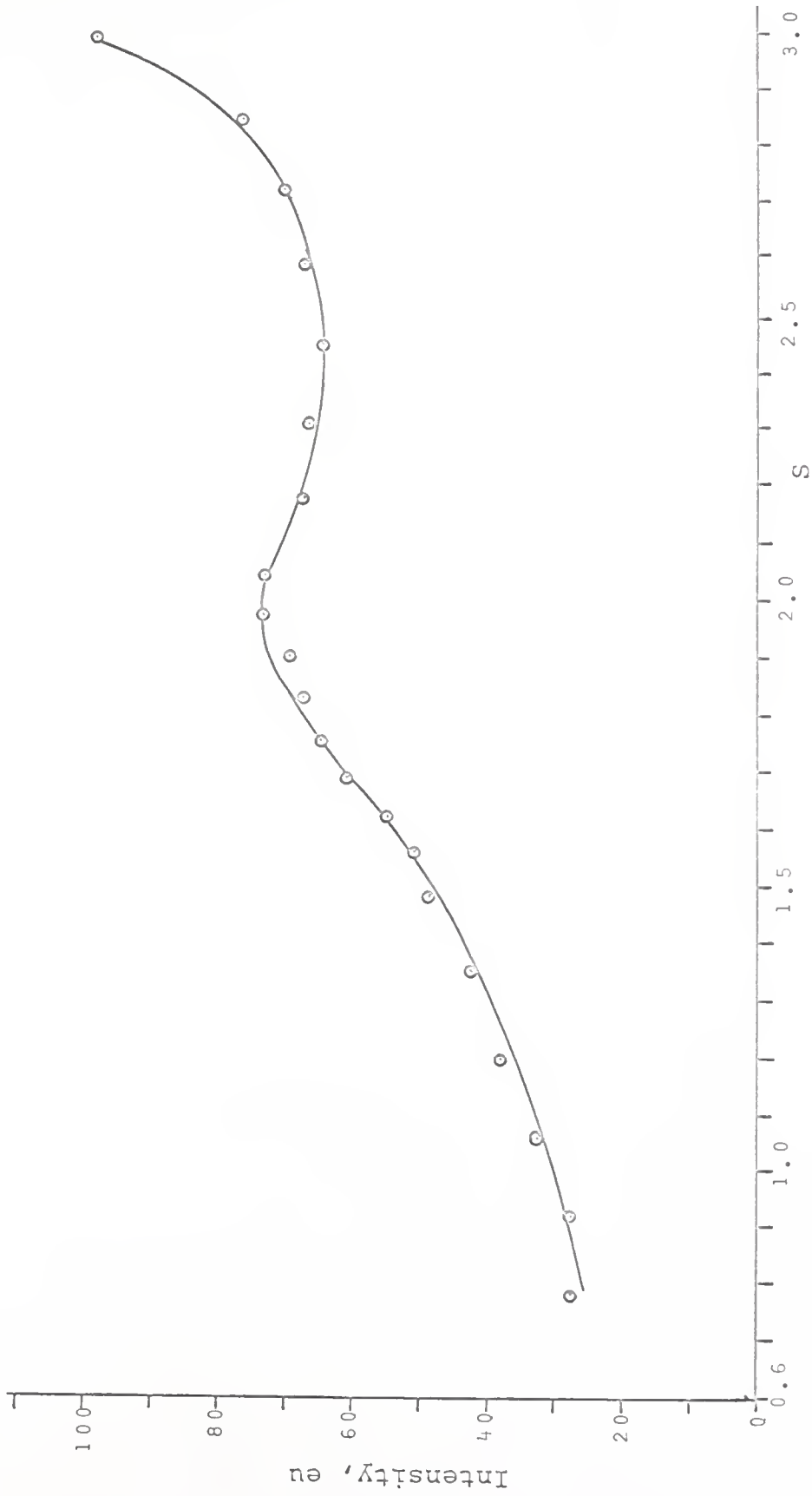

Fig. 37--Diffuse-scattering curve for specimen X-1 (10.5 a/o Mo) after solution-heat-treating.

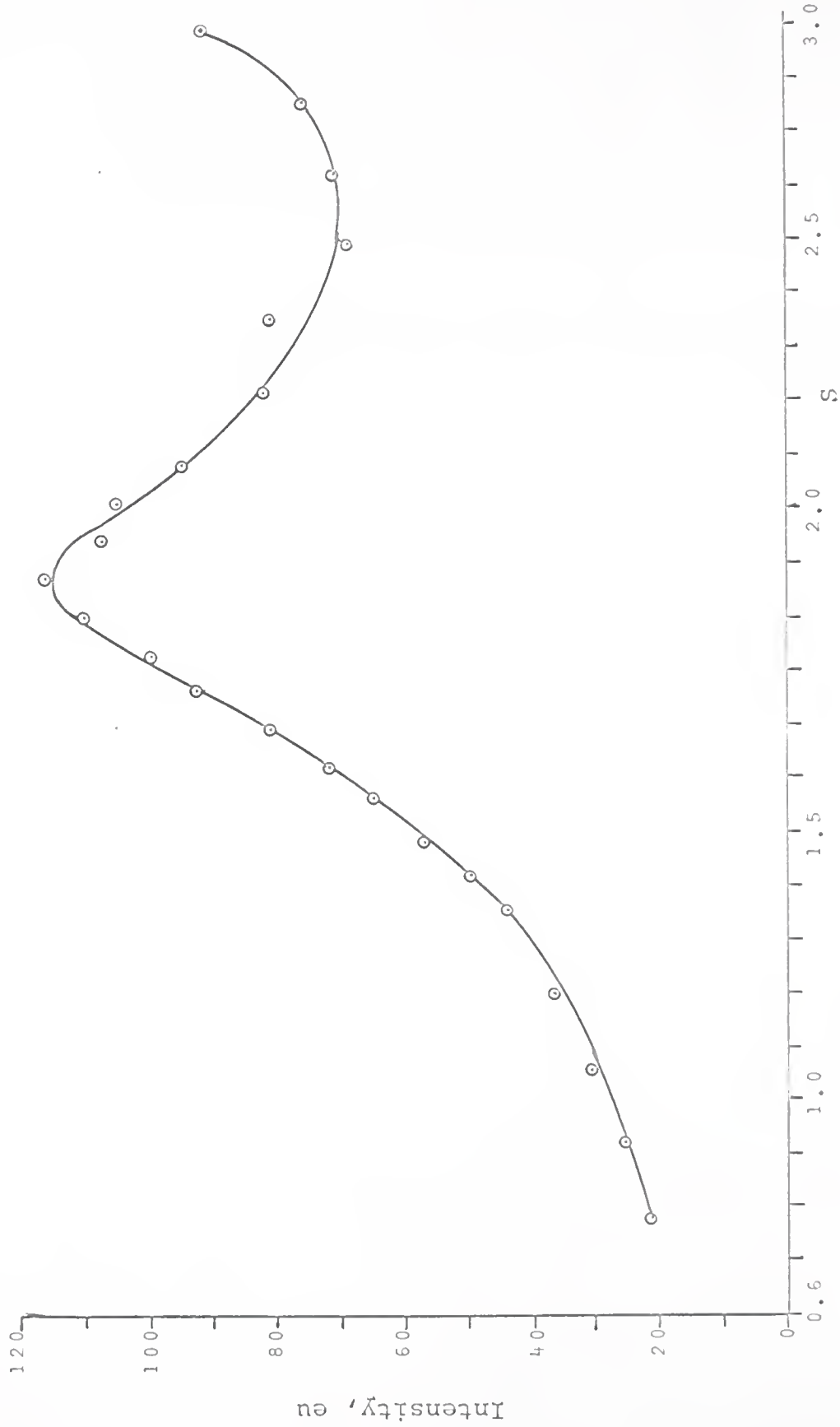

Fig. 38--Diffuse-scattering curve for specimen X-2 (14.0 a/o Mo) after solution-heat-treating.

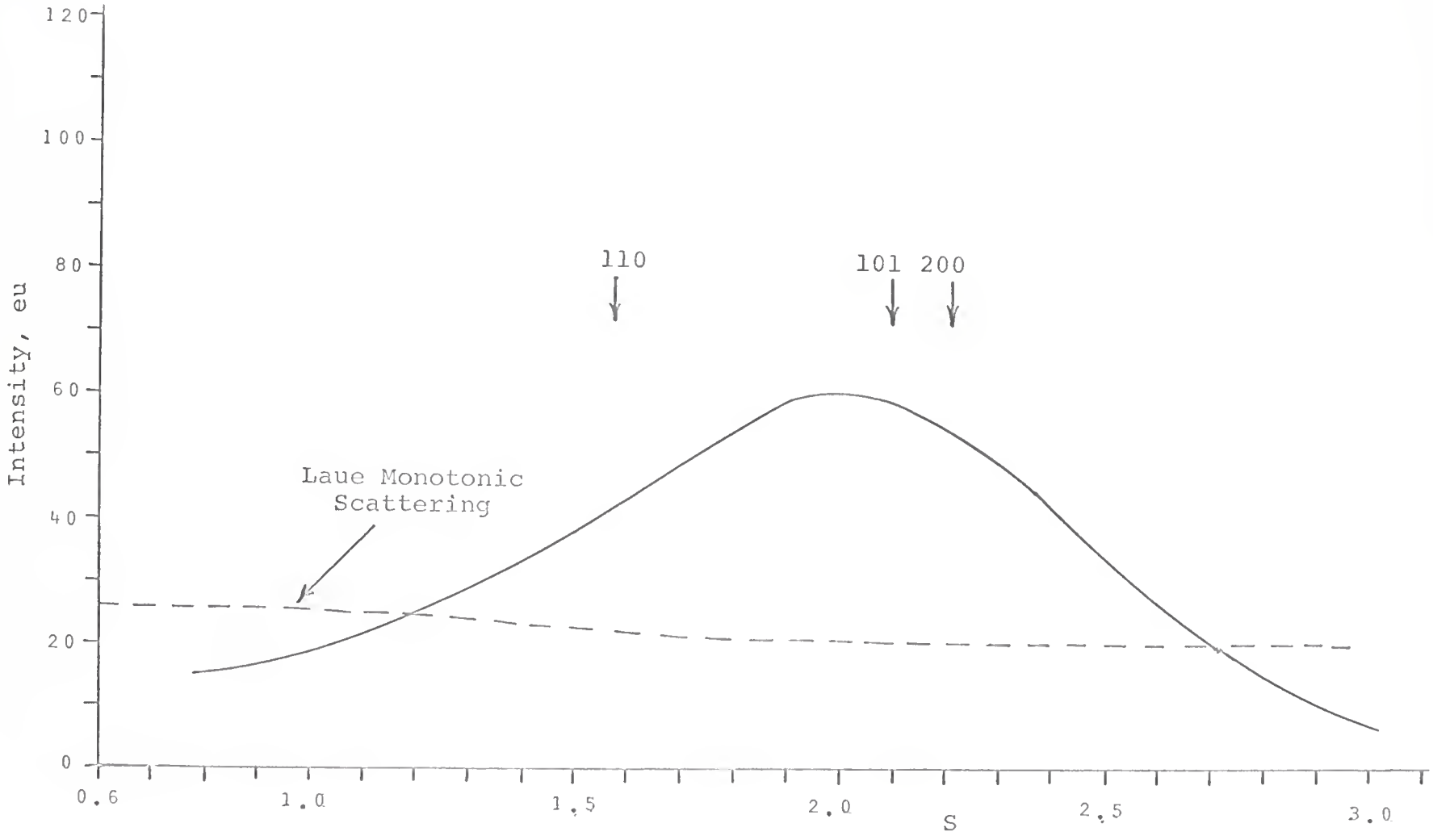

Fig. 39--Corrected diffuse scattering curve for specimen X-1 (10.5 a/o Mo) after solution-heat-treating.

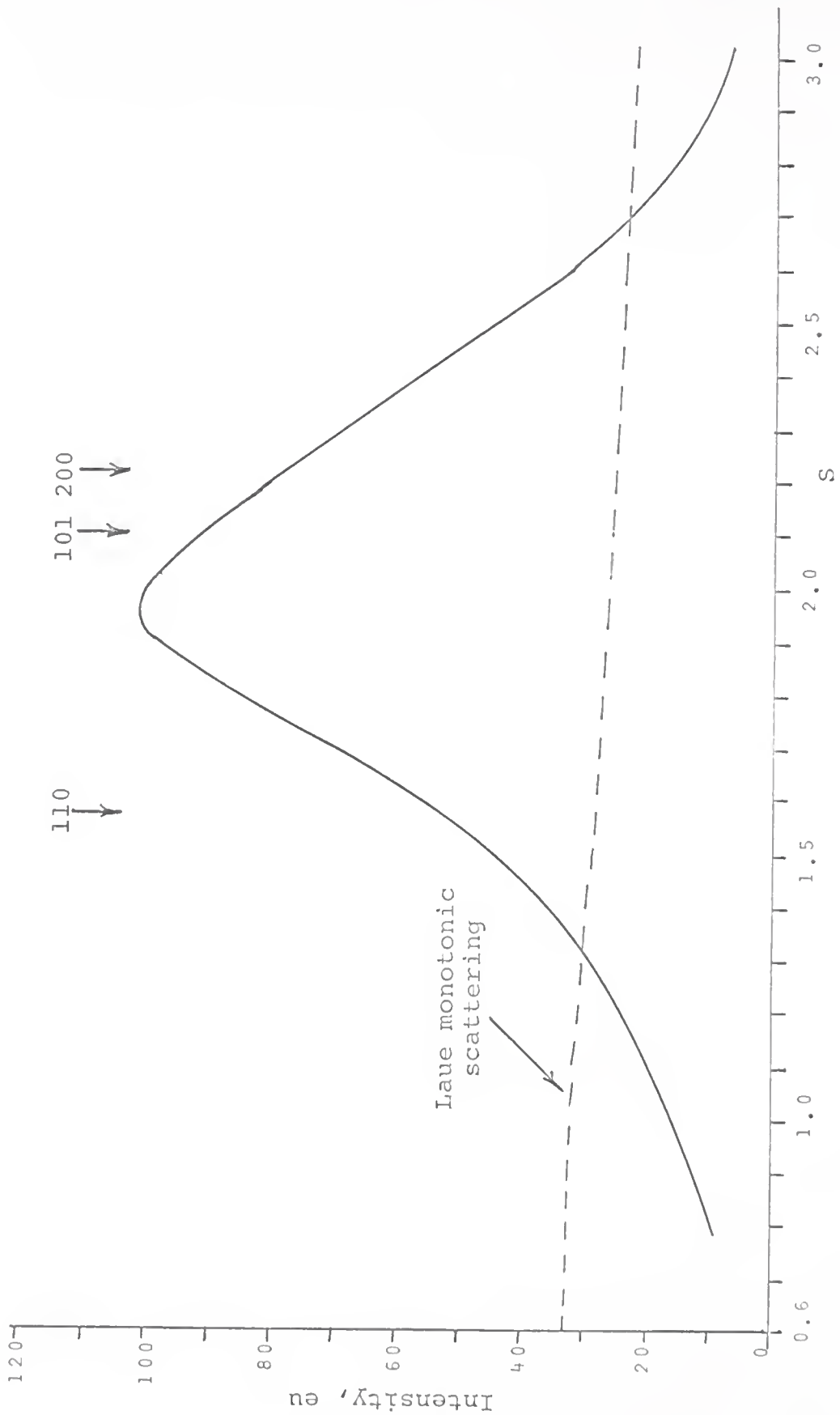

Fig. 40--Corrected diffuse-scattering curve for specimen X-2 (14.0 a/o Mo) after solution-heat-treating.

reflections of the Ni_4Mo long-range order.* The positions of these lines are indicated on the curves of Figures 39 and 40. In the work of Starke *et al.* [7] on Ni-Al a similar SRO maximum was found to occur at the lower value of S≈1.7. This SRO was produced by the partial destruction through cold-rolling of ordered G.P. zones of Ni_3Al. The superlattice lines existing in the ordered Ni_3Al were the (100) and (110) of the FCC lattice. The mean position of these lines is also approximately S = 2.0. This illustrates the point that the exact position of the diffuse maximum depends on the relative contributions of the α_i coefficients of equation (10) in Chapter I. Even in cases where the SRO is definitely produced by small domains or regions of LRO, the position of the diffuse maximum depends on the relative intensities of the superlattice lines that constitute the maximum. The diffuse maximum in the Ni - 10.5 a/o and in the Ni - 14.0 a/o Mo alloys was well within the range of S values that would be expected if the maximum were produced by a broadening of the (110), (101), and (200) superlattice lines of the β phase. It is entirely possible, therefore, that the SRO in dilute Ni-Mo alloys consists of small,

*The (110) and (101) superlattice reflections are indexed with reference to the body-centered tetragonal unit cell of the β phase. Within this lattice the (111) peak of the original FCC lattice has the indices (211). See references [91] and [97] for further details.

imperfect domains of the Ni_4Mo-type LRO as proposed by Spruiell [31].

It is obvious that a much greater degree of SRO existed in the 14.0 a/o alloy in the solution heat-treated state than in the 10.5 a/o alloy. This is to be expected since as pointed out previously the maximum degree of SRO is limited by the composition of the alloy. The higher the fraction of solute atoms the greater is the maximum possible departure from randomness. The fact that more SRO exists in the 14.0 a/o alloy in the solution-heat-treated state is consistent with the fact that a greater decrease in resistivity was observed upon cold-rolling the two alloys.

In Figures 41 and 42 the diffuse scattering curves for specimens X-1 and X-2 in the cold-rolled state are shown. In Figures 43 and 44 the same curves are shown after correcting for temperature-diffuse scattering, etc. In both alloys there is a marked decrease in the degree of SRO as compared with the solution-heat-treated state. The corresponding resistivity measurements (Figure 36) made on the same specimens show a marked decrease in resistivity upon cold working also. Although the specimens were cold-rolled to 70% and 65% reduction of area, some SRO still existed after the rolling operation.

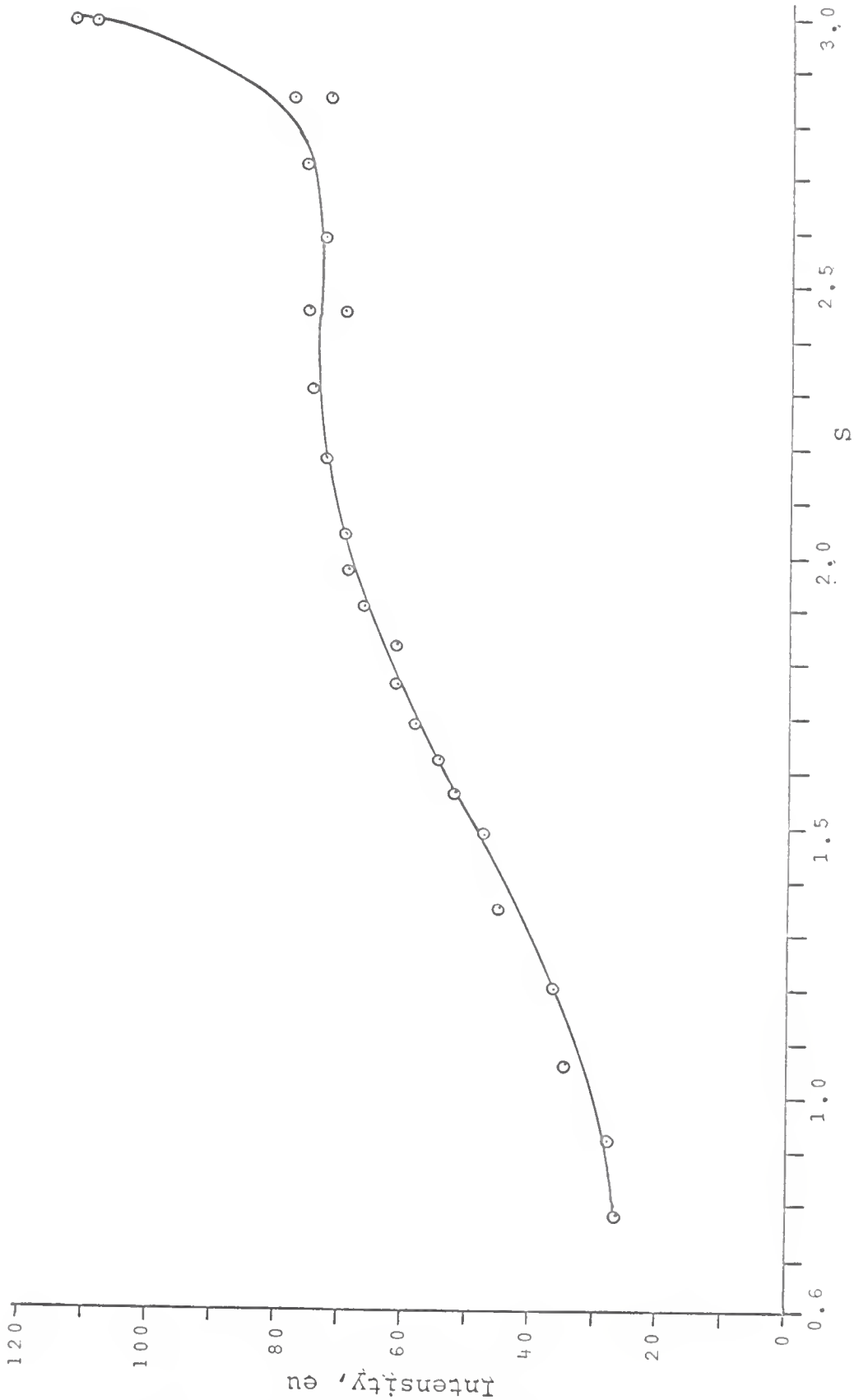

Fig. 41--Diffuse-scattering curve for specimen X-1 (10.5 a/o Mo) after cold-rolling to 70% reduction of area.

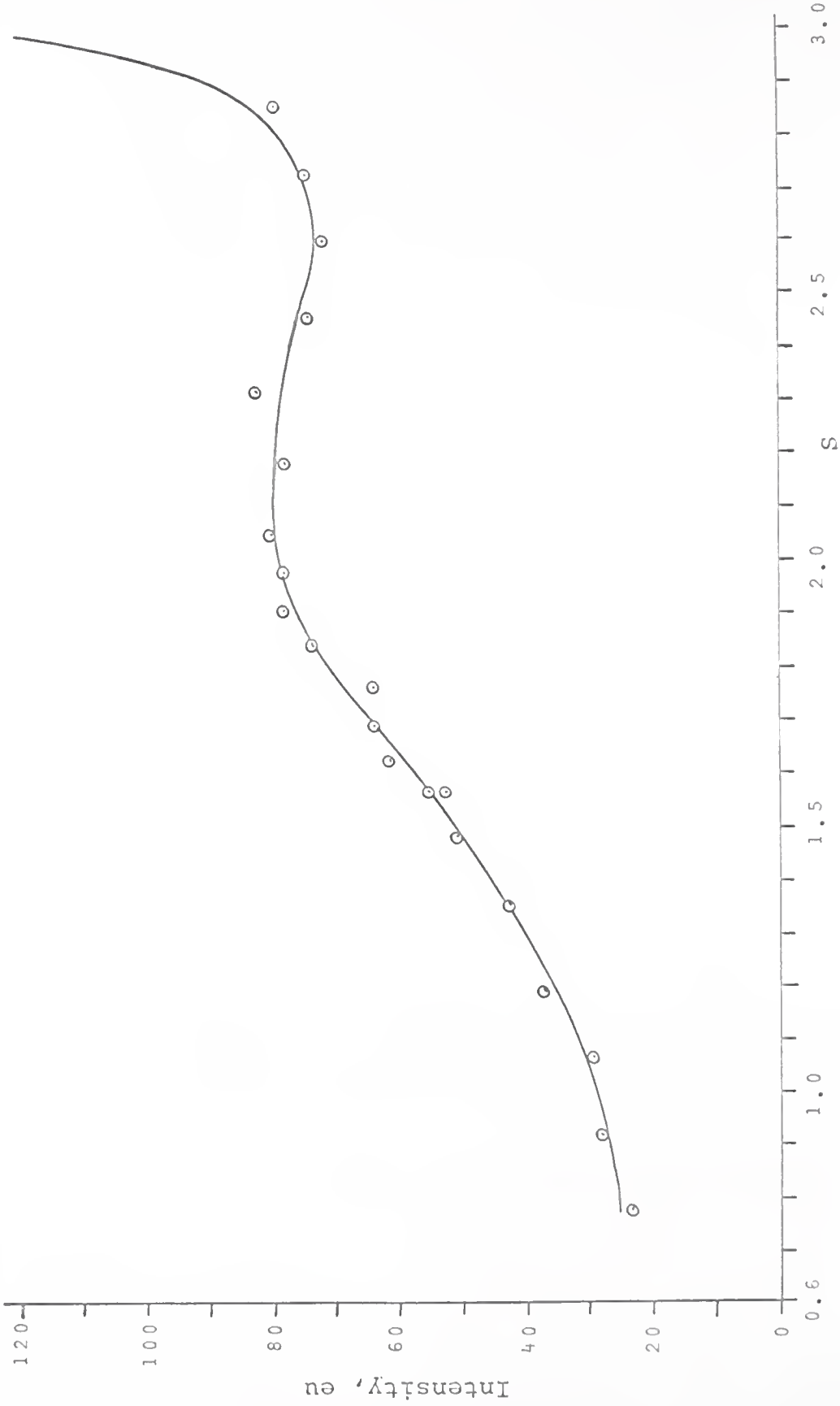

Fig. 42--Diffuse-scattering curve for specimen X-2 (14.0 a/o Mo) after cold rolling to 65% reduction of area.

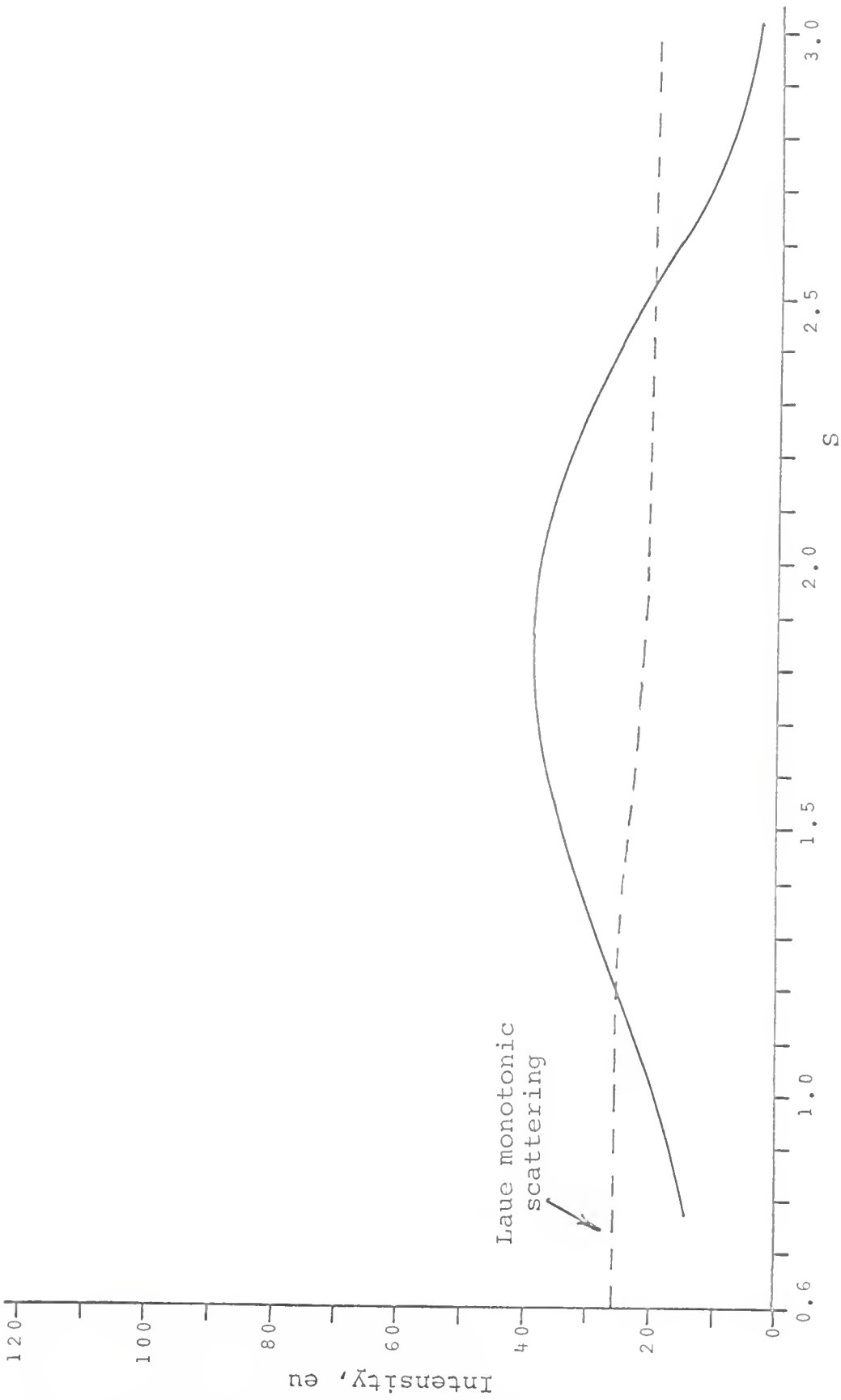

Fig. 43--Corrected diffuse-scattering curve for specimen X-1 (10.5 a/o Mo) after cold rolling to 70% reduction of area.

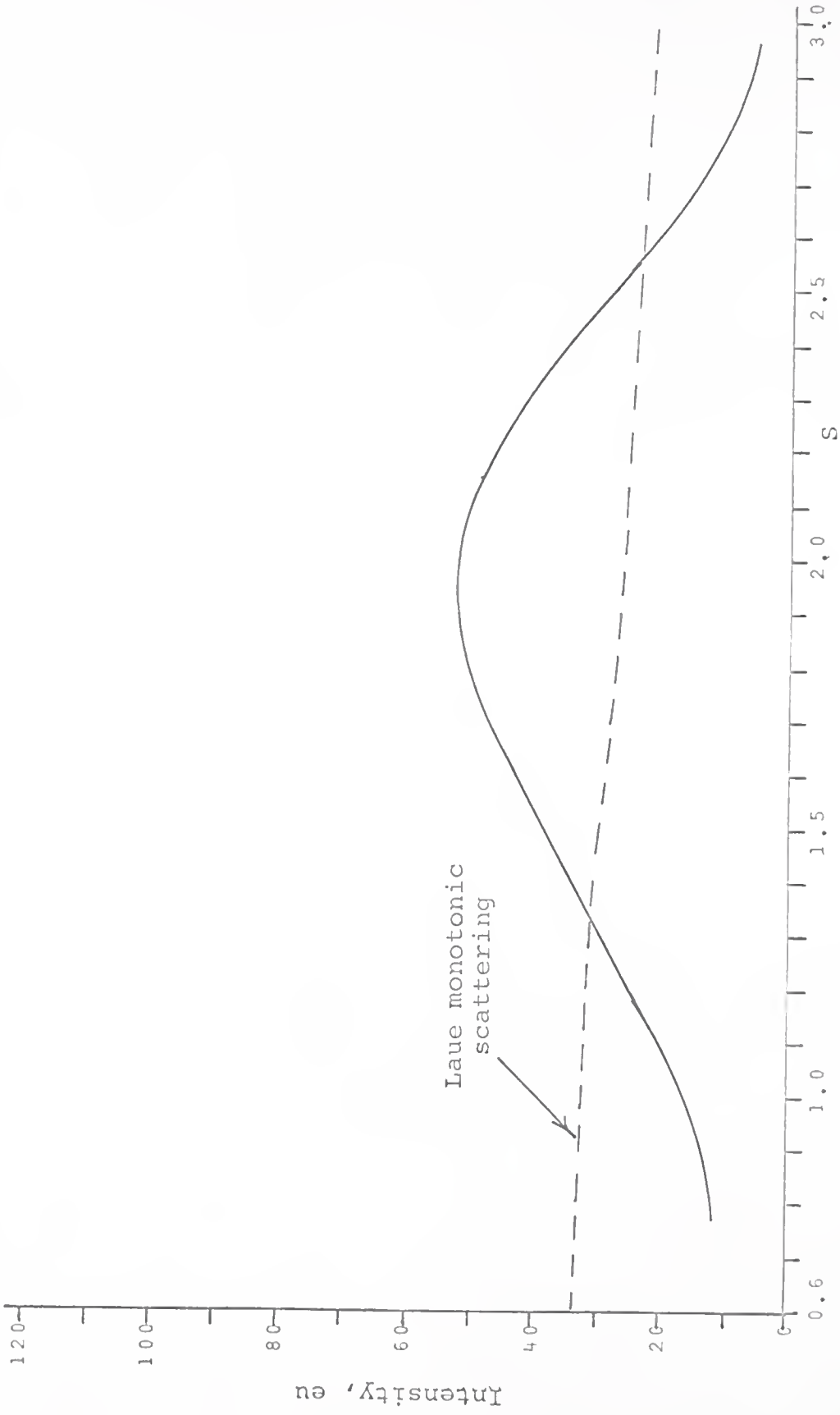

Fig. 44--Corrected diffuse-scattering curve for specimen X-2 (14.0 a/o Mo) after cold rolling to 65% reduction of area.

The above curves clearly demonstrate that SRO can be partially destroyed by cold-rolling and hence SRO is the likely explanation for the K-state in Ni-Mo alloys. It is a bit surprising, however, that a measurable amount of SRO still existed after severe cold-rolling. At first glance one would expect an essentially random structure after such an operation. On the other hand it has been shown by Starke *et al.* [7] and Hornbogen and Kreye [8] that in Ni-Al some SRO still exists after a rather severe deformation. It was found by Rudman and Averbach [119] that severely abrading the surface of a Cu-Au specimen resulted in only a 50% decrease of SRO. From this they concluded that slip had occurred on approximately one-third of all the available {111} planes. Hence it appears that cold work can partially destroy SRO but is not nearly as effective in "mixing" or "randomizing" a solid solution as might be expected.

Upon annealing specimens X-1 and X-2 at 500°C after cold-working there was a rapid increase in resistivity above that of the cold-worked state within a period of 30 minutes. In Specimen X-1 there was approximately a 4% increase and in X-2 approximately an 8.5% increase in resistivity. The increase in resistivity was accompanied by a sharp increase in the degree of SRO in both specimens

as shown in Figures 45 through 48. Following this initial rapid increase in resistivity, there was no significant change in either specimen upon prolonged annealing at 500°C. As shown in Figures 49 through 56, as the amount of SRO also remained essentially constant during this period.

Following the prolonged anneal at 500°C, specimen X-2 was heat-treated for short periods at 630°C, 650°C, and 750°C to precipitate the β phase. As a result of the precipitation the resistivity decreased sharply as shown in Figure 36. The effect of the precipitation on the diffuse-scattering curve is shown in Figures 57, 58, and 59. In Figure 57 it can be seen that after 3.75 hours at 630°C plus one hour at 650°C the diffuse-scattering curve was essentially unchanged from its appearance after 246 hours at 500°C. This lack of change can be attributed to the fact that the SRO of the matrix had not changed significantly and the superlattice lines of the β phase had not yet appeared as a result of the small size and low volume fraction of the β phase. After an additional 4 hours at 650°C, significant changes in the diffuse scattering curve had appeared. As shown in Figure 59 the tail of the curve on the low-angle side was considerably higher than in the previous curves; furthermore, the tail passed through a minimum at S = 0.9 as S decreased. This

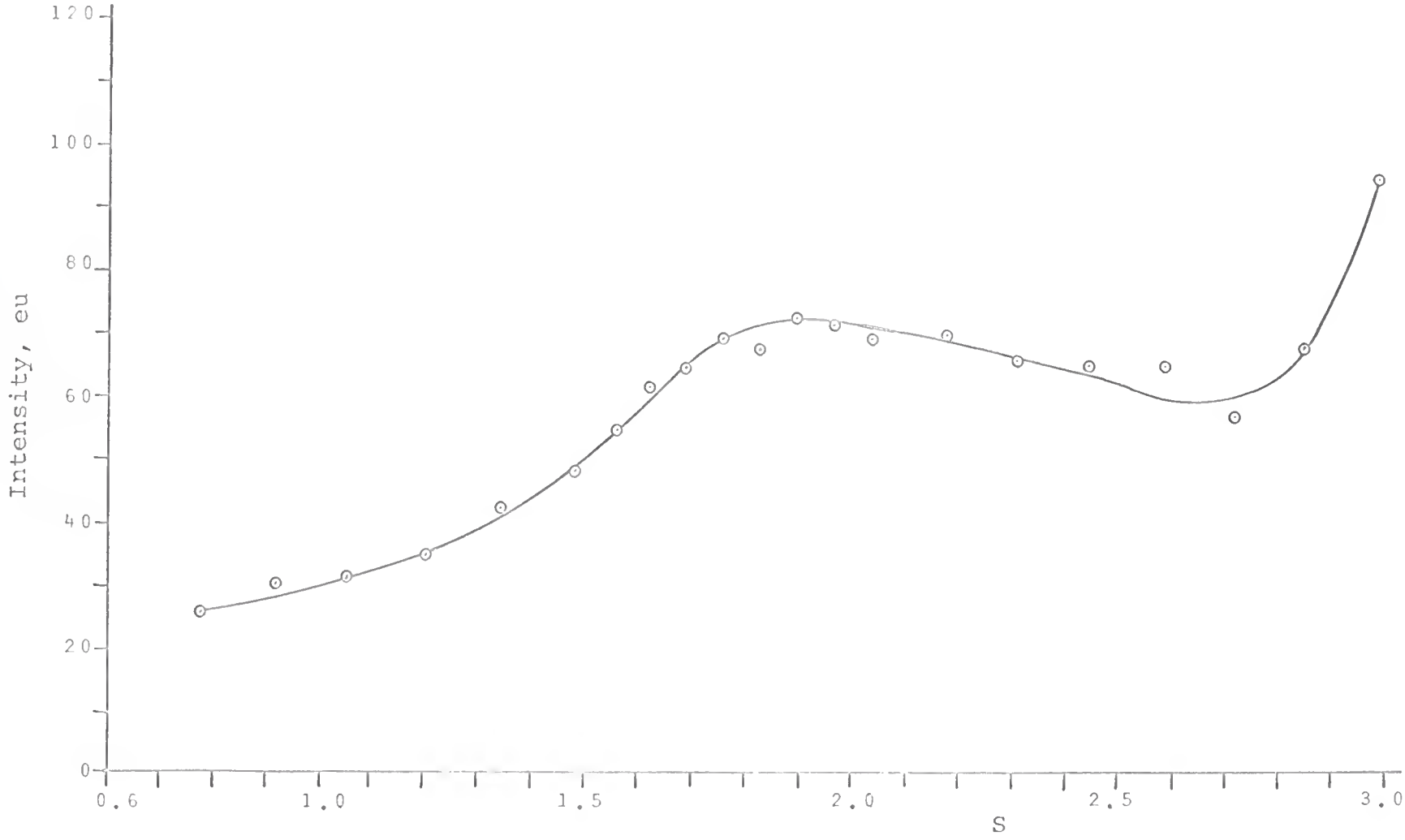

Fig. 45--Diffuse-scattering curve for specimen X-1 (10.5 a/o Mo) after cold rolling and annealing for 30 minutes at 500°C.

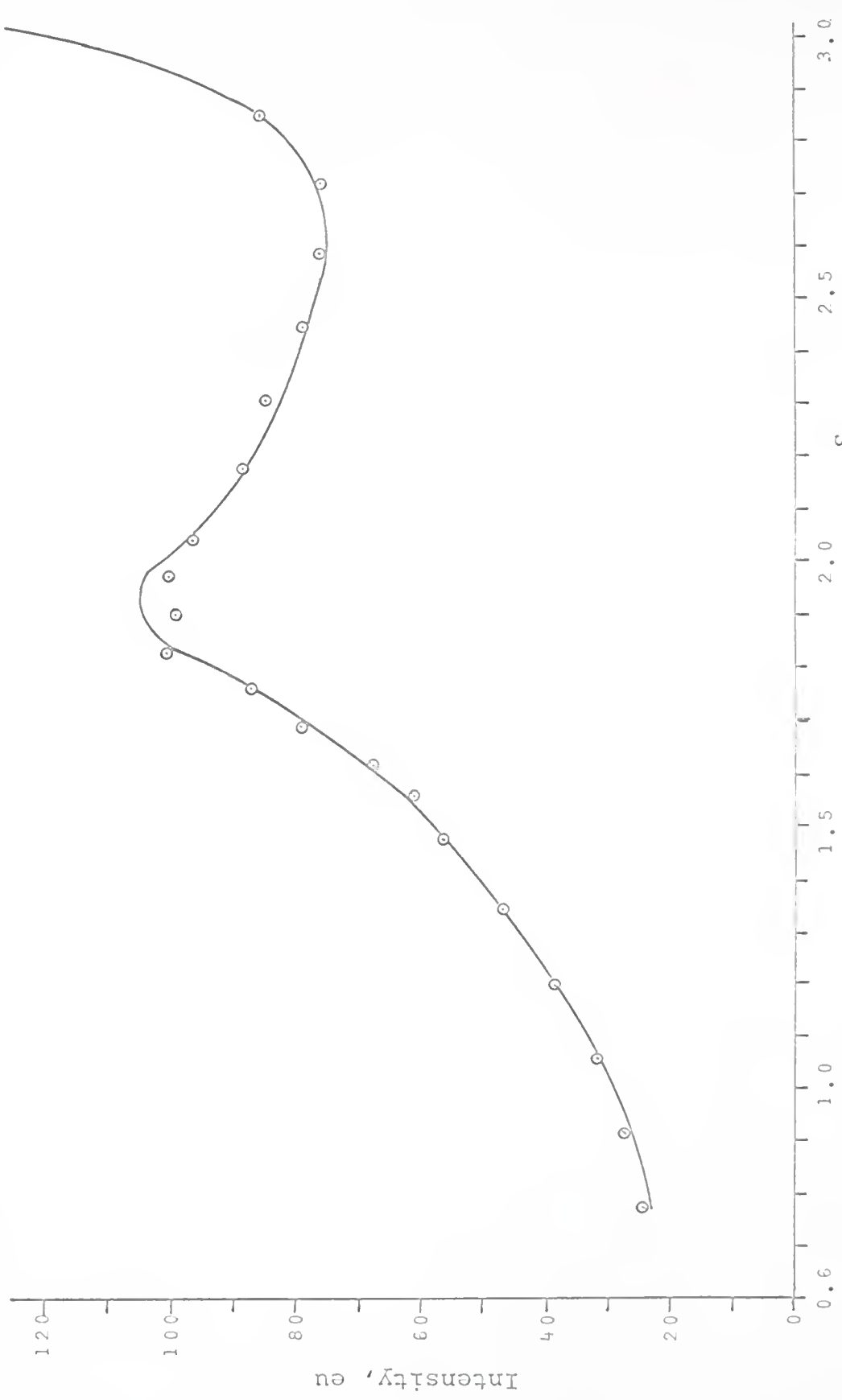

Fig. 46--Diffuse-scattering curve for specimen X-2 (14.0 a/o Mo) after cold rolling and annealing for 30 minutes at 500°C.

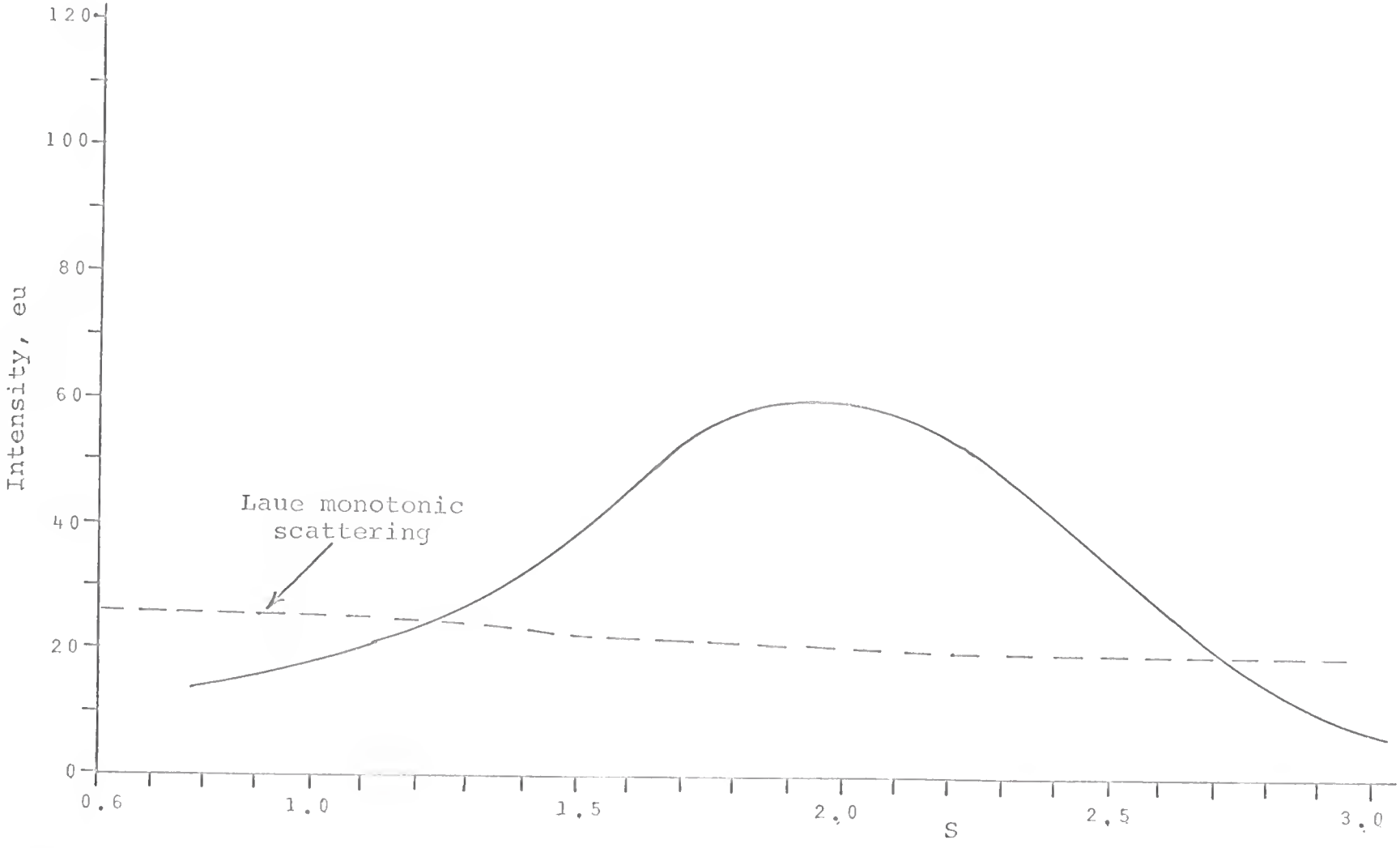

Fig. 47--Corrected diffuse-scattering curve for specimen X-1 (10.5 a/o Mo) after cold rolling and annealing for 30 minutes at 500°C.

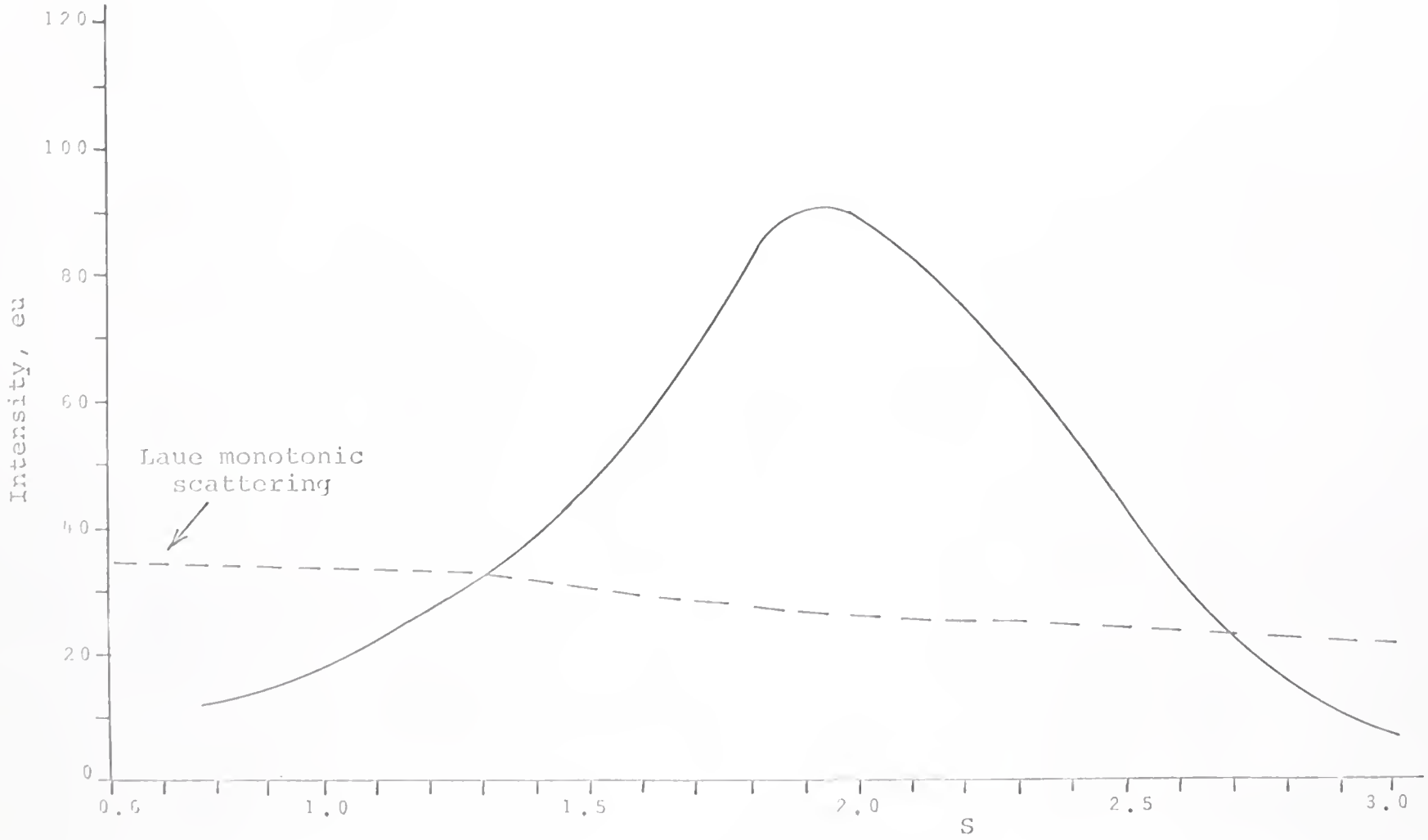

Fig. 48--Corrected diffuse-scattering curve for specimen X-2 (14.0 a/o Mo) after cold rolling and annealing for 30 minutes at 500°C.

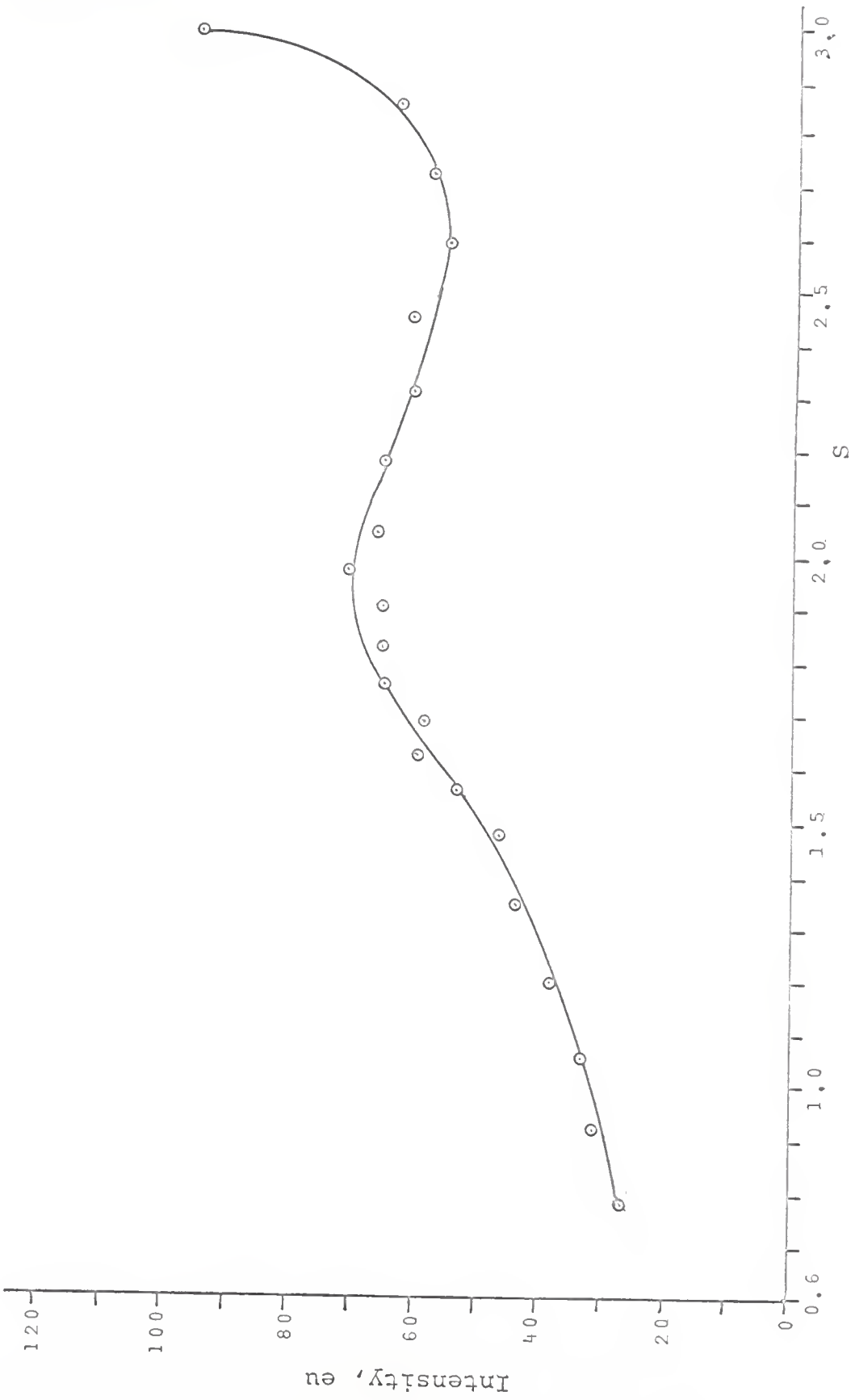

Fig. 49--Diffuse-scattering curve for specimen X-1 (10.5 a/o Mo) after cold rolling and annealing for 10 hours at 500°C.

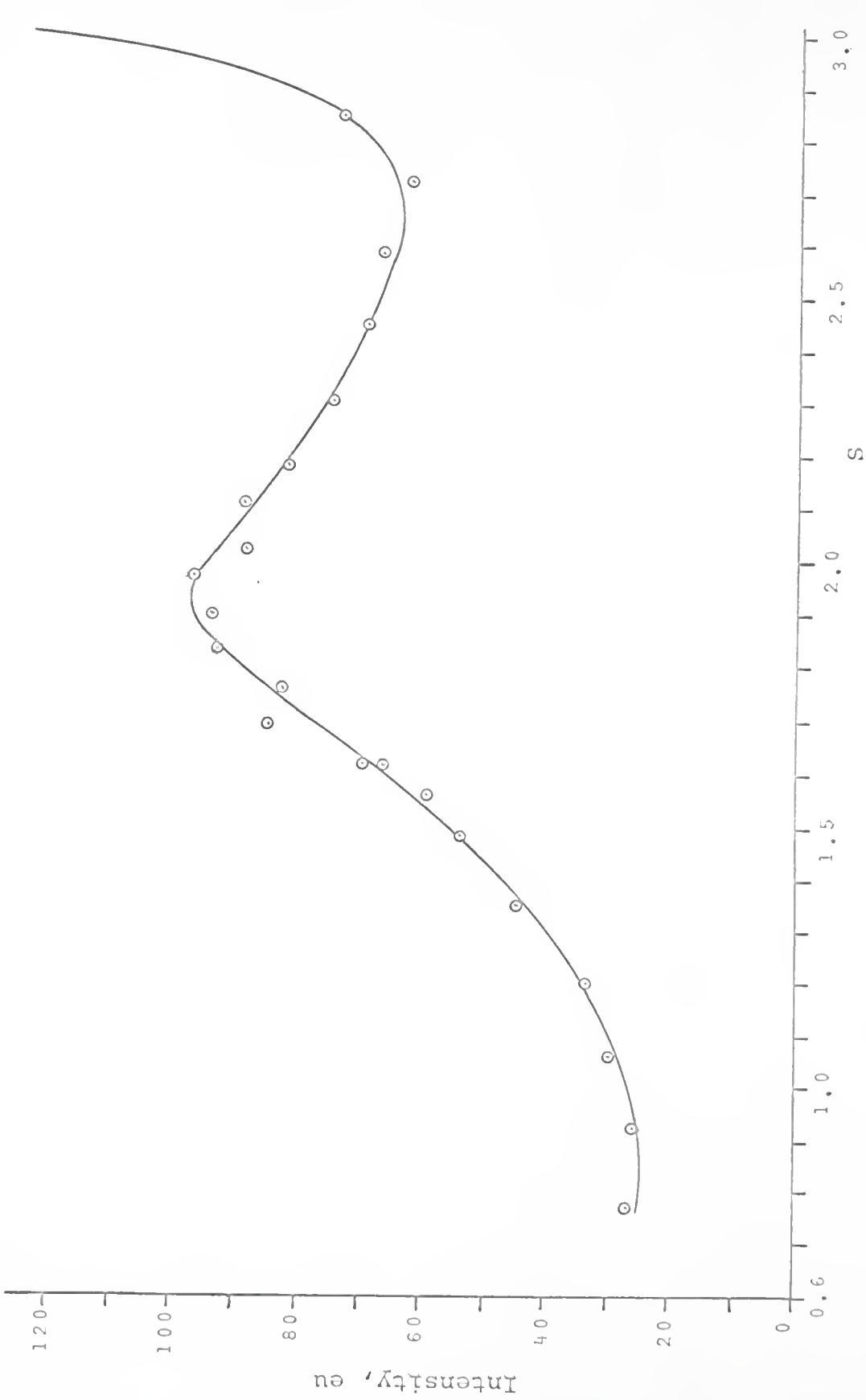

Fig. 50--Diffuse-scattering curve for specimen X-2 (14.0 a/o Mo) after cold rolling and annealing for 10 hours at 500°C.

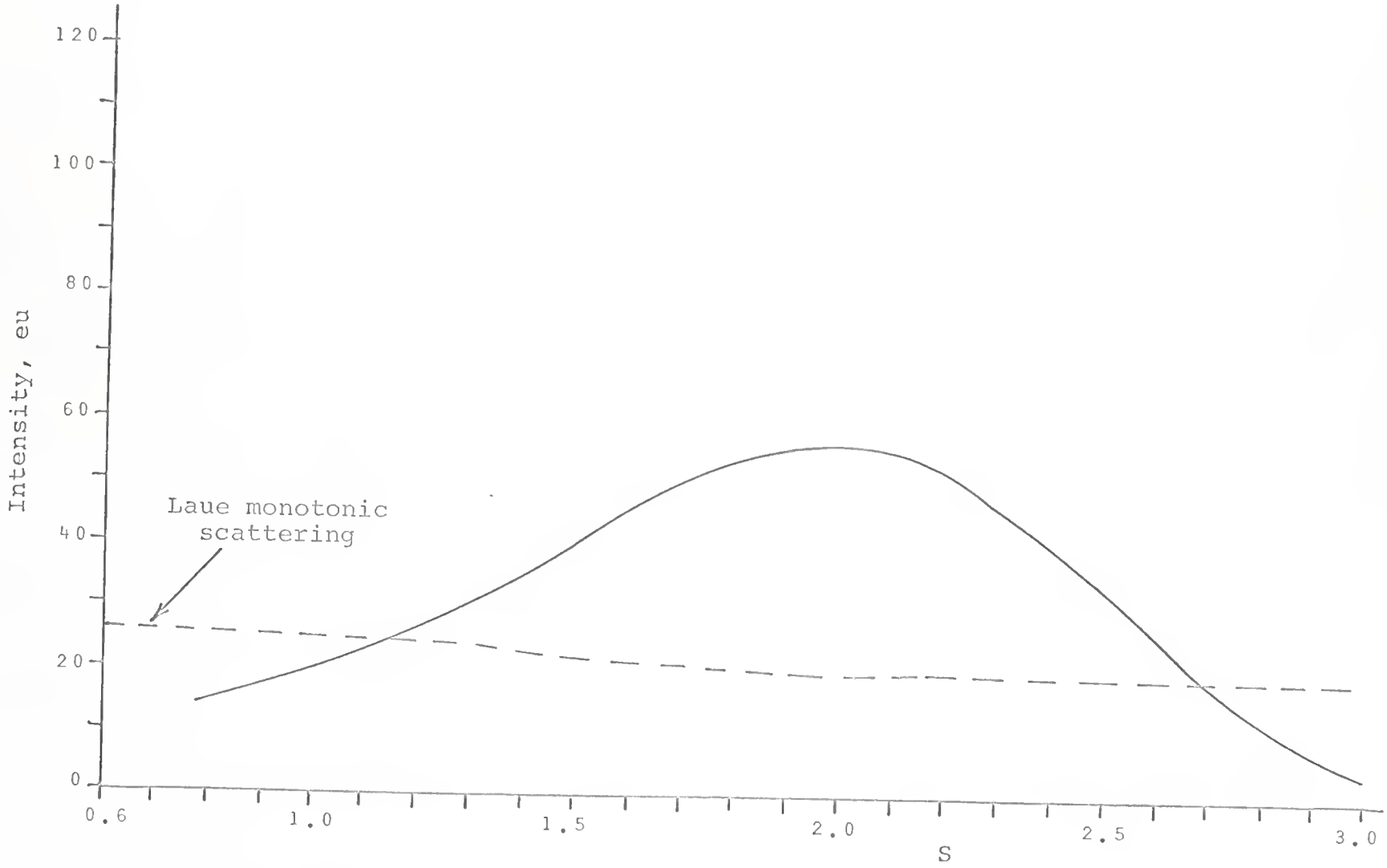

Fig. 51--Corrected diffuse-scattering curve for specimen X-1 (10.5 a/o Mo) after cold rolling and annealing for 10 hours at 500°C.

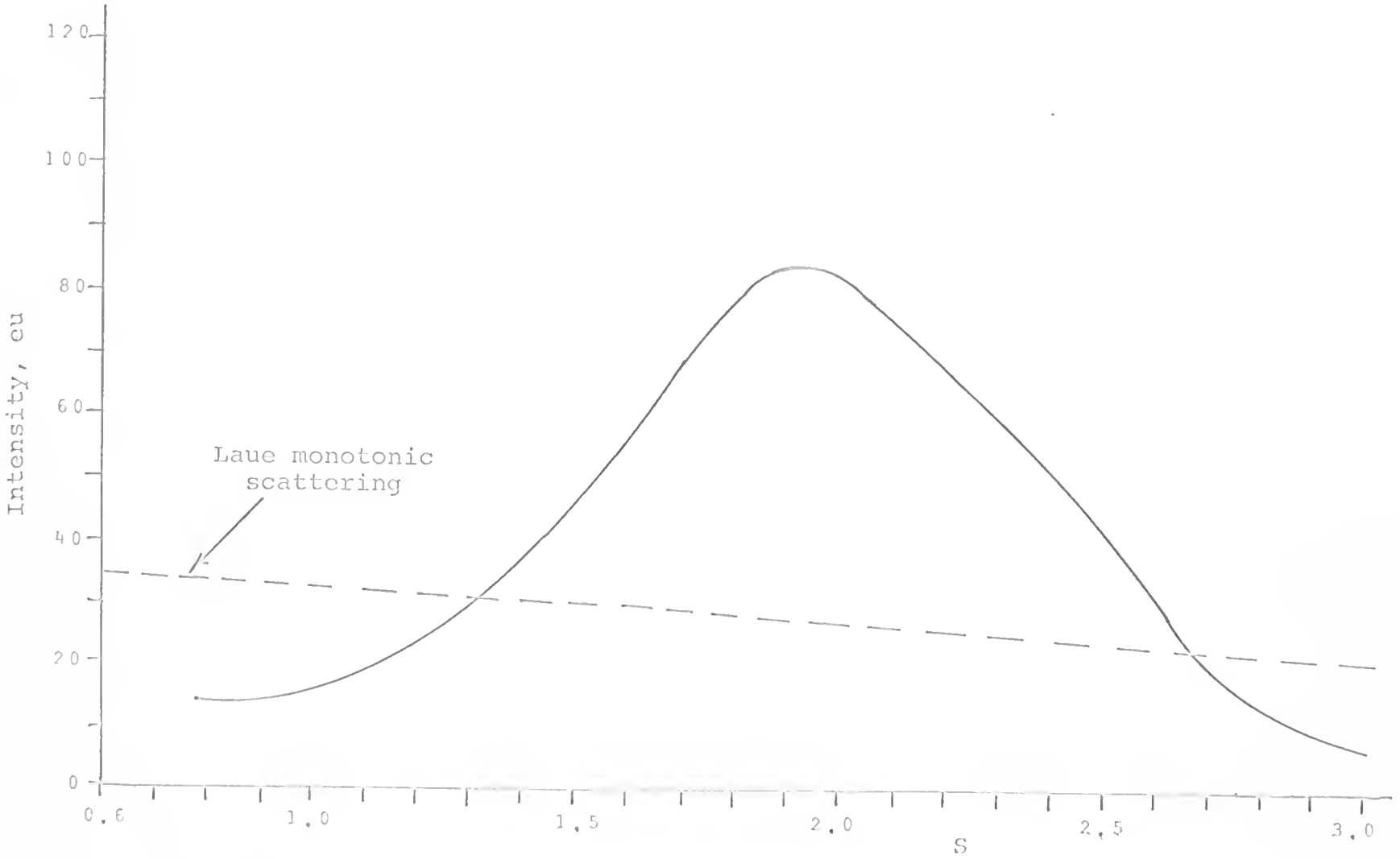

Fig. 52--Corrected diffuse-scattering curve for specimen X-2 (14.0 a/o Mo) after cold rolling and annealing for 10 hours at 500°C.

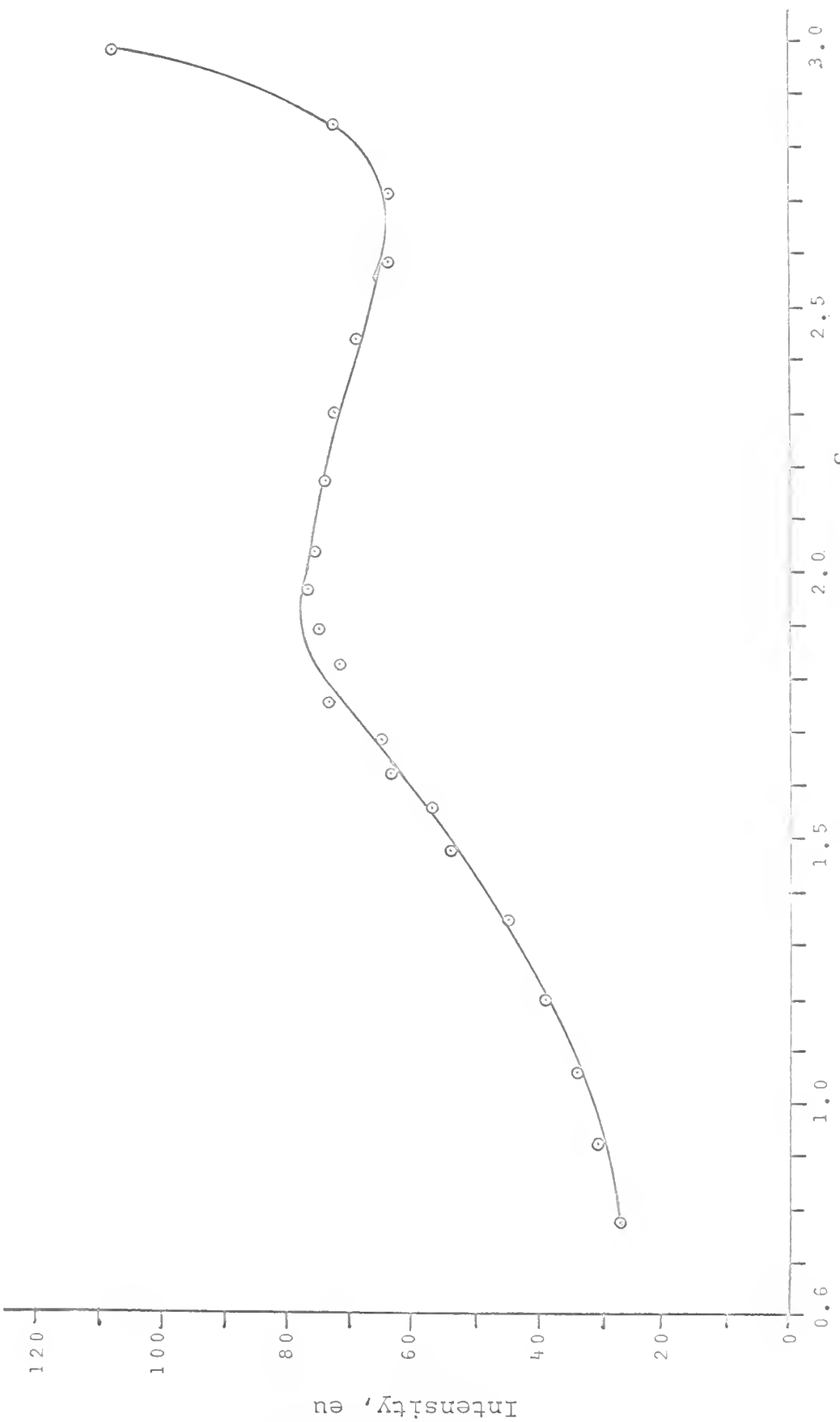

Fig. 53--Diffuse-scattering curve for specimen X-1 (10.5 a/o Mo) after cold rolling and annealing for 201 hours at 500°C.

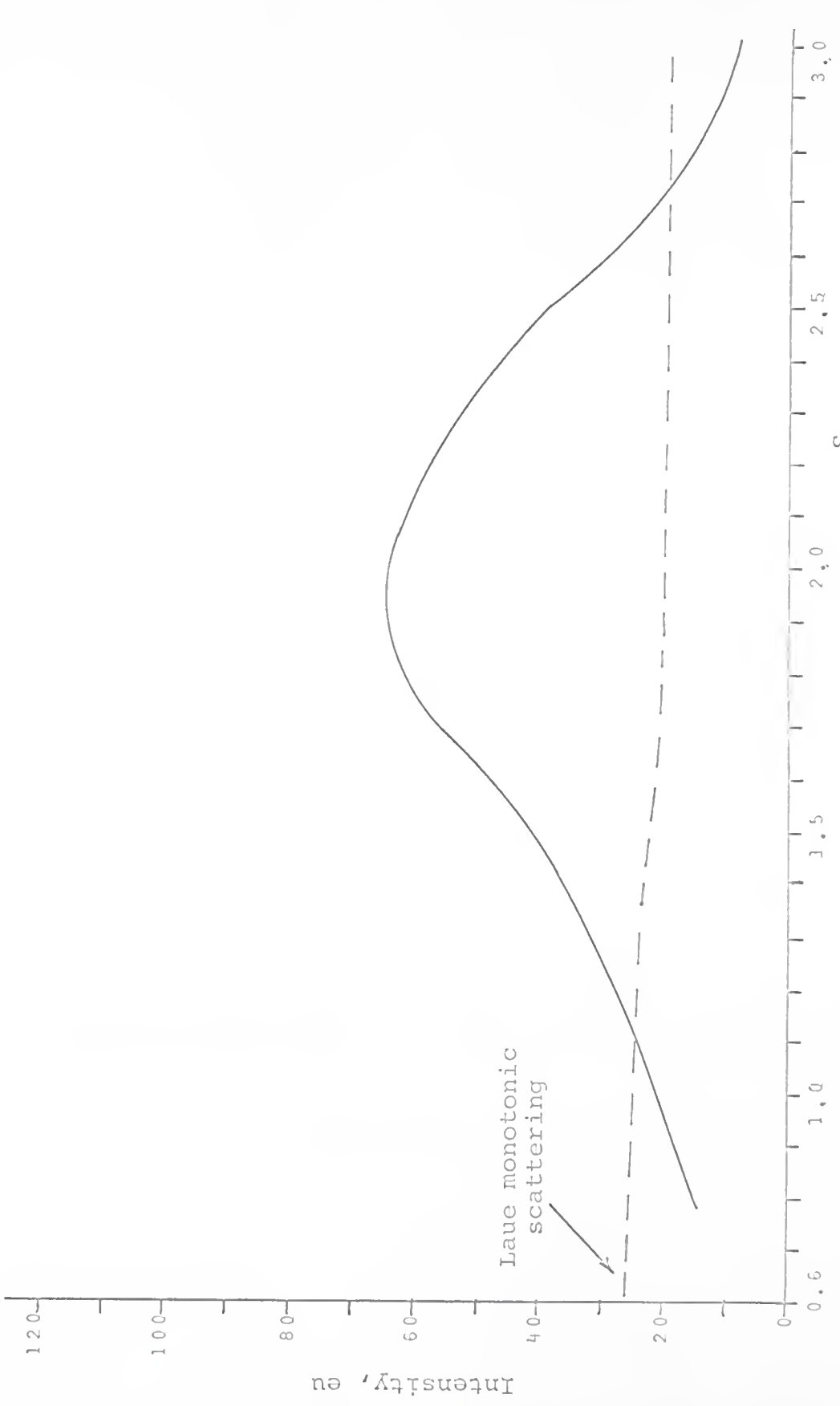

Fig. 54--Corrected diffuse-scattering curve for specimen X-1 (10.5 a/o Mo) after cold rolling and annealing for 201 hours at 500°C.

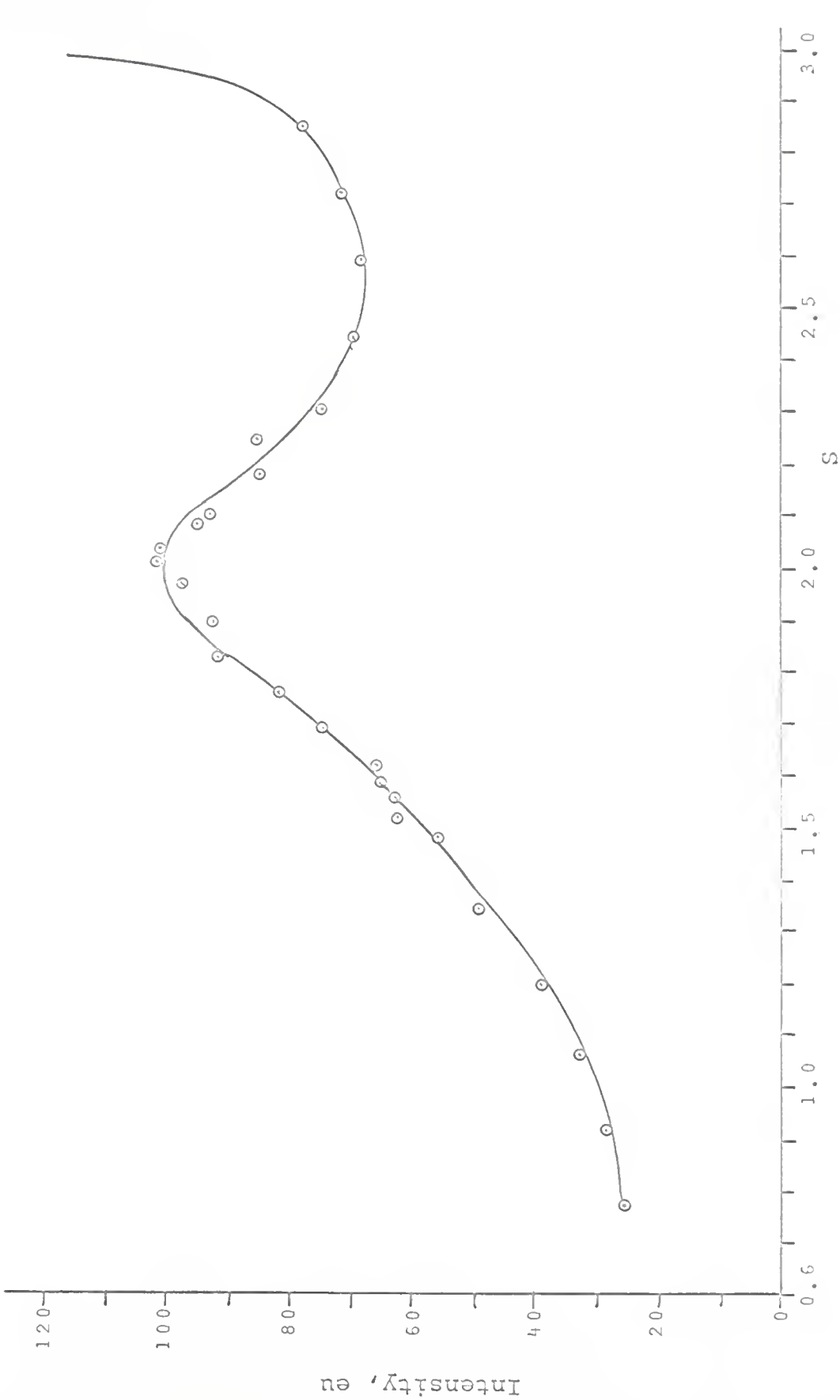

Fig. 55--Diffuse-scattering curve for specimen X-2 (14.0 a/o Mo) after cold rolling and annealing for 246 hours at 500°C.

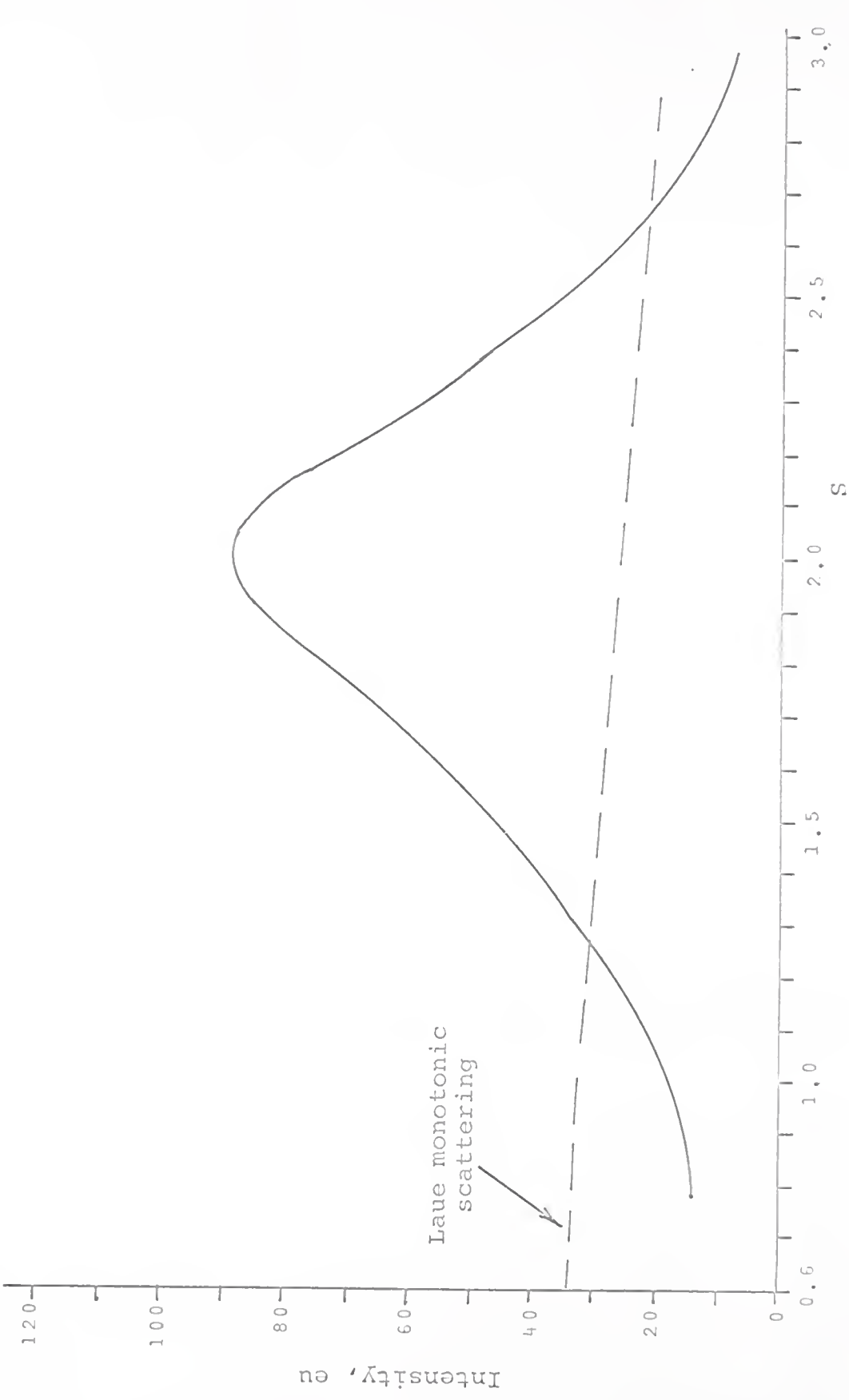

Fig. 56--Corrected diffuse-scattering curve for specimen X-2 (14.0 a/o Mo) after cold rolling and annealing for 246 hours at 500°C.

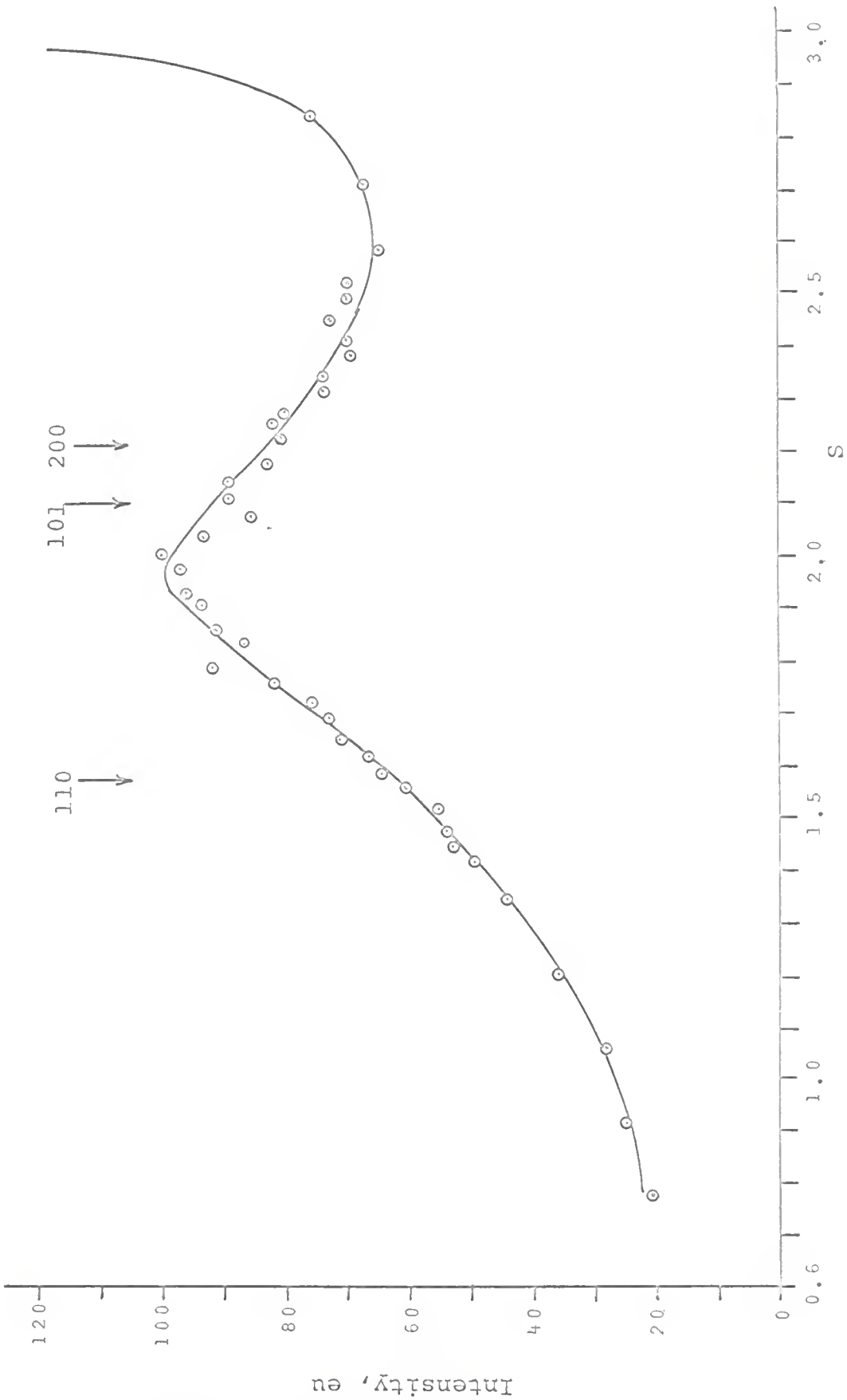

Fig. 57--Diffuse-scattering curve for specimen X-2 (14.0 a/o Mo) after cold rolling and annealing for 3.75 hours at 630°C and 1 hour at 650°C.

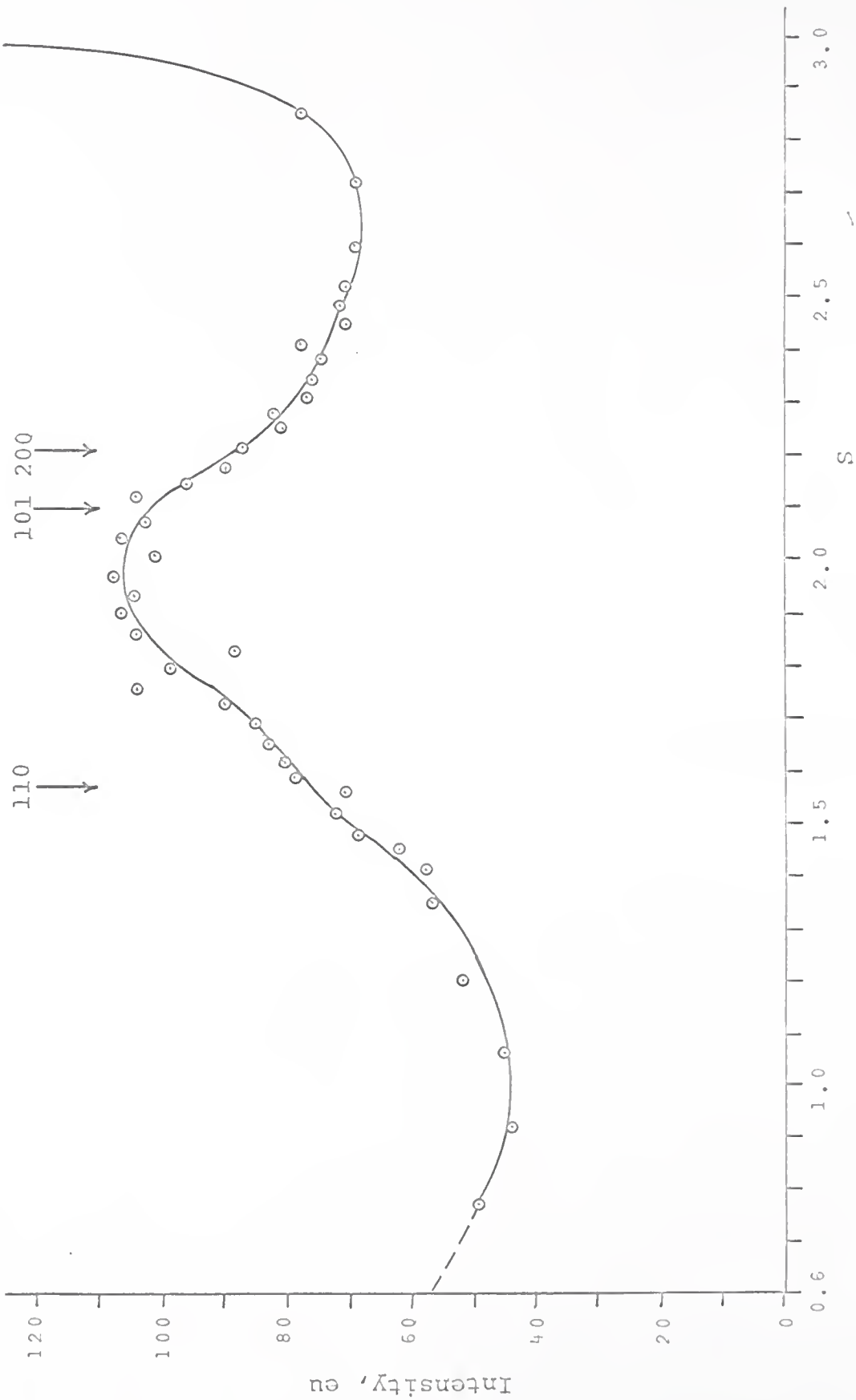

Fig. 58--Diffuse-scattering curve for specimen X-2 (14.0 a/o Mo) after cold rolling and annealing for 3.75 hours at 650°C and 5 hours at 650°C.

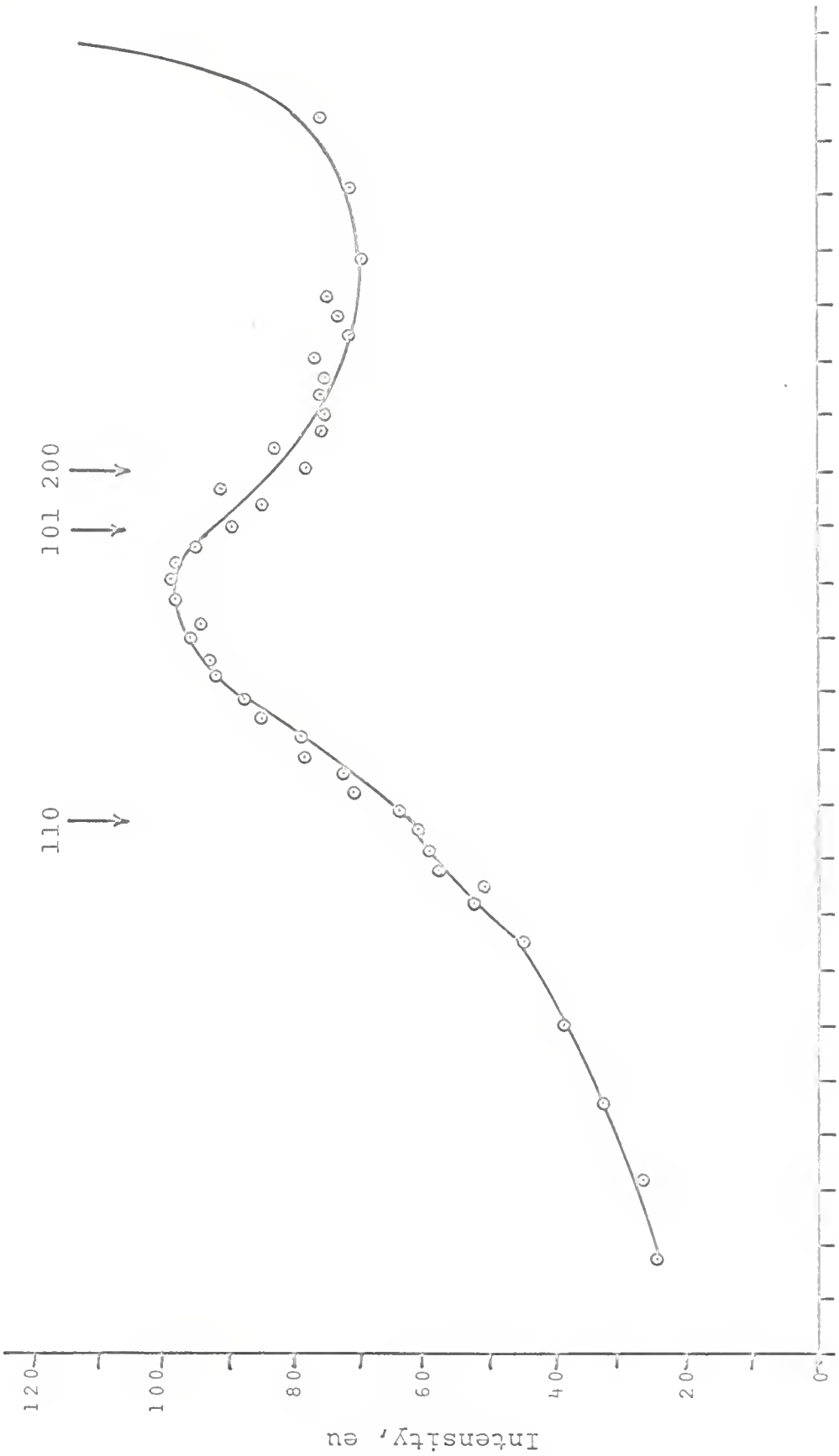

Fig. 59---Diffuse scattering curve for specimen X-2 (14.0 a/o Mo) after cold rolling and annealing for 3.75 hours at 630°C, 5 hours at 650°C, and 1.5 hours at 750°C.

effect can be attributed to interference from the tail of the small-angle scattering corresponding to the precipitation of the β phase. The presence of a measurable amount of small-angle scattering means that a number of the β-phase particles were less than 100 Å in size at this stage. Another feature in Figure 59 is the occurrence of small broad "hump" in the diffuse scattering curve at S≈1.55 which is apparently due to the emergence of the (110) superlattice line.

After annealing for an additional 1.5 hours at 750°C, the interference from the small-angle-scattering curve had disappeared. One would expect therefore that the average size of β nuclei after 1.5 hours at 750°C was several hundred angstroms. The slight perturbation from the (110) peak was still present and the large amount of scatter in the vicinity of the (101) and (200) superlattice lines indicated that these peaks were trying to emerge. The superlattice lines of the β phase did not occur as strong peaks for two reasons: (1) Superlattice lines are by nature very weak. (2) The volume fraction of β phase in the 14.0 a/o Mo alloy even after complete precipitation at 750°C is only about 10% according to the phase diagram of Guthrie and Stansbury.

In summary it is apparent that sharp increases in SRO were accompanied by sharp increases in resistivity upon

annealing both the 10.5 and 14.0 a/o Mo alloys. It is also apparent that as the resistivity decreased upon cold-rolling so did the amount of SRO. Furthermore the K-effect was more pronounced in the 14.0 a/o alloy and the amount of change in its SRO was greater upon cold-working and annealing. Most of these features can be seen clearly in the uncorrected diffuse-scattering curves and are especially obvious in the curves that have been corrected for Compton scattering, temperature-diffuse scattering, and interference from the {111} peak.

4.3 *Field-Ion Micrographs of Ni - 14.0 a/o Mo and Ni - 20.0 a/o Mo Alloys*

Field-ion micrographs were obtained from specimens W-1, W-2, and W-3 for the purpose of determining the nature of the SRO in dilute Ni-Mo alloys. The histories of these specimens are given in Table 1. Specimens W-1 and W-2 contained 14.0 a/o Mo and W-3 contained 20.0 a/o Mo. Specimen W-1 was quenched from 850°C in order to retain the SRO existing above the solvus at this composition. Specimen W-2 was quenched from 850°C and was then annealed for 2.5 hours at 700°C to develop the two-phase structure of β precipitates in the α matrix. Specimens W-1 and W-2 were then compared with specimen W-3 which was annealed for 110 minutes at 750°C to develop the fully-ordered Ni_4Mo structure.

In Figures 60-63 micrographs of specimens W-1 are shown. These micrographs correspond to the α matrix with no LRO. Figures 64-69 show the fully ordered Ni_4Mo structure of specimen W-3. The difference in appearance between the LRO and SRO was striking. The LRO appeared as a very regular structure with well developed crystallographic poles, whereas the α matrix, exhibiting only SRO, appeared as a very spotty and irregular structure. The reasons for this contrast were discussed in Chapter I, Section 4. One of the most important conclusions to be drawn from these micrographs is that there were no small well-developed domains of LRO existing above the critical temperature as reported by Southworth and Ralph [88] for Co-Pt. Instead the micrographs of W-1 appeared to be uniformly disordered. From this observation it was concluded that if SRO in Ni-Mo consists of domains of LRO, the domains are quite imperfect. On the other hand, certain features of specimen W-1 suggest that a domain structure does indeed exist in the single-phase α region. These features are the lines which have the appearance of domain boundaries as indicated by arrows in Figures 60-63. In Figures 62 and 63 the visibility of the boundaries was enhanced by photographing while the tip was being field evaporated.

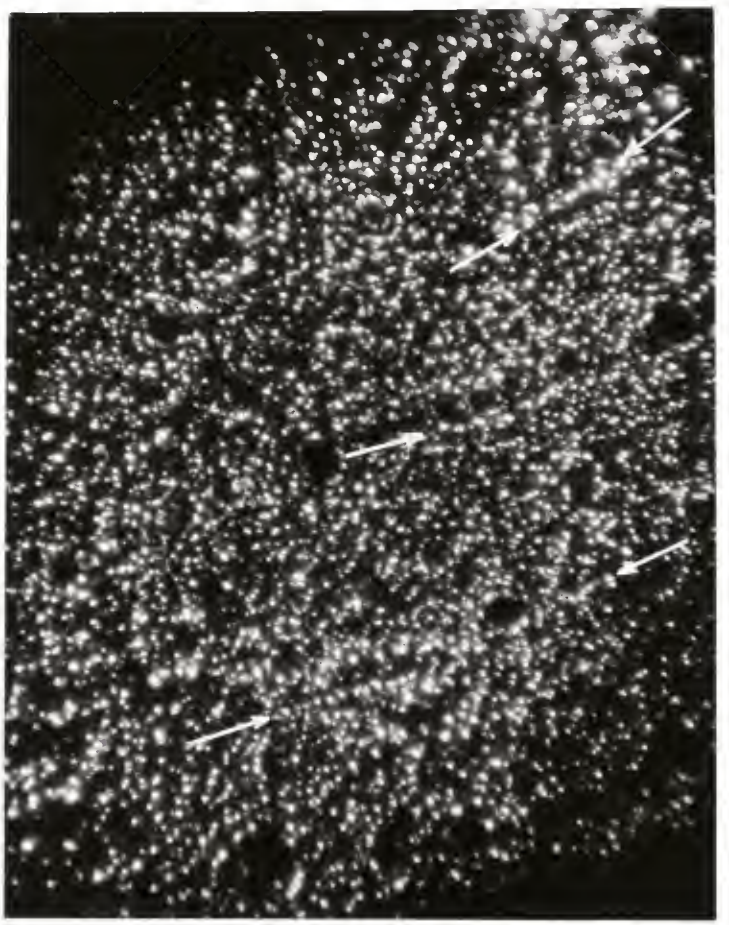

Fig. 60--Field-ion micrograph of the Ni-14.0 a/o Mo alloy (specimen W-1) quenched from 850°C.

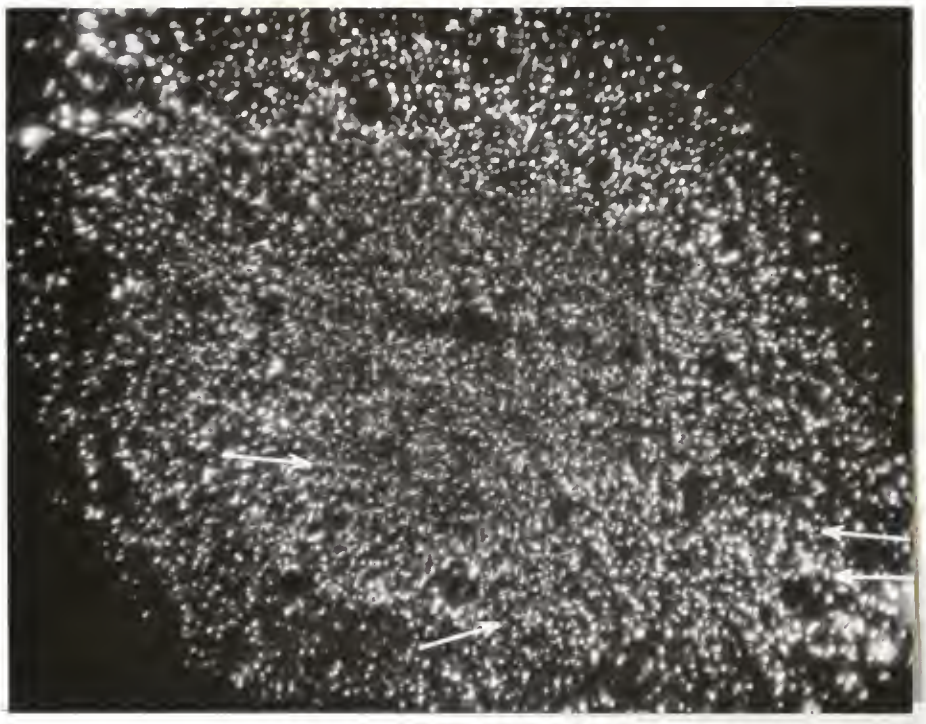

Fig. 61--Field-ion micrograph of the Ni-14.0 a/o Mo alloy (specimen W-1) quenched from 850°C.

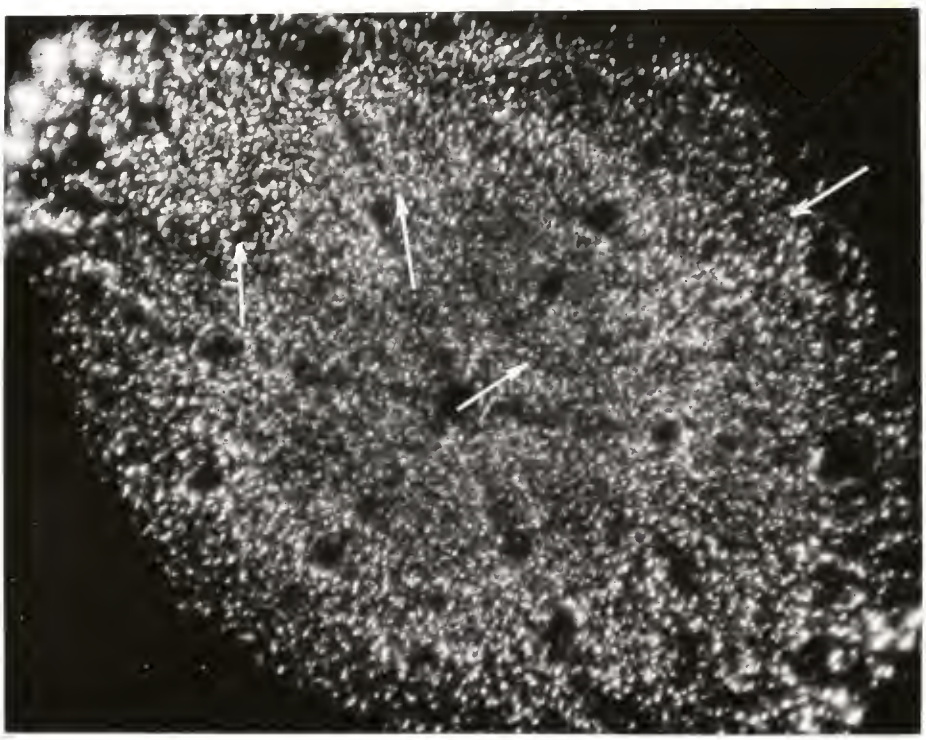

Fig. 62--Field-ion micrograph of the Ni-14.0 a/o Mo alloy (specimen W-1) quenched from 850°C and photographed during the process of field evaporation.

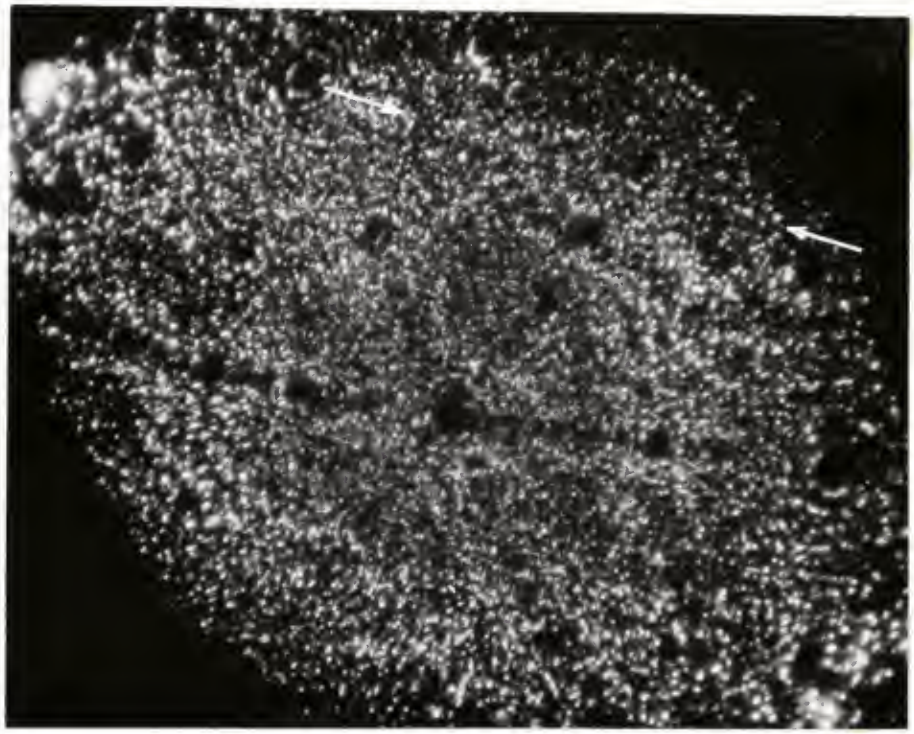

Fig. 63--Field-ion micrograph of the Ni-14.0 a/o Mo alloy (specimen W-1) quenched from 850°C and photographed during the process of field evaporation.

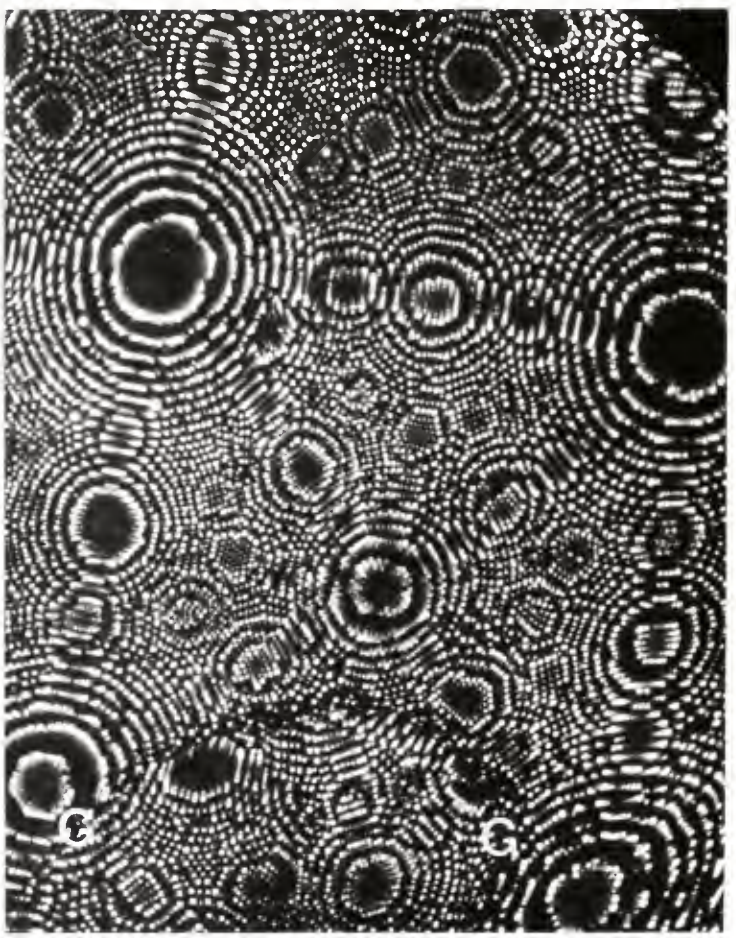

Fig. 64--Field-ion micrograph of fully-ordered Ni_4Mo (specimen W-3) showing a grain boundary.

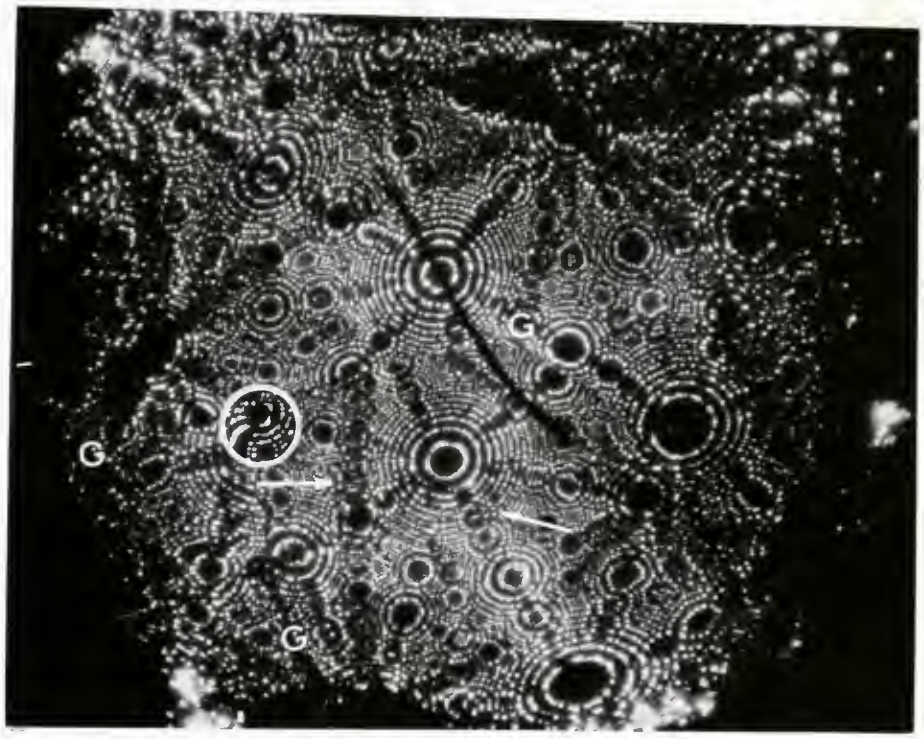

Fig. 65--Field-ion micrograph of fully-ordered Ni_4Mo (specimen W-3) showing grain boundaries and at antiphase domain boundary.

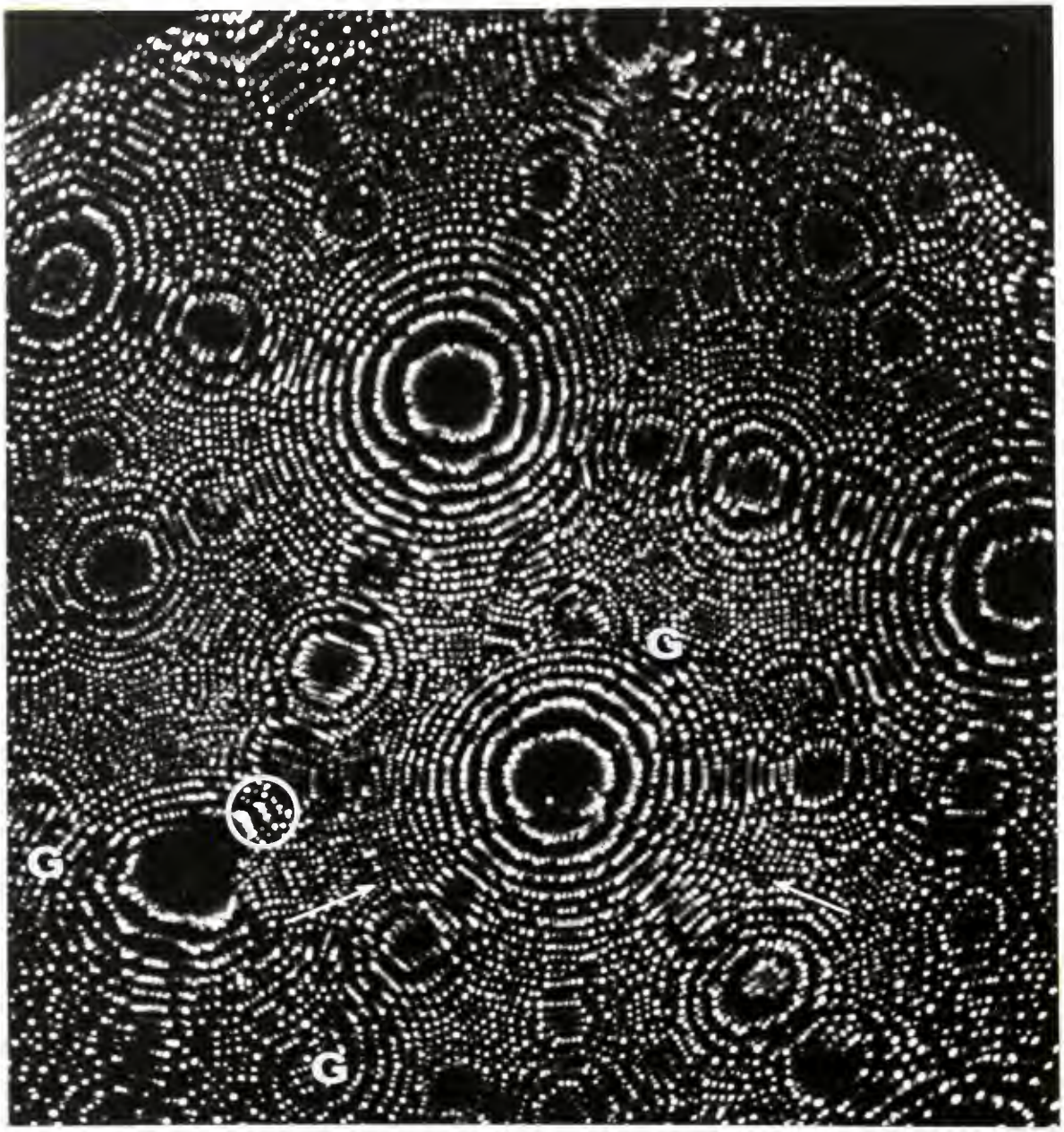

Fig. 66--Field-ion micrograph of fully-ordered Ni_4Mo (specimen W-3) showing grain boundaries and an antiphase domain boundary.

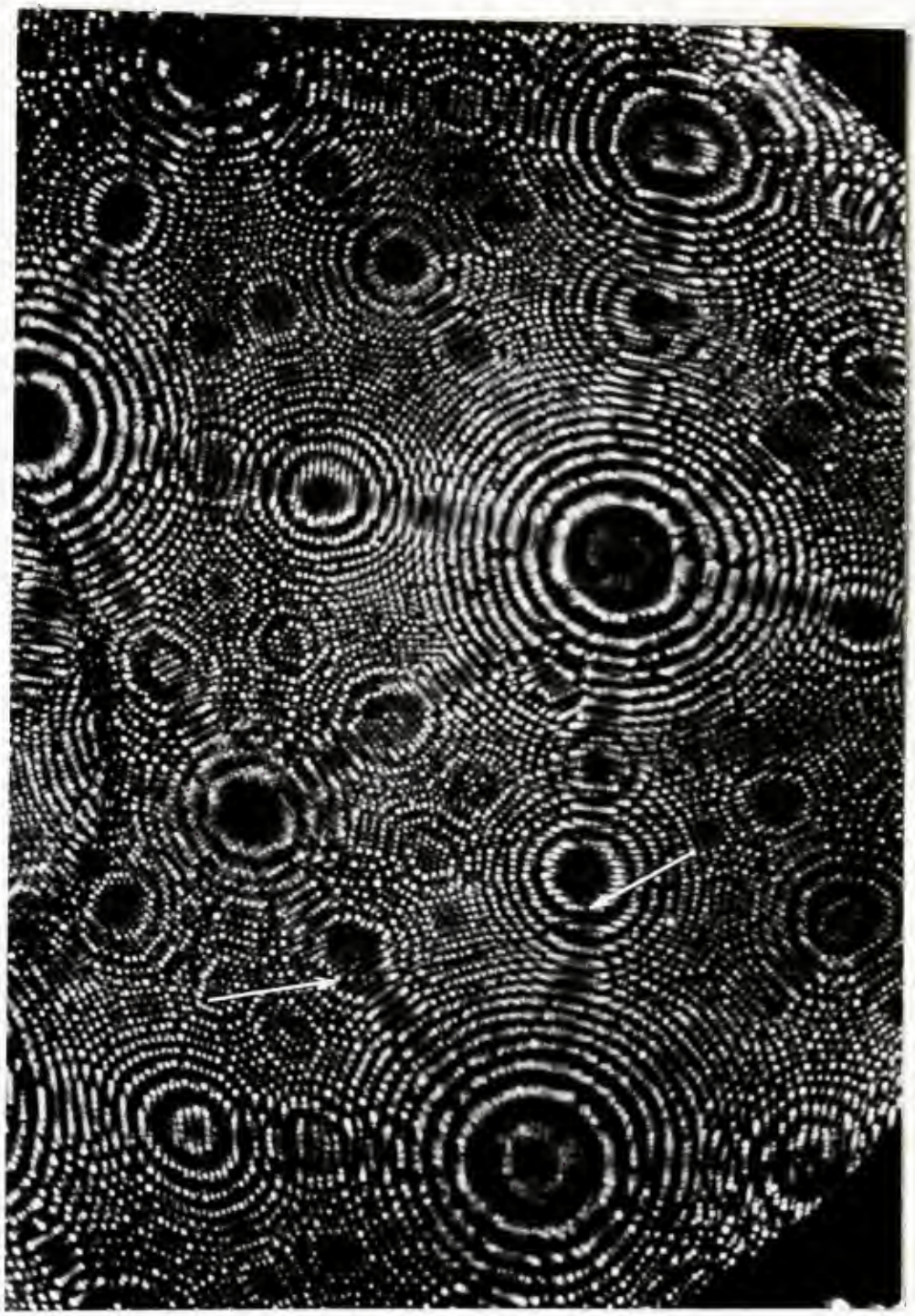

Fig. 67--Field-ion micrograph of fully-ordered Ni_4Mo (specimen W-3) showing a translational antiphase domain boundary.

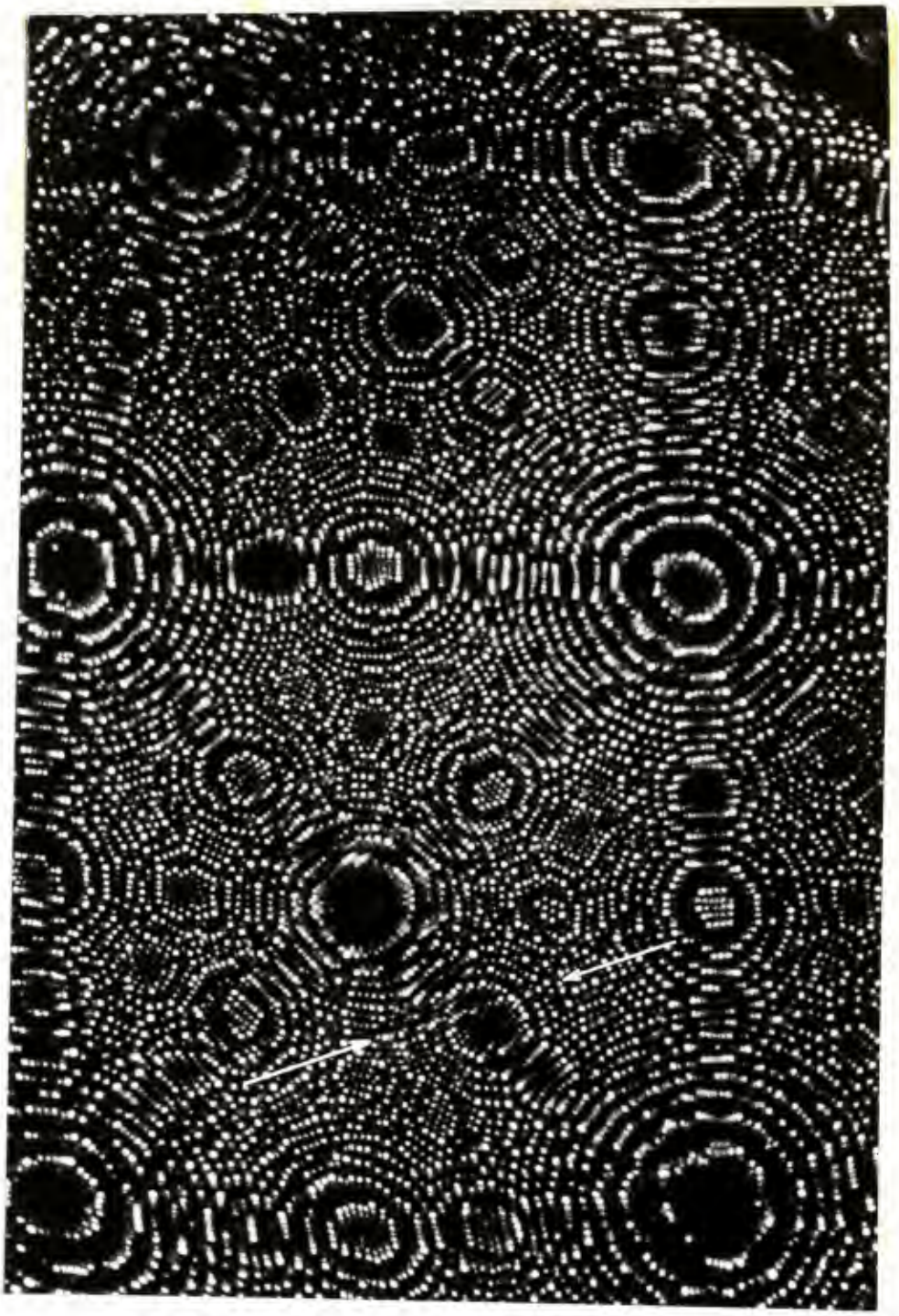

Fig. 68--Field-ion micrograph of fully-ordered Ni_4Mo (specimen W-3) showing a translational antiphase domain boundary.

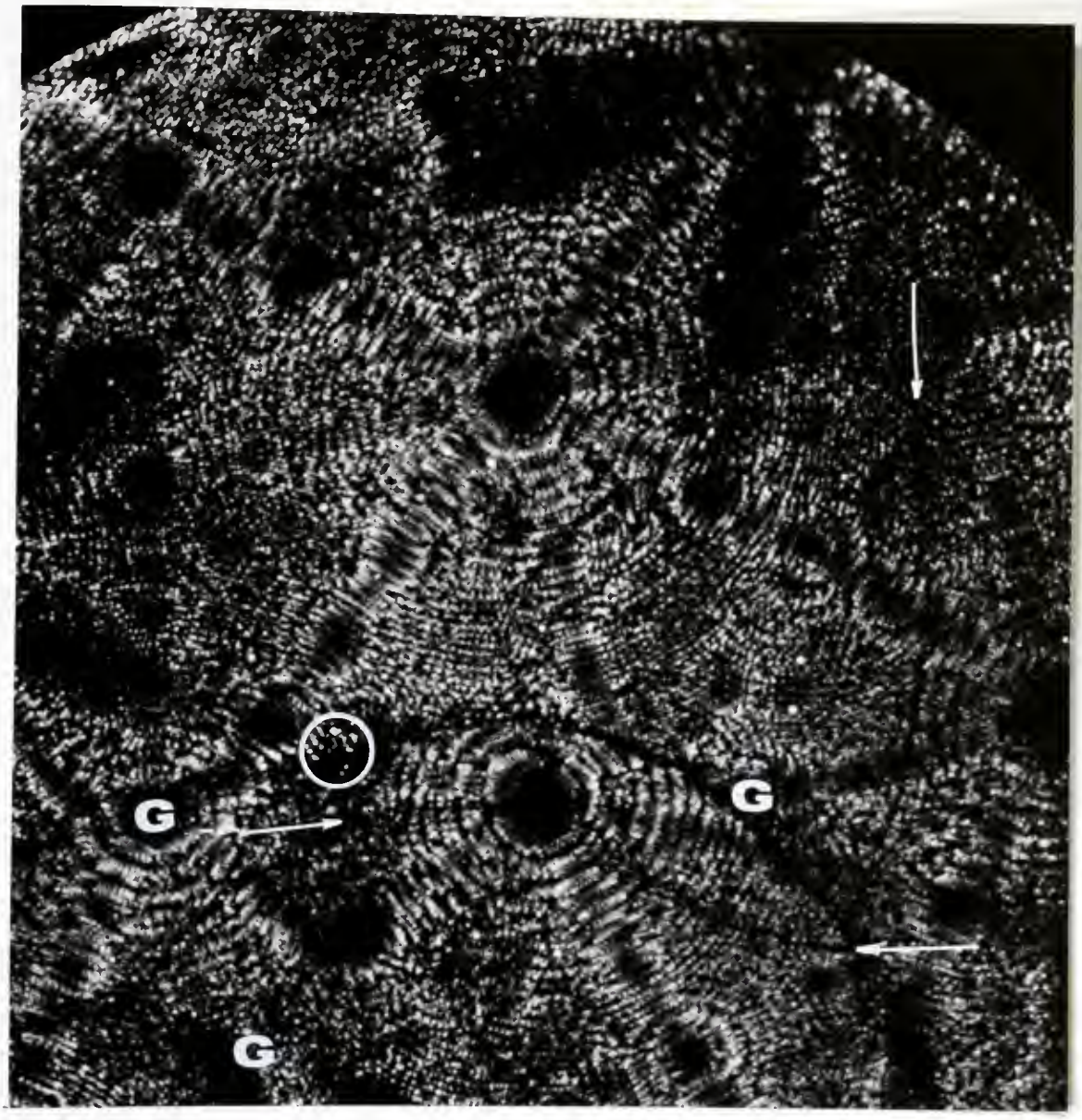

Fig. 69--Field-ion micrograph of fully-ordered Ni_4Mo (specimen W-3) photographed during the process of field evaporation.

There were several interesting features in the micrographs of specimen W-3 representing the fully-ordered state (Figures 64-69). These photographs showed numerous domain boundaries, which are again indicated by arrows. There was also a complete absence of any disordered regions. This observation is in agreement with the TTT curve of Lampe and Stansbury [106], which shows that the α to β transformation is complete after approximately 80 minutes. Also present in the micrographs of specimen W-3 were grain boundaries, which are indicated by the letter "G".

In Figure 65 the difference in appearnce between grain boundaries and antiphase domain boundaries is shown. Two grain boundaries meet at the encircled point to form a triplet point. The symmetry of the specimen is completely changed by a grain boundary because large rotations of the lattice take place. In the same photograph a rotational domain boundary is present and is indicated by arrows. This boundary causes a slight shear or misfit of the rings of crystallographic pole but no significant displacement or rotation of the lattice occurs. In Figure 66 the previous area is shown enlarged after several atomic layers were removed by field evaporation. The misfit of the rings due to the antiphase domain boundary can be seen more clearly in this photograph.

It was pointed out in Chapter I, Section 1.4 that various types of antiphase domain boundaries are possible in alloy systems for which ordering changes the lattice symmetry. Boundaries caused by the meeting of two domains in which the tetragonal axes are not parallel, for example, are called rotational boundaries. If the tetragonality is accompanied by a slight lattice shrinkage, as is frequently the case, such boundaries may be only partially coherent as a result of misfit of the two lattices. This is the nature of the domain boundary shown in Figures 65 and 66. Boundaries caused by the meeting of two domains which have their tetragonal axes parallel are called translational boundaries. There is no misfit of the opposing lattices along such a boundary; however, it may still be visible in a field-ion micrograph, as was discussed in Chapter I. A good example of what appears to be a translational domain boundary is shown in Figure 67. In Figure 68, the same boundary is shown after field evaporation of several atomic layers. Note that in Figure 67 the boundary appears primarily as a dark line, whereas in Figure 68 it appears as a bright row of atoms.

In Figure 69 a micrograph of the same general area as that of Figure 66 is shown, except that the image was photographed during field evaporation to enhance the visibility of the boundaries. A close inspection of this

photograph reveals the presence of many boundaries which are not readily visible in the preceeding figures. One can see therefore that even though an antiphase boundary is present it may not be clearly visible. For this reason it is difficult to tell how many domains are present or what the average size is. It can be said however that many of the domains are of the order of 50 Å in diameter since the entire field of view is roughly 1,000 Å.

Because of the low volume fraction of the β phase present in specimen W-2, no β particles were found though many layers of atoms were field evaporated. The area shown in Figure 70 is the α phase. This image appears slightly more regular than the images from specimen W-1 in Figures 60-63 indicating that the degree of local order was greater in specimen W-2 than in W-1. It is reasonable to expect the degree of local order to be greater in specimen W-2 since it was annealed at a lower temperature. Also present in Figure 70 are several domain boundaries, again indicated by arrows.

The presence of the domain boundaries in the α phase of specimens W-1 and W-2 is evidence that SRO in dilute Ni-Mo alloys consists of small, imperfect domains of Ni_4Mo-type LRO. The density and general appearance of the boundaries in specimens W-1 and W-2 were similar to those

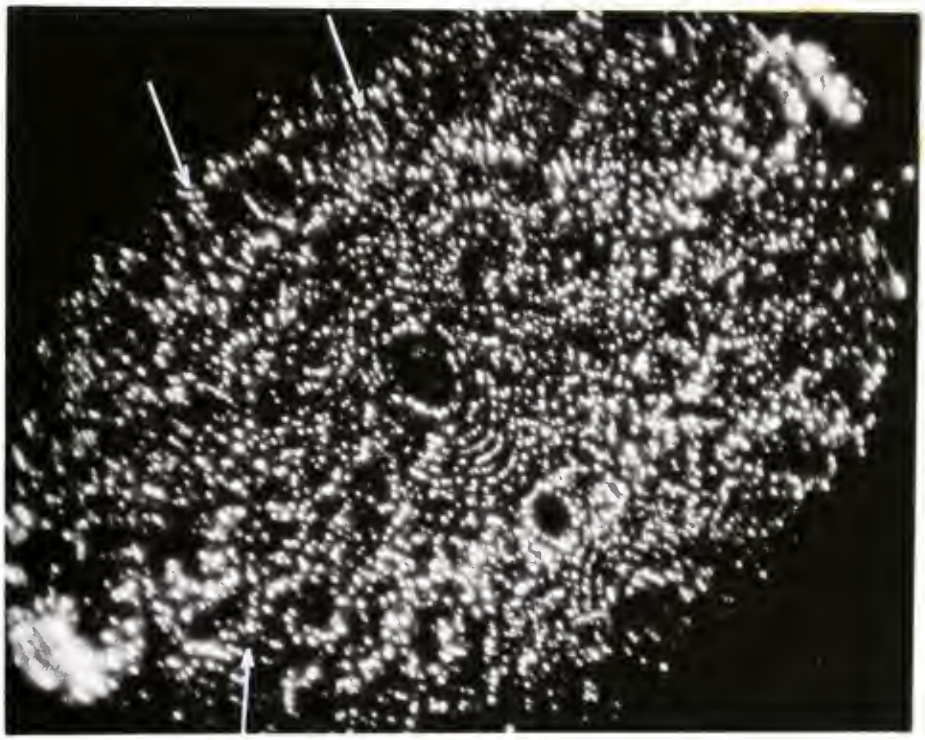

Fig. 70--Field-ion micrograph of the Ni-14.0 a/o Mo alloy (specimen W-2) annealed for 2.5 hours at 700°C.

found in specimen W-3 representing the fully-ordered Ni_4Mo structure. It appears that the domains in the "disordered" specimens were perfect enough to form boundaries that are visible with the field-ion microscope but not perfect enough to appear as small, highly-regular regions such as those observed by Southworth and Ralph in the alloy CoPt.

4.3 *Precipitation of the β Phase*

The precipitation of the β phase was studied in Ni-14.0 a/o Mo using electron transmission microscopy and small-angle x-ray scattering. The primary purpose of this portion of the work was to determine whether or not any intermediate metastable phases form during the precipitation process. Such metastable phases, if present, would shed doubt upon the suggestion that "nuclei" of the β phase exist above the solvus in the form of small, imperfect domains. Specimens F-3, F-5, and F-6 were examined in the electron microscope. Specimen F-3 was quenched from 1,000°C, cold-rolled approximately 20%, and annealed at 650°C. Accompanying small-angle scattering measurements were made on specimen F-3. Precipitation of the β phase was studied directly in specimens F-5 and F-6 which were annealed in the microscope by means of the hot stage. F-5 was cold-rolled approximately 20% prior to annealing, and F-6 was

quenched from 1,000°C. Small-angle scattering measurements were also made on specimens F-2 and F-4.

From the above studies the following information was obtained concerning the precipitation of the β phase in Ni-14.0 a/o Mo alloys:

1. No intermediate metastable phases were observed during the precipitation process. In specimens F-5 and F-6 the β phase precipitated directly from the supersaturated solid solution as platelets along certain specific habit planes. In Figure 71 an example of precipitates formed in the hot stage in specimen F-5 is shown.

2. The dispersion of precipitates was extremely inhomogeneous in specimens F-3 and F-5, which were cold-rolled prior to annealing. Certain areas were found to be heavily populated with platelets whereas others were completely devoid of platelets. The inhomogeniety was particularly apparent in specimen F-3. In specimen F-6, which had been quenched from 1,000°C prior to annealing in the hot stage, the dispersion of platelets was found to be quite uniform. With regard to uniformity of size and dispersion of the β platelets the order was F-6, F-5, and F-3, with F-6 being the most uniform and F-3 the least. An example of precipitates found in specimen F-6 is shown in Figure 72. In Figure 73 an example of precipitates formed in specimen F-3 is shown.

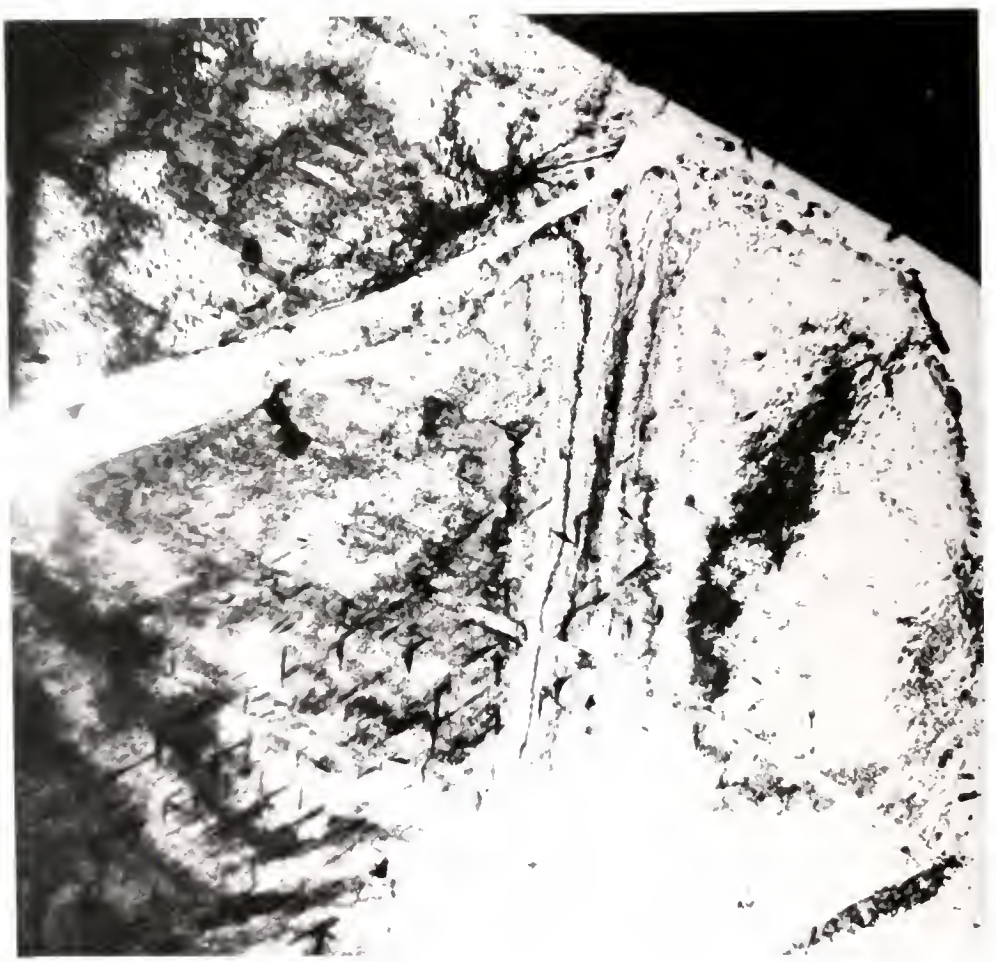

Fig. 71--Electron-transmission micrograph of β-phase platelets in the Ni-14.0 a/o Mo alloy (specimen F-5), cold-rolled and annealed in the hot stage. Magnification x 21,500.

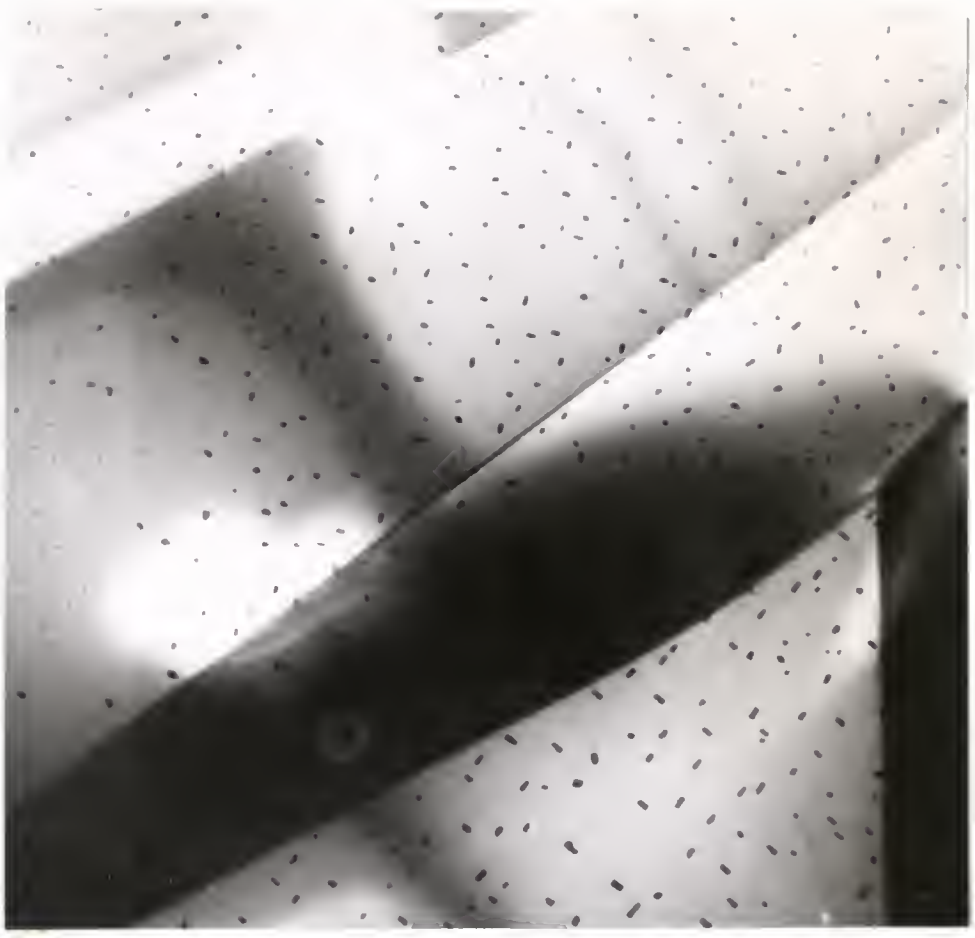

Fig. 72--Electron-transmission micrograph of β-phase platelets in the Ni-14.0 a/o Mo alloy (specimen F-6), quenched from 1000°C and annealed in the hot stage. Magnification x 6,500.

Fig. 73--Electron-transmission micrograph of β-phase platelets in the Ni-14.0 a/o Mo alloy (specimen F-3) cold-rolled to 20% reduction of area and annealed for 5 hours at 650°C. Magnification x 31,500.

3. The β platelets formed by heating specimens F-5 and F-6 in the hot stage grew to final size very rapidly. Although there was some variation in size, the particles could not be caused to grow or coalesce upon further heating.

4. The precipitates which were grown in the hot stage could not be re-dissolved by further heating. The temperature of the specimen could not accurately be determined during annealing because of the design of the hot stage. However, even after heating the foils to a point at which local melting began at the edges of the foil, the platelets remained unchanged. It is reasonably certain that under such conditions the foils were at a temperature above the solvus line.

5. During the precipitation process the β platelets appeared to remain either as very small nuclei (Figure 35) or as full-sized platelets (Figure 34). This conclusion is based in part upon the observations stated in paragraph 3, but it was shown more clearly by the small-angle-scattering and electron-microscopic results from specimen F-3. In Figure 74 a small-angle-scattering curve is shown for specimen F-3 after five hours at 650°C. The average particle radius was determined by use of the Guinier approximation (Chapter I, Section 1.5) to be approximately

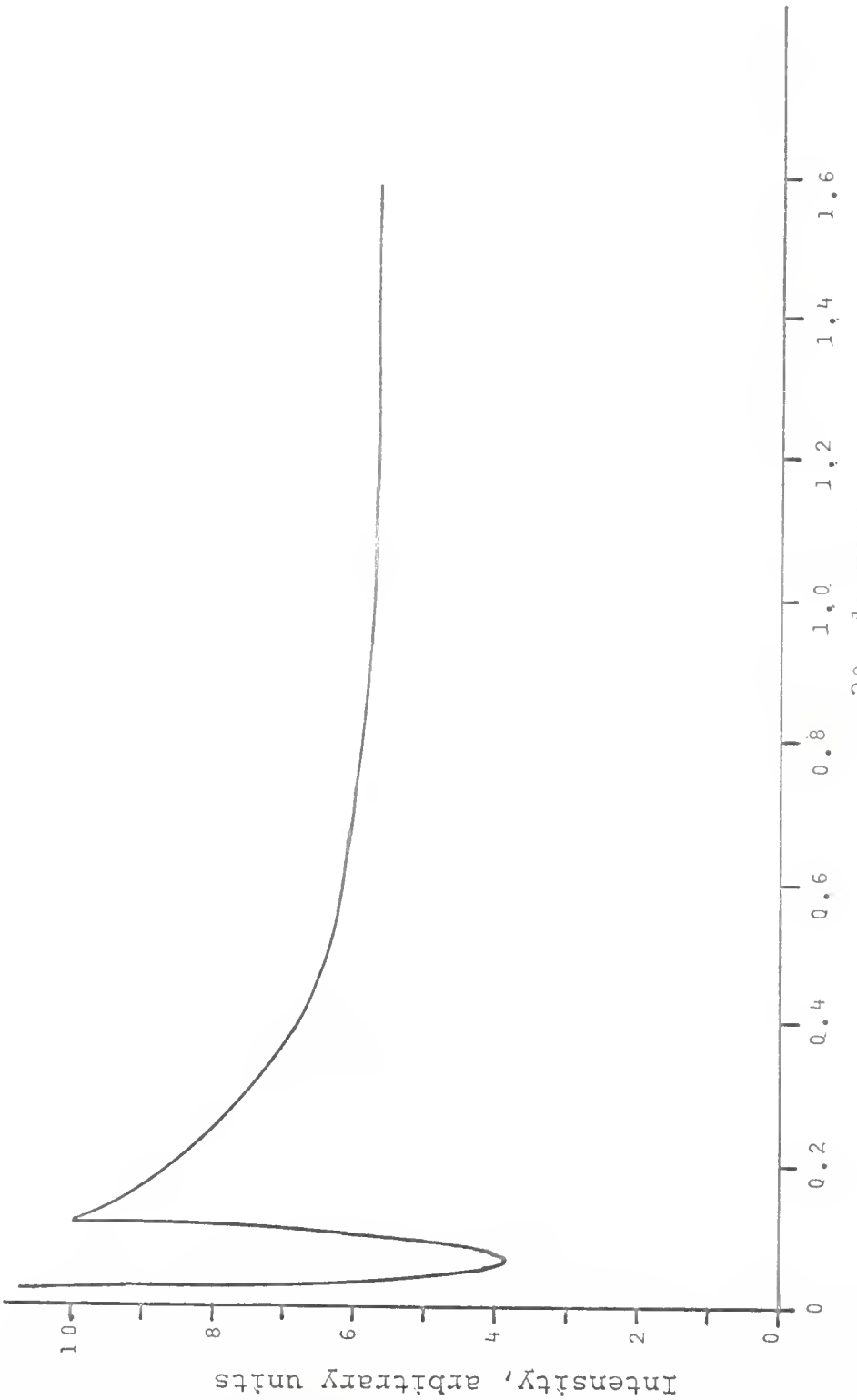

Fig. 74--Small-angle-scattering curve for the Ni-14.0 a/o Mo alloy (specimen F-3) after annealing for 5 hours at 650°C.

20 Å. Even though electron microscopy revealed a few large platelets five hours at 650°C, no intermediate-size precipitates of a few hundred angstroms in size were found. Furthermore, according to the small-angle-scattering curve of Figure 74, most of the β precipitates are present either as small nuclei approximately 50 Å in diameter or as the large platelets which are at the upper limit of detection by the small-angle scattering technique (approximately 1,000 Å). Apparently the small nuclei and the larger platelets can co-exist in the same foil with no intermediate sizes present. Raising the temperature evidently triggers the rapid growth of more of these nuclei into larger platelets as shown in Figures 32, 33, and 36.

The erratic behavior of the precipitation process described in paragraphs 2, 3, 4, and 5 can be attributed to the high degree of strain that accompanies the formation of β platelets. It can be seen in Figures 32, 33, and 36 that when precipitation began at a given temperature, the resistivity dropped quickly to a certain plateau. When the annealing temperature was increased the resistivity dropped quickly to a still lower plateau. It appears that the precipitation process is opposed by the high degree of strain which accompanies the α to β transformation.

Apparently the extent to which the transformation will progress at any given temperature depends on the rate at which the accompanying strains can be accomodated or relieved which in turn depends upon the annealing temperature as well as the local density of defects produced by prior cold work.

6. The β phase platelets precipitated preferentially on {111} planes. An analysis of one of the better diffraction patterns obtained from specimen F-5 gave good agreement with the {111} habit plane proposed by Spruiell [31]. It also showed that at least for this particular foil the platelets did not precipitate parallel to {100} planes as proposed previously [91].

CHAPTER V

CONCLUSIONS AND RECOMMENDATIONS FOR FURTHER STUDY

The primary objective of this study was to determine the role of local order in the formation of the K-state in dilute Ni-Mo alloys. It was known from previous work of other investigators that short-range order exists in dilute Ni-Mo alloys and that the K-state can be produced in these alloys with proper treatment; however, it had not been shown conclusively that short-range order contributed to the formation of the K-state. During the course of this work alloys of various compositions (10.5 a/o Mo, 14.0 a/o Mo, 20.0 a/o Mo) were examined after a variety of thermal and mechanical treatments. Although emphasis was placed on the use of resistivity and polycrystalline x-ray diffuse-scattering measurements, the techniques of field-ion microscopy, electron microscopy, and x-ray small-angle scattering were also used to some extent. From an analysis of the results obtained by these techniques and from previous work of other investigators, the following conclusions can be drawn:

1. The K-state in dilute Ni-Mo alloys can be attributed directly to the formation of SRO in the α solid solution. This conclusion is based upon the fact that a

one-to-one correlation was shown between increasing resistivity and increasing SRO in Ni-10.5 a/o and Ni-14.0 a/o Mo alloys. The structural states of the alloys were equivalent for the x-ray and resistivity measurements since both were made on the same specimens.

Consideration must be given to the possibility that since the SRO was destroyed by cold-rolling and restored by subsequent annealing, local lattice distortions could have been partly or wholly responsible for the resistivity changes as suggested by the theories of Logie *et al.* [77], Jaumot and Sawatzky [79], and Aarts and Houston-MacMillan [80]. Since the K-state can also be produced in Ni-Mo alloys simply by quenching and annealing, in which case there is an insignificant change in the dislocation structure, it is doubtful that local lattice distortions play a significant part. The same argument can be applied to rule out the possibility that solute atmospheres at dislocations could have caused the resistivity changes.

2. SRO in dilute Ni-Mo alloys consists of small, imperfect domains of LRO of the type Ni_4Mo. This conclusion is based principally on the results of the field-ion micrographs obtained from the Ni-14.0 a/o and the Ni-20.0 a/o Mo alloys. In these micrographs boundaries were found in the α matrix of the Ni-14.0 a/o alloy which were quite

similar in appearance and density to antiphase domain boundaries found in the fully-transformed Ni_4Mo alloy. It was concluded that the SRO existing in the α region consists of small imperfect domains of Ni_4Mo LRO approximately 50 Å in diameter. Domains of this size could account for the maximum in the diffuse-scattering curves of the 10.0 and the 14.0 a/o alloys since the (110), (101), and (200) superlattice lines would be broadened sufficiently to merge into one large "hump." The position of the diffuse maximum, in fact, occurred approximately at the mean position of these three lines. It is also noteworthy that the precipitation of the β phase was observed to be a continuous process during the heating of foils in the hot stage of the electron microscope. If intermediate phases had been observed, it would have cast doubt on the hypothesis that nuclei, or small domains, of the β phase exist above the solvus. Apparently the reversals in hardness sometimes found upon aging the two-phase alloys are due to a loss of coherency strains as the original β nuclei grow into full-size platelets, as suggested by Guthrie and Stansbury [91].

The above concept of the nature of SRO in dilute Ni-Mo alloys is in agreement with the structure proposed by Spruiell and Stansbury [31], but is in disagreement

with a model proposed by Baer [109]. Baer's model is best described as alternate double layers of (420) planes of the original FCC lattice in which the stems are slightly enriched and depleted in Ni atoms. An antiphase domain structure is also possible for this type of SRO, but according to the calculations of Baer the amount of enrichment and depletion in these layers amounts to about 4%. It is difficult to imagine that this slight departure from randomness could be responsible for the observed domain boundaries.

3. The increase in resistivity in dilute Ni-Mo alloys with increasing SRO could be explained in terms of the "superzone" concept [73-75]. One of the main points made by Baer was that more than one model for SRO may adequately describe the observed diffuse intensity; however, for his model there is no adequate explanation for the resistivity anomaly. On the other hand, the superzone concept may be used to explain the resistivity rise with increased SRO if one assumes that the SRO consists of small domains of Ni_4Mo LRO. Neglecting the change in electronic structure due to the addition of Mo atoms, the number of s electrons is 0.54 per atom [120]. Assuming that the Fermi surface is spherical, its radius will be approximately 0.735 R, where R is the radius of the tangent

sphere to the first Brillouin zone. Since there are three superlattice nodes which are closer to the origin of the reciprocal lattice than the {111} node, ordering within the lattice will cause a splitting of the first Brillouin into four smaller "sub-zones." The lower boundary of the uppermost one of these new zones occurs at approximately 0.730 R. Therefore ordering of the Ni_4Mo type may be expected to decrease the number of effective electrons since the Fermi surface is very near to a Brillouin zone boundary.

With the above idea in mind one might expect that perfect LRO of the Ni_4Mo type would cause a net increase in resistivity; whereas just the opposite is true (106). Once again it must be born in mind that the resistivity is related not only to the number of effective electrons, but also the collision probability [equation (3), Section 1.1] of these electrons. While ordering may decrease the number of effective electrons, it also decreases the collision probability due to the creation of a more perfect lattice. It is suggested that for a relatively imperfect degree of order such as that which is characteristic of SRO in the α phase, the first effect predominates, causing a resistivity increase. As the order progresses to a degree such as that found in an equilibrium state of LRO,

the latter effect predominates, causing a net decrease in resistivity.

It should be pointed out that with the "superzone" concept, the K-effect is not restricted to transition element alloys. It has been generally felt that the presence of a transition element is essential, and that some significant change in s electrons to d states or perhaps an increase in s-d scattering accompanies the K-state. However, in Ni-Mo one may expect a significant increase in resistivity simply on the basis of the occurrence of new Brillouin-zone boundaries without attributing any significance to the presence of the vacant d shell. The change in s and d states may also be important. It may in fact prove to be the most important effect as further studies are done on this system.

4. The β phase precipitates directly from the α solid solution as thin platelets without the formation of intermediate metastable phases. It seems reasonable that the small domains of Ni_4Mo type of order existing above the solvus serve as nuclei for the transformation. Based upon the appearance of decorated dislocations in the partially transformed 14.0 a/o Mo alloy it appears that dislocations serve as preferential nucleating sites for the β phase. This is supported by the difference in

morphology and density of platelets observed in specimens which were either cold-rolled or fully-annealed prior to precipitation of the β phase. Since there is a lattice strain associated with the α to β transformation it is reasonable to assume that the strain field around a dislocation has some effect on the precipitation process.

The following suggestions for further study in the Ni-Mo system are made:

1. Measurements of the Hall coefficient, thermoelectric power and the magnetic susceptibility could be correlated with the changes in resistivity and used to either support or refute the proposals made here for the cause of the K-state in Ni-Mo. Each of these techniques yields certain information about the electronic structure of an alloy which compliments the information obtained from resistivity measurements. A point of particular interest would be whether or not there is a significant change in the vacant states of the d shell upon formation of the K-state. If so this would indicate that the number of conduction electrons is lowered by a shift of electrons from s to d states during the formation of SRO. Under these conditions the superzone concept would have to be discarded or at least modified to take this into account.

2. Further studies with the field-ion microscope would be very valuable for the study of SRO in Ni-Mo. The evidence to date may be taken only as an indication that SRO consists of small, imperfect domains of LRO of the Ni_4Mo type. This conclusion is based primarily on the appearance of "domain" boundaries. It would be very helpful if one could distinguish Ni atoms from Mo atoms with the field-ion microscope, either by the variation of intensity with different imaging voltages or by preferential field evaporation of the different atomic species. Recent improvements in photographic technique have been made at the University of Florida [121] which have resulted in improved atomic resolution. It is possible that with these improvements a suitable technique could be developed for distinguishing different atomic species.

3. The application of the Monte Carlo computer method of Gehlen Cohen could be used to determine a suitable model for SRO in Ni-Mo alloys. At present there is no guarantee that such a model would be the correct one, but it would be interesting to compare such results with the models obtained by Spruiell and Baer. For this work it would be desirable to have the best possible order parameters; therefore, three-dimensional single crystal data would be needed. So far as the author is aware, only two-dimensional single-crystal data has been obtained to date.

4. Further studies with the electron microscope could be correlated with the field-ion microscope studies. Even though the boundaries observed in the field-ion micrographs of this work were interpreted as antiphase domain boundaries, it is possible that they are instead due to a mosaic substructure. Using the dark-field illumination from a selected superlattice spot it should be possible to determine the density, size, and shape of the antiphase boundaries in a suitably-annealed Ni - 20.0 a/o Mo specimen. It should also be possible to determine the approximate size and shape of the sub-grain boundaries by electron microscopy since they are composed of dislocation networks. From such observations it should be possible to determine whether the observed boundaries are indeed due to antiphase domains.

APPENDIX

APPENDIX

CONVERSION OF X-RAY INTENSITIES TO ELECTRON UNITS

The diffuse x-ray intensities in this study were expressed in electron units (eu) by comparing with a polystyrene standard. Equations (12) and (13) give the necessary relationships for this conversion. The equations are:

$$I_p = K\left[\frac{N}{2\mu}\right]_p P(\theta_p) I_p^{eu} \qquad (1)$$

$$I_s = K\left[\frac{N}{2\mu}\right]_s P(\theta_s) I_s^{eu} \qquad (2)$$

I_p and I_s are the experimentally measured intensities of the polystyrene and the specimen respectively, whereas I_p^{eu} and I_s^{eu} are the intensities of each expressed in eu. $P(\theta)$ is the polarization factor which depends upon the scattering angle; N is the number of scattering centers (atoms or molecules) per unit volume; μ is the linear absorption coefficient; and K is an experimental constant which is independent of the scattering angle.

The expression $N/2\mu$ may be rewritten as $\frac{N_0}{2(\mu/\rho)M}$ where N_0 is Avagodro's number; (μ/ρ) is the mass absorption coefficient; and M is the molecular weight. By making this substitution, dividing equation (1) by equation (2)

and then rearranging terms, the following expression can be derived:

$$I_s^{eu} = I_p^{eu} \frac{M_s}{M_p} \frac{(\mu/\rho)_s}{(\mu/\rho)_p} \frac{P(\theta_p)}{P(\theta_s)} \frac{I_s}{I_p} \qquad (3)$$

For polystyrene $M_p = 104.14$ and (μ/ρ) for copper radiation is 4.01 cm^2/gm. At $\theta_p = 50°$. The intensity of polystyrene is 66.2 eu with copper radiation. Assuming the specimen to be 10.5 a/o Mo the following values can be derived:

$$M_s = 62.60$$

$$(\mu/\rho)_s = 67.74 \ cm^2/gm$$

Using a value of 0.515 for $P(\theta_p)$ equation (3) can be written

$$I_s^{eu} = \frac{346.5}{P(\theta_s)} \frac{I_s}{I_p}$$

For this example suppose that the specimen was measured at $\theta_s = 11°$. Suppose further that the ratio of the intensity of the specimen to that of the polystyrene standard at $\theta_p = 50°$ was found to be 0.200. Using $P(\theta_s) = 0.930$ the value of I_s^{eu} is:

$$I_s^{eu} = \frac{346.5}{0.930} \times 0.200 \text{ eu} = 74.4 \text{ eu.}$$

REFERENCES

1. Thomas, H., "On Resistance Alloys," Z. für Physik, 129 (1951) 219.

2. Nordheim, R. and Grant, N. J., "Resistivity Anomalies in the Nickel-Chromium System," J. Inst. Metals, 82 (1954) 440.

3. Lifshitz, B. G., Izv. Akad. Nauk SSSR, 21 (9) (1957) 1225.

4. Kurdyumov, G. V., *et al.*, "Variations of Interatomic-Bond Strength in a Single Phase Solid Solution of Nickel and Aluminum," Dokl. Nauk SSSR, 124 (1959) 76.

5. Davies, R. G., "An X-ray and Dilatometric Study of the K-state in Iron-Aluminum Alloys," J. Phys. Chem. Solids, 24 (1963) 985.

6. Chen, W. and Nicholson, M. E., "The Influence of Annealing on the Electrical Properties of Cold-Worked Silver-Palladium Alloys," Acta Met., 12 (1964) 687.

7. Starke, E. A., Jr., Gerold, V. and Guy, A. G., "An Investigation of the K-effect in Nickel-Aluminum Alloys," Acta Met., 13 (1965) 957.

8. Hornbogen, V. E. and Kreye, H., "Anomalous Changes in Resistivity in Nickel-Aluminum Alloys," Z. Metall, 57 (2) (1966) 123.

9. Stansbury, E. E., Brooks, C. R. and Arledge, T. C., "Specific Heat Anomalies in Solid Solutions of Chromium and Molybdenum in Nickel: Evidence for Short-Range Order," J. Inst. Met., 94 (4) (1966) 136.

10. Müller, H. G. and Muth, P., "Interpretation of the K-state," Z. Metall., 50 (1959) 217.

11. Yano, Z., "Anomaly in the Nickel-Rich Solid Solution Of the Nickel-Chromium Binary System," Bull. Inst. Phys./Chem. Research (Tokyo), 19 (1940) 110.

12. Taylor, A. and Hinton, K. G., "A Study of Order-Disorder and Precipitation Phenomena in Nickel Chromium Alloys," J. Inst. Met., 81 (1952/53) 169.

13. Manec, J., "Study of Precipitation in Several Nickel Base Alloys," Acta Met., 7 (1959) 124.

14. Roberts, B. W., Swalin, R. A., "Concerning an Order-Disorder Transition in the Nickel-Chromium System," Trans. AIME, 209 (1957) 845.

15. Bagaryatskii, Yu. A. and Tyapkin, Yu. D., "On the Atomic Structure of Solid Solutions of Chromium in Nickel," Dokl. Akad. Nauk SSSR, 122 (1958) 806.

16. Köster, W. and Rocholl, P., "Conductivity and Hall Constant in Nickel-Chromium Alloys," Z. für Metall., 48 (1957) 485.

17. Starikova, G. V. and Presnyakov, A. A., Phys. Met. and Metall., 10 (1960) 943.

18. Baer, H. G., "Superstructure and the K-State in the Ni-Cr System," Z. für Metall., 49 (1958) 614.

19. Ibragimov, Sh. Sh. and Dimitriyev, V. D., "Effect of Neutron Bombardment on K-State Formation in Nickel-Chromium Alloy," Phys. Met. and Metall., 15 (4) (1963) 119.

20. Popov, L. E. and Karpov, G. I., "Effect of Quenching Temperature on the Formation of Short-Range Order," Dokl. Akad. Nauk SSSR, 129 (5) 1028.

21. Semenova, N. V., "Question of the Anomaly in the Electrical Resistance of Ni_3Cr," Phys. Met. and Metall., 6 (6) (1958) 57-66.

22. Sukhovarov, V. F., "Temperature-Velocity Dependence of the Resistance to Deformation of Nichrome in the Region of Existence of the K-State," Phys. Met. and Metall., 11 (1961) 302.

23. Progrushchenko, A. V., "X-ray Study of the Thermal Expansion of Nickel-Chromium Alloys," Nauk Dokl. Vyssh. Shkoly. Metallurgia I, (1958) 218-221.

24. Dekhtyar, M. V., Phys. Met. and Metall., 3 (1956) 55.

25. Gerold, V., "Physical Properties of Solid Solutions Containing Spherical Guinier-Preston Zones," J. Phys. Radium, 23 (1962) 812.

26. Mott, N. F., J. Inst. Met., 60 (1937) 267.

27. Baer, H. G., "Short-Range Ordering and the K-state," Z. Metall., 56 (2) (1965) 79.

28. Kudryavtseva, L. A., Panova, L. M., Popov, L. E., Sukhovarov, V. F., Phys. Met. and Metall., 15 (3) (1963) 108.

29. Popov, L. E., *et al.*, "Influence of Relaxation of Atomic Defects on Diffusional Transformation in Ni-Mo Alloys," Issl. Stali i Splavov, Akad. Nauk SSSR, (1964) 150.

30. Sukhovarov, *et al.*, "Investigation of the Process of Atom Redistribution in the Alloy Ni-10 a/o Mo," Phys. Met. and Metall., 15 (5) (1963) 53.

31. Spruiell, J. E., "X-ray Study of Short-Range Order in Nickel Alloys Containing 10.7 and 20 Atomic Per Cent Molybdenum," Ph.D. Thesis, University of Tennessee (Dec., 1963).

Spruiell, J. D. and Stansbury, E. E., J. Phys. Chem. Sol., 26 (1965) 811.

32. McManus, G. M., "Short-Range Order in Some Nickel-Base Alloys," J. Appl. Phys., 36 (11) (1965) 3631.

33. Westerlund, R. W. and Nicholson, M. E., "Effect of Plastic Deformation on the Resistivity and Hall Constant of Silver-Palladium Alloys," Acta Met., 14 (1966) 596.

34. Guy, A. G., "Structural Changes Accompanying the Formation of the K-state," Trans. ASM, 55 (1962) 737.

35. Korevaar, B. M., "The Influence of Lattice Defects on the Electrical Resistivity of a Gold-Copper Alloy (7 a/o Cu)," Acta Met., 6 (1958) 572.

36. Korevaar, B. M., Physica, 25 (1959) 1021.

37. Damask, A. C., "Residual Resistivity vs. Short-Range Order in Cu_3Au," J. Phys. Chem. Solids, 1 (1956) 23.

38. Presnyakov, A. A., *et al.*, "Anomalies in the Electrical Resistivity of Brasses and Aluminum Bronzes," Phys. Met. and Metall., 10 (5) (1960) 41.

39. Dekker, A. J., *Solid State Physics*, Prentice-Hall, Inc., Englewood Cliffs, N. J. (1963) 275.

40. Bardeen, J., "Electrical Conductivity of Metals," J. Appl. Phys., 11 (1940) 88.

41. Krivoglaz, M. A. and Smirnov, A. A., *The Theory of Order-Disorder in Alloys*, American Elsenier Publishing Co. Inc., New York (1965) 363.

42. Drude, P., Ann. d. Physik, 1 (1900) 566.

Drude, P., Ann. d. Physik, 3 (1900) 370, 869.

Drude, P., Ann. d. Physik, 7 (1902) 687.

Drude, P., Ann. d. Physik, 14 (1904) 936.

Lorentz, H. A., *Electromentheorie des Metalle*, Leipsig (1909).

43. Sommerfeld, A., Z. für Physik, 47 (1928) 1.

Sommerfeld, A. and Frank, N. H., Rev. Mod. Phys., 3 (1931) 1.

44. Mott, N. F. and Jones, H., *Theory of Properties of Metals and Alloys*, Dover Publication, Inc. New York (1958).

45. Bloch, F., Z. für Physik, 52 (1928) 555.

Bloch, F., Z. für Physik, 53 (1929) 216.

Bloch, F., Z. für Physik, 59 (1930) 208.

46. Linde, J. O., Ann. d. Physik, 15 (1932) 219.

47. Nordheim, L., Ann. d. Physik 9 (1931) 607, 641.

48. Johansson and Linde, Ann. d. Physik 25, (1936), 1.

49. Svensson, B., Ann. d. Physik, 14 (1932) 699.

50. Matyas, Z., Phil. Mag., 40 (1949), 324.

51. Warren, B. E. and Averbach, B. L., "The Diffuse Scattering of X-rays," in *Modern Research Techniques in Physical Metallurgy*, American Society for Metals, Cleveland (1953) 95.

52. Warren, B. E., "Temperature Diffuse Scattering for Cubic Powders," Acta Cryst., 6 (1953) 803.

53. Walker, C. B. and Keating, D. T., "The Effect of Temperature on Local Order Diffuse Scattering From Alloys," Acta Cryst., 14 (1961) 1170.

54. Paskin, A., "Contributions of One and Two Phonon Scattering to Temperature Diffuse Scattering," Acta Cryst., 11 (1958) 165.

55. Flinn, P. A., "Electronic Theory of Local Order," Phys. Rev. 104 (2), (1956), 350.

56. Cowley, J. M., "X-ray Measurements of Order in Single Crystals of Cu_3Au," J. Appl. Phys., 21 (1950) 24.

57. Warren, B. E., Averbach, B. L., and Roberts, B. W., "Atomic Size Effect in the X-ray Scattering by Alloys," J. Appl. Phys., 22 (12) (1951) 1493.

58. Borie, B. and Sparks, C. J., Metals and Ceramics Div. An. Prog. Rep. ORNL - 3870 (June, 1965).

59. Flinn, P. A., Averbach, B. L., Rudman, P. S., "Interpretation of Diffuse X-ray Scattering from Powder Patterns of Solid Solutions," Acta. Cryst., 7 (1954) 153.

60. Walker, C. B. and Guinier, A., "The Phenomenon of Pre-precipitation in Aluminum-Silver Alloys," Comptes Rendus, 234 (1952) 2379.

61. Huang, K., "X-ray Reflections From Dilute Solid Solutions," Proc. Roy. Soc., A190 (1947) 120.

62. Borie, B. S., "X-ray Diffraction Effects on Atomic Size in Alloys . II," Acta Cryst., 12 (1959) 280.

63. Roberts, B. W., Jr., "Short and Long-Range Order in CuAu," Ph.D. Thesis, MIT, (1951).

64. Sato, K., Watanabe, D. and Ogama, S., "Electron Diffraction Study on CuAu at Temperatures Above the Transition Point," J. Phys. Soc. Japan, 17 (10) (1962).

65. Walker, C. B., "X-ray Measurement of Order in CuPt," J. Appl. Phys., 23 (1952) 118.

66. Gehlen, P. C. and Cohen, J. B., "Computer Simulation of the Structure Associated with Local Order in Alloys," Phys. Rev., 139 (3A) (1965) A844.

67. Takagi, Y., Proc. Phys. Math Soc. (Japan), 23 (1941) 44.

68. Flinn, P. A., Averbach, B. L. and Cohen, M., "Local Atomic Arrangements in Au-Ni Alloys," Acta Met., 1 (1953) 664.

69. Münster, A., and Sagel, K., "Short-Range Order and Thermodynamic Properties of Metallic Solid Solutions," in *Phys. Chem. of Met. Solid Solutions . I*, New York Chem. Publ. Co. (1960) 196.

70. Friedel, J., Adv. in Phys., 3 (1954) 446.

71. Rudman, P. S., "A Theory of Atom Size Difference Induced Short Range Order," Acta Met., 13 (1965) 387.

72. Copeland, W. D. and Nicholson, M. E., "X-ray Evidence for Short-Range Order in Au-Pd," Acta Met., 12 (3) (1964) 321.

73. Gibson, J. B., J. Phys. Chem. Solids, 1 (1956) 27.

74. Muto, T., Sci. Paper Inst. Phys. Chem. Res. Tokyo, 34 (1938) 377.

75. Slater, J. C., Phys. Rev., 84 (1951) 179.

76. Nicholas, Proc. Phys. Soc. London, A66 (1953) 201.

77. Logie, H. J., Jackson, J., Anderson, J. C. and Nabarro, F. R. N., "Effect of Plastic Deformation on Resistivity of Gold-Palladium Alloys," Acta Met., 9 (1961) 707.

78. de Morton, M. E., Nature, London, 181 (1958) 477.

79. Jaumot, F. E. and Sawatzky, A., "Order-Disorder and Cold-Work Phenomena in Copper-Palladium Alloys," Acta Met., 4 (1956) 127.

80. Aarts, W. H. and Houston-MacMillan, A. S., "Anomalous Behavior of Silver-Palladium Alloys on Plastic Deformation," Acta Met., 5 (1957) 525.

81. Westerlund, R. W. and Nicholson, M. E., "Effect of Plastic Deformation on the Resistivity and Hall Constant of Silver-Palladium Alloys," Acta Met., 14 (1966) 569.

82. Dehlinger, U., "Der Widerstandsverlauf in Mischkristallen mit Nahordung," Z. Metall., 53 (9) (1962).

83. Bennet, W. D., J. Iron and Steel Inst., 171 (1952) 372.

84. Müller, E. W., "Das Feldionmikroskop," Z. für Physik, 131 (1951) 136.

85. Müller, E. W., "Field Ionization and Field-Ion Microscopy," Adv. in Elec. and Elec. Phys., 13 (1960) 83.

86. Ralph, B. and Brandon, D. G., "A Field-Ion Microscope Study of the Order-Disorder Reaction in Equiatomic Cobalt-Platinum," J. Int. Appl. Cobalt, 9 (1964) 1.

87. Ralph, B. and Brandon, D. G., "A Field-Ion Microscope Study of the Order-Disorder Reaction in Equiatomic Cobalt-Platinum Alloy in the Permanent Magnetic State," *Proc. Third European Reg. Conf. on Elec. Micr.*, Publ. House of Czech. Acad. Sci., Prague (1964) 303.

88. Southworth, H. N. and Ralph, B., "The Interpretation of Field-Ion Micrographs: The Image of an Order/Disorder Alloy," Phil. Mag., 14 (128) (1966) 383.

89. Guinier, A. and Fournet, G., *Small-Angle Scattering of X-rays*, John Wiley and Sons, Inc., New York (1955).

90. Hansen, M., *Constitution of Binary Alloys*, McGraw-Hill, Inc., New York (1958).

91. Guthrie, P. V. and Stansbury, E. E., "X-ray and Metallographic Study of the Nickel - Rich Alloys of the Nickel-Molybdenum System . II," USAEC Report ORNL - 3078, Oak Ridge, Tennessee, Oak Ridge National Laboratory (July, 1961).

92. Stoffel, D. W. and Stansbury, E. E., USAEC Report AECU - 3105, (1955).

93. Grube, G. and Schlecht, H., "Elektrische Leitfähigkeit und Zustands-diagram bei binären Legierungen Das System Nickel-Molybdän," Z. Elektrochem., 44 (1938) 413.

94. Grube, G. and Winkler, O., "Magnetische Suszeptibilitat und Zustands-Diagram von Binären Legierungen Das System Nickel-Molybdän," Z. Elektrochem., 44 (1938) 423.

95. Saito, S. and Beck, P., Trans. AIME, 215 (1959) 300.

96. Ellinger, F. H., "The Nickel-Molybdenum System," Trans. ASM, 30 (1942) 607.

97. Harker, D., "The Crystal Structure of Ni_4Mo," J. Chem. Phys., 12 (1944) 315.

98. Mikheev, V. S., Tr. Inst. Met. im. A. A. Baikova, Akad. Nauk SSSR, 1957 (2) 154; Chem. Abstr., 52 (1958), 8884.

99. Riddle, J. R., USAEC Report ORNL - 2839 (1959), 300.

100. Smiryagin, A. P., Potemkin, A. Ya. and Martynyuk, R. P., Zh. Neorgan. Khim., 3 (1958), 853.

101. Bagaryatskii, A. and Ivanovskaya, Dokl. Akad. Nauk SSSR, 132 (1960), 339.

102. Shoemaker, C. B., Fox, A. H. and Shoemaker, D. P., Acta Cryst., 13 (1960) 587.

103. Obrowski, W., Naturwissenshaften, 46 (1959) 490.

104. Guthrie, P. V., "An X-ray Investigation of the Nickel-Molybdenum Alloy System," M. S. Thesis, University of Tennessee, (1960).

105. Block, S. J., "Hardness Changes During the Ordering Reaction of Three Nickel-Molybdenum Alloy Systems," M. S. Thesis, University of Tennessee, (1960).

106. Lampe, B. T. and Stansbury, E. E., "An Investigation of the Order-Disorder Transformation in the Nickel-Molybdenum Alloy By Electrical Resistivity Measurements," M. S. Thesis, University of Tennessee, (1963).

107. Kritskaya, V. K., *et al.*, "Nature of the Variation of Young's Modulus During Heat Treatment of Single-Phase Nickel-Base Alloys," Dokl. Akad. Nauk SSSR, 129 (3) (1959) 550.

108. Polotskii, I. G. and Benieva, T. Ya., Issl. po Zh. Splav., 4 (1959) 202.

109. Baer, H. G., "Short-Range Order in the Nickel-Tungsten System," Z. Metall., 57 (4) (1966) 318.

110. Sosin, A. and Brinkman, J. A., Acta Met., 7 (1959) 478.

111. Clarebough, L., Hargreaves, M., Loretto, M., West, G., Acta Met., 8 (1960) 797.

112. Schumacher, D., Schule, W. and Seeger, A. Z. Naturforschung, 17A (1962) 228.

113. Popov., L. Ye. *et al.*, Paper presented at Ukr. Conf. on Atomic Ordering and its Infl. on Prop. of Alloys, Kiev (1962).

114. Wilson, L. V. and Gregg, R. Q., "A Note on the Use of the Curved-Crystal Monochromator on the X-ray Diffractometer at Low Angles," Norelco Reporter, 12 (4) (1965) 114.

115. Sagel, K., *Tabellen zür Röntgevstrukturanalyze*, Springer-Verlog, Berlin (1958) 166.

116. Gould, R. W. and Gerold, V. K., "Adaptation of the Norelco High-Angle Diffractometer For Small-Angle Scattering Studies of Pre-Precipitation," Norelco Reporter, 12 (1) (1965) 7.

117. Bollman, W., *Proc. Stockholm Conf. Elec. Micr.*, Almqvist and Wiksell, Stockholm (1957) 316.

118. Iida, S., "Formation Energy of Superlattice in Ni_3Fe," J. Phys. Soc. Japan, 10 (9) (1955) 769.

119. Rudman, P. S. and Averbach, B. L., "Effect of Cold Work on Local Order," Acta Met., 4 (1956) 382.

120. Argyres, P. and Kittel, C., Acta Met., 1 (1953), 241.

121. Hren, J. J. and Newman, R. W., To be published.

BIOGRAPHICAL SKETCH

Bruce Gordon LeFevre was born in Warren, Arkansas in 1937. He attended high school in Texarkana, Arkansas, and for a short time in Aurora, Colorado. In 1959, he received his B.S. degree in metallurgical engineering from the Colorado School of Mines in Golden, Colorado, near Denver. From 1959 until 1963 he was employed by the duPont company at their Savannah River Laboratory near Aiken, South Carolina.

In September, 1963, Mr. LeFevre began work on his Ph.D. degree at the University of Florida. His research at the University of Florida has been supported by a National Science Foundation grant. On receiving his Ph.D., Mr. LeFevre will be employed as an assistant professor by the Chemical Engineering School of the Georgia Institute of Technology in Atlanta, Georgia. His work there will consist of teaching and research in the field of metallurgy and materials science.

Mr. LeFevre is married and has two children. His wife is the former Elaine Annette Richter of Jefferson City, Missouri. His children are Christopher Alan, age 4 years and Cecily Adrienne, age 5 months. Mr. LeFevre is a

member of the American Institute of Mining and Metallurgical Engineers, the American Society for Metals, Sigma Nu, Tau Beta Pi and Sigma Xi.

This dissertation was prepared under the direction of the chairman of the candidate's supervisory committee and has been approved by all members of that committee. It was submitted to the Dean of the College of Engineering and to the Graduate Council, and was approved as partial fulfillment of the requirements for the degree of Doctor of Philosophy.

December 17, 1966

Dean, College of Engineering

Dean, Graduate School

Supervisory Committee:

Chairman